AUTHOR: TEBOWEI, R.

TITLE: Computational fluid dynamics (CFD) modelling of critical velocity for sand transport flow regimes in multiphase pipe bends.

YEAR: 2016

Computational Fluid Dynamics (CFD) Modelling of Critical Velocity for Sand Transport Flow Regimes in Multiphase Pipe Bends

Roland Tebowei

A thesis submitted in partial fulfilment of the
requirements of the
Robert Gordon University
for the degree of Doctor of Philosophy
(School of Engineering)

September 2016

Computational Fluid Dynamics (CFD) Modelling of Critical Velocity for Sand Transport Flow Regimes in Multiphase Pipe Bends

PhD Candidate

Roland Tebowei

Supervisory team

Dr Mamdud Hossain (Principal supervisor)

Dr Sheikh Z. Islam

Dr Gbenga O. Oluyemi

School of Engineering, Robert Gordon University, The Sir Ian Wood Building, Riverside East, Garthdee Road, Aberdeen, AB10 7GJ, United Kingdom.

Funding organisation

Niger Delta Development Commission (NDDC), Port Harcourt, Nigeria

To my late dad, **G. T. Tebowei** (rtd. Navy Cdr.) who passed away in the year I started my PhD programme.

Acknowledgements

"If I have seen further than my peers it is by standing on the shoulders of Giants." – Isaac Newton (1676). Similarly, I will like to acknowledge and express my heartfelt gratitude to my principal supervisor **Dr Mamdud Hossain** and the members of my supervisory team, Dr Gbenga Oluyemi and Dr Sheikh Islam who I describe as academic giants, for their valued guidance and encouragement throughout my PhD programme.

My sincere appreciation to my sponsor Niger Delta Development Commission (NDDC) for funding my PhD programme. I am also grateful to the entire staff at School of Engineering, Robert Gordon University (RGU) Aberdeen for their support. Very importantly, I must acknowledge the staff at RGU-Library department for their effort in providing materials that were outside my reach. In addition, I will like to thank my research colleagues at the Research hub of the school of engineering for their support and encouragement.

I will like to thank my dear mother Mrs Esther Titilayo Tebowei and my siblings, Sonia, Nelly and Paul Tebowei for their encouragement. Finally, I will like to thank my entire family members and friends for their support and encouragement. The words I present here are not enough to express my gratitude to everyone. I thank you all!

Roland Tebowei

June 2016.

Dedication

I will like to dedicate my thesis to Almighty God the supreme provider of my needs. The Lord God has been good to me.

Abstract

The production and transportation of hydrocarbon fluids in multiphase pipelines could be severely hindered by particulate solids deposit such as produced sand particles which accompany hydrocarbon production. Knowledge of the flow characteristics of solid particles in fluids transported in pipelines is important in order to accurately predict solid particles deposition in pipelines. This research thesis presents the development of a three-dimensional (3D) Computational Fluids Dynamics (CFD) modelling technique for the prediction of liquid-solids multiphase flow in pipes, with special emphasis on the flow in V-inclined pipe bends. The Euler-Euler (two-fluid) multiphase modelling methodology has been adopted and the multiphase model equations and closure models describing the liquid-solids flow have been implemented and calculated using the finite volume method in a CFD code software. The liquid phase turbulence has been modelled using a two-equation $k-\varepsilon$ turbulence model which contains additional terms to account for the effects of the solid-particles phase on the multiphase turbulence structure.

The developed CFD numerical framework has been verified for the relevant forces and all the possible interaction mechanisms of the liquid-solids multiphase flow by investigating four different numerical frameworks, in order to determine the optimum numerical framework that captures the underlying physics and covers the interaction mechanisms that lead to sand deposition and the range of sand transport flow regimes in pipes. The flow of liquid-sand in pipe has been studied extensively and the numerical results of sand concentration distribution across pipe and other flow properties are in good agreement with published experimental data on validation. The numerical framework has been employed to investigate the multiphase flow in V-inclined pipe bends of $\pm 4^{o}-6^{o}$, seemingly small inclined bend angles. The predicted results which include the sand segregation, deposition velocity and flow turbulence modulation in the pipe bend show that the seemingly small pipe bends have significant effect on the flow differently from that of horizontal pipes. The pipe bend causes abrupt local change in the multiphase flow characteristic and formation of stationary sand deposit in the pipe at a relatively high flow velocity. The threshold velocity to keep sand entrained in liquid in pipe bends is significantly higher than that required for flow horizontal pipes. A critical implication of this is that the correlations for predicting sand deposition in pipelines must account for the effect of pipe bend on flow characteristics in order to provide accurate predictions of the critical sand transport velocity (MTV) in subsea petroleum flowlines, which V-inclined pipe bends are inevitable due to seabed topology.

Identifying words:

Sand transport flow regimes, sand concentration profile, CFD modelling, V-pipe bend effect, stationary sand deposit, minimum transport velocity, turbulence modelling, multiphase flow, Eulerian-granular model, petroleum flowlines.

Table of Contents

List of Figures

List of Tables

Nomenclature

Symbol	Description	Unit
C_D	Drag coefficient	-
C_v	Solids volume fraction	-
D	Pipe diameter (size)	M
$D_{t,sl}$	Turbulent quantities for solids phase	-
d_s	Particle diameter (size)	M
e_{ss}	Coefficient of restitution of particles	-
ε	Turbulence dissipation rate	m^2s^{-2}
F_D	Drag force	N
F_{td}	Turbulent dispersion force	N
F_{vm}	Virtual mass force	N
g	Gravitational constant	ms^{-2}
$g_{0,ss}$	Radial distribution function	-
I_{2D}	Second invariant of the deviator of the strain	-
k_l	Turbulent kinetic energy of liquid phase	m^2s^{-2}
k_{ls}	Covariance of velocities of liquid and solids	m^2s^{-2}
k_s	Turbulent kinetic energy of solids phase	m^2s^{-2}
M_{ls}	Interfacial momentum transfer	Ns^{-1}
Pr	Prandtl number	-
P_{sf}	Solids frictional pressure	Nm^{-2}
P_s	Solids pressure	Nm^{-2}
R	Ratio of liquid and solids phase stress	-
Re	Reynolds number	-

U^*	Normalised velocity magnitude	-
v_l	Velocity of liquid phase	ms^{-1}
v_s	Velocity of solids phase	ms^{-1}
y^*	Normalised height of near wall mesh node	-

Greek letters

Θ_s	granular temperature	m^2s^{-2}
$\mu_{s,col}$	solids collisional viscosity	Pa.s
$\mu_{s,kin}$	solids kinetic viscosity	Pa.s
$\mu_{s,fr}$	solids frictional viscosity	Pa.s
$\alpha_{s,min}$	minimum frictional volume fraction	-
$\alpha_{s,max}$	maximum packing fraction limit of solids	-
Π_{kl}, $\Pi_{\varepsilon l}$	Influence of solids phases on liquid phase	-
$\tau_{F,sl}$	Characteristic particle relaxation time	s
$\tau_{t,sl}$	Lagrangian time scale	s
α_l	volume fraction of liquid phase	-
α_s	volume fraction of solids phase	-
η_{sl}	the ratio of the two characteristic times	-
ρ_m	mixture density	kg/m^3
ρ_i	liquid density	kg/m^3
ρ_s	solids density	kg/m^3
λ_s	Solids phase bulk viscosity	Pa.s
τ_w	Wall shear stress	Nm^{-2}
$\bar{\bar{\tau}}_l$	Viscous stress tensor for liquid phase	Nm^{-2}
μ_l	molecular viscosity of liquid phase	Pa.s

$\mu_{t,l}$	liquid turbulent viscosity	Pa.s
$\mu_{t,m}$	mixture turbulent viscosity	Pa.s
γ_{Θ_s}	granular energy dissipation	$\mathrm{kgm^{-3}s^{-1}}$
Φ	angle of internal friction	-
ϕ_{ls}	energy exchange between particles and liquid	$\mathrm{kgm^{-3}s^{-1}}$

Chapter 1

Introduction

1.1 Motivation for the Present Study

The global demand for energy has been on the increase in the past decades and is set to grow by 30-40% by 2040, according to the International Energy Agency world-energy-outlook report (2015). The rapid growth in worldwide energy use is reported to be driven primarily by China, India, Africa, Southeast Asia and the Middle East, considering the growth in population and the strong need to improve the standard of living using modern technology in the countries that lack sufficient modern energy services such as electricity. Although, the world produces electricity using three major sources, which include fossil fuels, nuclear and renewable sources (World Energy Council 2013). However, fossil fuels are still the dominant sources of the world energy despite the growing concern over their link to global climate change.

Fossil fuels consist of crude oil, natural gas and coal, and the renewable energy sources include wind, hydro, solar and geothermal energy. Fossil fuels account for almost 76% of the global energy supply (World Energy Council 2013). The crude oil and natural gas account for 87% of the fossil fuels constituent consumption for global energy use and may continue to dominate, despite the global collaborative efforts to reduce the use of carbon emitting energy sources by encouraging expansion and development of clean and renewable energy sources such as solar power, hydropower and hydrogen fuel-cell (Cusick 2013). Therefore, the high consumption of crude oil and natural gas for energy production is a strong indication that hydrocarbon energy are mostly relied upon globally and may remain dominant than any other source of energy.

The petroleum and process industries will have to continue increasing the production and supply of oil and gas in order to meet the high consumption of hydrocarbon energy. This need has challenged the oil and gas operators to step-out the search for hydrocarbons in ultra-deep water and more extreme environments where access is very challenging (Whitfield 2016). The challenges associated with developing hydrocarbon discoveries in offshore environment are enormous. An area of critical concern is issues related to design of pipeline (flow-line) infrastructures required to transport the hydrocarbons from subsea fields to the platforms and onshore terminals. This challenge of pipeline infrastructures development for production from offshore fields pose more complications with water-depth and distance from the shore (Ewida et al. 2004).

Fortunately, continued advances and improvement of offshore technology in petroleum industry have enhanced accessibility to deep-water offshore environments. The advancement in offshore technology has led to development of many subsea wells for extraction of crude oil and natural gas from subsea reservoirs in challenging and harsh offshore environments (Stevenson and Thorpe 1999). However, operational experiences from oil and gas fields have revealed that solids such as sand is often produced with the oil and gas during production, particularly from sandstone reservoirs, which complicates the issues of oil and gas production and transportation from offshore fields (Danielson 2007; Salama 2000)

The recent studies by Dabirian, Mohan and Shoham (2015), Spillane and Leggoe (2011), Bello, Oyeneyin and Oluyemi (2011) and Zhu et al. (2010) have reported that most of the prolific reservoirs with hydrocarbon reserve in commercial quantity worldwide are mainly formed of unconsolidated sandstone formations and are prone to produce sand with the hydrocarbon fluids. Therefore, petroleum multiphase pipelines would generally contain a flow-stream of liquid, gas and solid particles (sand) phases or mainly liquid and sand for hydrocarbons with very low gas-oil ratio (GOR). The knowledge of the nature of the sand particles interaction with the fluids and movements in pipelines is imperative, in order to understand the implications of sand particles transport in hydrocarbon flow stream in pipelines.

1.2 Problems of Produced Sand

The presence of sand particles in hydrocarbon flow-stream is a major risk factor to pipe blockage that may lead to reduced oil-well performance which increases work-over frequency (London, Cameron and Pierce 2012). Sand deposition may occur in pipelines due to changes in flow conditions, which may include flow-rates and pipe inclination, to mention a few. The sand deposit may cause flow impediment, erosion and corrosion of pipes, and other flow assurance issues. These problems due to produced sand may occur more often in offshore subsea pipelines, which are usually route through undulating seabed topology (Guzman and Zenit 2011). The undulating nature of seabed terrain causes pipe bend (pipe-dip) sections in long subsea pipelines route through seabed to production platform, as shown in Figure 1.1. The figure shows a schematic of a pipeline installed on seabed for extraction of oil and gas, with various pipe bend (dip) sections formed as result of the seabed undulation and the pipe riser base in contact with the seabed. Consequently, a typical long subsea pipeline system would generally comprise of series of horizontal and pipe bend sections.

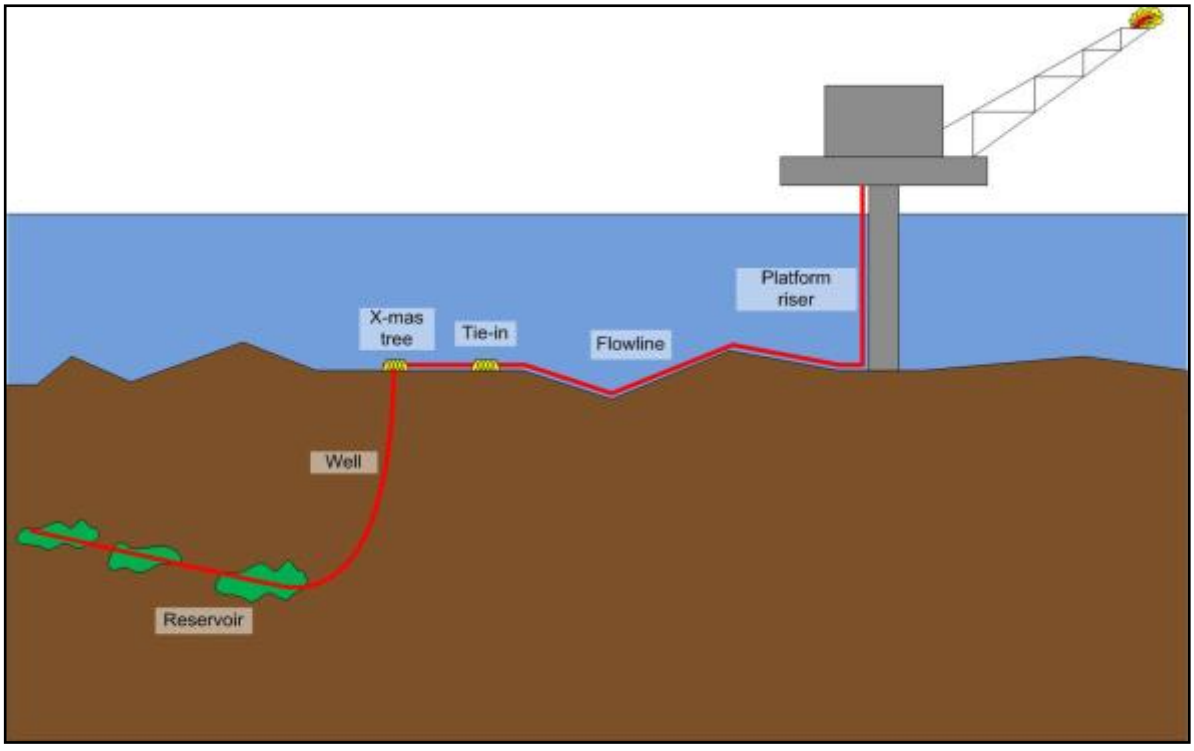

Figure 1.1: Schematic of offshore production systems and seabed topology

The pipe bend section is formed of downward, dip and upward inclined sections as shown in Figure 1.1. The dip points are generally known as low-points of pipelines where stationary solids bed may accumulate and the likely spot where pipe leaks may occur (Soepyan et al. 2014; Danielson 2007; De Henau and Raithby 1995). Stationary sand deposit in pipe and pipe bend sections may result in additional pressure loss in pipelines, which may eventually impede production and consequently result in economic risks (Al-lababidi, Yan and Yeung 2012). Therefore, it is vital to ensure multiphase pipelines are designed and operated such that transport of sand particles can be managed to avoid stationary sand deposit and abrasion of pipes in order to ensure oil and gas flow assurance.

Flow assurance refers to ensuring unhindered simultaneous flow of oil and gas mixture in pipelines economically over the lifetime of a field (Jordan et al. 2001). The need for economic production of oil and gas has motivated several production companies to integrate approaches to address issues of produced sand into their portfolios for field development planning (Wilson 2013). According to Rawlins (2013), the methods used by petroleum operators for addressing produced sand issues are sand control and sand management methods. The sand control involves exclusion of sand from reservoir fluids by the use of completion components such as gravel pack and screens to prevent sand influx. However, the presence of the sand screens may result to build-up of sand in the wellbore, which may reduce the inflow from the reservoir (Wilson 2013). In addition, the cost of intervention for repair of failed sand screens is high (Whitfield 2016), which is a major drawback of the sand control method.

The sand management method involves producing sand particles with the hydrocarbon fluids and transporting the mixture in pipelines to the platforms where the sand phase can be separated. The underlying concept in sand management method is to design and operate flow-lines to tolerate certain amount of produced sand and as well avoid the problems of sand (Al-lababidi, Yan and Yeung 2012). This method has enabled increased hydrocarbon production from sand producing wells, extension of oil-well life and restart of shut-in wells due to sand blockage in several producing regions globally (Rawlins 2013).

The benefit of allowing produced sand to a certain amount based on the concept of sand management is exploited in Western Canada, where petroleum production operators have observed that by encouraging produced sand with the hydrocarbon can lead to improved and economical production of heavy-oil from tight reservoirs (Tremblay 2005). The study by Meza-Diaz and Sawatzky (2012) refers to the heavy-oil production strategy as cold heavy-oil production with sand (CHOPS), which involves aggressively producing sand in order to increase the permeability of a reservoir and in turn enhances oil recovery. However, the problem with the CHOPS is that high sand volume may be produced with the hydrocarbon and eventually plug the flow-line due to rapid build-up of sand deposit as shown in Figure 1.2, which shows a partially plugged pipe due to sand deposit, and a broken pipe bend section. Meza-Diaz and Sawatzky (2012) also report issues of plugged pipe which resulted from aggressively produced sand. Therefore, a robust understanding of the hydrodynamics mechanisms which play critical roles in the transport of solids in pipelines is imperative, in order to provide accurate guidance to optimize pipe design for efficient sand management.

Figure 1.2: Images of plugged pipe by sand and damage caused by wear (Andrzej and Susan 2001)

The characteristics of sand transport in pipelines may be described by flow regime, which represents the distribution pattern of the sand-phase in the fluid phase, as shown in Figure 1.3. From hydrodynamics perspective, at a sufficiently high flow velocity, the sand-phase may be fully suspended in the carrier fluid, this phenomenon is known as homogeneous flow regime (Doan et al.1996). However, if the flow velocity reduces to a certain threshold, the sand may segregate towards the pipe-bottom and transported as heterogeneous flow pattern. At a much reduced velocity, the heterogeneous flow may further result in moving sand bed flow regime and eventually formation of a stationary sand deposit in pipes (Oudeman 1992). Therefore, it is essential to investigate the conditions, particularly, the critical transport velocity that leads to the various sand transport flow regimes.

Several studies have been carried out by researchers such as Bello et al. (2011), Salama (2000), Danielson (2007), Oudeman (1992) and Doron and Barnea (1995), in order to determine the critical conditions for various sand flow regimes pipe, particularly the velocity leading to stationary sand deposit in pipes. However, most of the studies focused on flow in horizontal and other forms of inclined pipes with little or no attention given to flow in V-inclined pipe bend similar to the pipe bend section of the undulating pipeline shown in Figure 1.1. The pipe bend angles considered in the few studies by Osho et al. (2012) and Yan et al. (2011) and King et al. (2011) that investigated flow in V-inclined bend pipes, do not represent a typical gradient of offshore seabed undulation dip. The typical gradient of seabed topology is formed of undulations of approximately $1-6^{o}$ upward and downward slope angles (Tippet and Priestmans, 1997). This seemingly small bend angles may have effect on sand transport flow differently from flow in horizontal pipes.

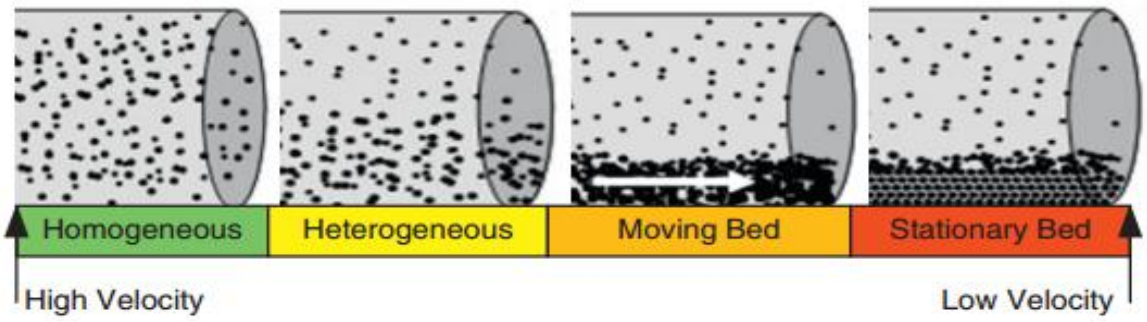

Figure 1.3: Sand transport flow regimes in pipes (Faraj, Wang and Jia 2015).

A matter of practical importance in the oil industry is predicting multiphase flow phenomena in pipeline systems of various inclinations such as the V-inclined pipe bend of the seemingly small bend angles. There exist several predictive correlations for predicting critical sand transport velocity in pipes. However, correlations are mostly valid for the particular type of system producing the data in which the correlation has been developed. In practise, generic application of the existing correlations has often led to erroneous conclusions been drawn for predictions of flow in V-inclined pipe bend (Guzman and Zenit 2011). This drawback necessitates the need for more investigations for sand transport flow in pipe bends of angles that represent a typical gradient of seabed topology in order to improve the accuracy of predictions for sand transport phenomena in subsea multiphase pipelines.

The majority of the existing published studies on sand transport in pipes are experimental studies, including recent studies by Faraj, Wang and Jia (2015), Kesena et al. (2014) and Al-lababidi, Yan and Yeung (2012). However, experimental methods are considered expensive, time consuming and usually require complex construction process, particularly for industrial scale investigations (Matousek 2005). In addition, there is scarcity of experimental methods that provide complete and accurate measurement of the flow mechanisms present in multiphase flow, particularly for flow with solid-phase in which information of the local values of the solid phase distribution and the flow turbulence energy may be necessary (Brennen 2005).

For example, experimental methods for determination of sand transport flow regimes in pipes is usually performed by visual observation of the flow through transparent pipe section (Faraj, Wang and Jia 2015). However, there may be discrepancy in precise determination of the transition velocity between the flow regimes by just visual observation due to the gradual change of the transition conditions between the various flow regimes. Particularly, the transition velocity which leads to formation of a stationary sand bed in pipe bottom may be difficult to determine precisely experimentally (Turian, Hsu and Ma 1987). The stationary bed regime occurs at a very low velocity such that an undetected layer of stationary solid particles bed may be present beneath a moving solid particle bed layer as have been reported by Doron and Barnea (1993) in their study in which they developed a mechanistic three-layer model for solid-liquid flow in horizontal pipe.

The possible discrepancies that may occur in results obtained from experimental methods have also been reported in the experimental study by Kesena et al. (2014) in which it was mentioned that using Pitot-style probes measuring instrument for sand concentration distribution measurement in pipes will give erroneous results, particularly at the bottom of pipe bends. They attributed the erroneous result in the pipe bend to the additional secondary flow induced in the flow-stream by the pipe bend curvature, which caused unstable flow in the pipe and in turn caused the flow to behave differently from that of horizontal pipe flow. This unstable flow observed in the pipe bend in the experimental study also confirms that sand transport phenomena in pipe bend may be significantly different from those in horizontal pipe flow.

The issue of discrepancies in research data may consequently lead to inaccurate predictive correlations and inappropriate design of pipeline systems for transporting sand in hydrocarbons flow-stream. The formation of an obstructive stationary sand bed height may occur earlier than expected in inappropriate designed pipes. In view of optimizing pipeline design, it is also useful to simultaneously obtain detailed information of the interactions between particle-fluid, particle-particle, shear stress, particle-pipe-wall and turbulence intensity in order to know the critical hydrodynamics mechanisms that are mostly responsible

for the various sand-liquid flow regimes in pipes. Experimental evidence of the local parameters may be difficult to obtain. For this reason, it is highly desirable to develop a methodology with considerable accuracy which incorporates comprehensive flow interactions between liquid and sand phase in order to accounts for relevant local information which may be difficult or impossible to obtain experimentally.

The advances and developments of computer technology over the past years have resulted in the provision of a new methodology known as computational fluid dynamics (CFD) for investigating complex flow problems (Pletcher, Tanehill and Anderson 2012). CFD is a numerical method for analysing engineering process systems involving fluid flow, heat transfer and related phenomena such as chemical reactions by means of computer-based simulation (Versteeg and Malalasekera 2007). CFD investigation approach is becoming a vital component in the design of industrial products and processes, such as multiphase pipes for transport of multiphase fluids.

The advantages of CFD method include ability to perform three-dimensional (3D) investigation of flow problems under various conditions rapidly compared to experimental method. The CFD advantages mentioned do not suggest that CFD method will completely replace experimental investigation methods for obtaining information for design purposes, but it is believed that computational methods will be widely preferably used in the future (Pletcher, Tanehill and Anderson 2012). The CFD method is capable of accounting for the actual physics of a flow process and it is possible to obtain detailed local information of the simulated system, in which experimental measurement of the local information may be almost impossible (Kaushal et al. 2012; Ekambara et al. 2009; Syamlal, Roger and O'Brien 1993). However, it should be noted that in order to take advantage of CFD method, the researcher must master certain fundamentals in the disciplines that are unique to computer simulation process and the problem of interest. This requirement suggests that CFD simulation without proper fundamental knowledge can be a very uncertain tool. Therefore, more research aimed at development of CFD methods with the objective of investigating solutions to practical engineering problems is essential.

1.3 Research Aim and Objectives

This section presents the overall aim and objectives of this research

1.3.1 Aim

The overall aim of this PhD project is to develop a unified three-dimensional (3D) CFD model framework to numerically investigate the critical transport conditions for various sand transport flow regimes in pipes and the effect of V-inclined pipe bends on sand transport characteristics in pipes.

1.3.2 Objectives

The following objectives summarize how the aim of this study is achieved:

i. Investigate numerical approaches and multiphase models that take into account the different interaction mechanisms in liquid-solids flow in order to predict the various conditions for sand transport flow regimes in pipe, with special attention to the nature of inter-particle interaction which leads to stationary sand deposit in pipes.

ii. Validate CFD simulation predictions with suitable published experimental data to determine the accuracy of the CFD model framework predictions of the critical flow mechanisms that exist in solids transport in liquid flow in pipes.

iii. Investigate the effect of low angles ($\pm$2-6^{o}) V-inclined pipe bends on sand transport characteristics in pipes, with particular attention to the minimum transport velocity (MTV) by comparing the predicted flow characteristics in pipe bend to that of an equivalent horizontal pipe.

iv. Interpret predicted results to reveal useful critical trends in flow quantities pertinent to solids transport in pipe bends, which may be difficult to measure, in order to provide better understanding of how sand transport characteristics change as pipeline inclination changes.

1.4 Thesis outline

Chapter 1 introduces the background of the problem that the present PhD thesis is concerned and addressed. It includes the motivation which explains the relevance of the present study, and the study aim and objectives.

Chapter 2 presents a critique of the literature of research investigation methods for solids transport in multiphase pipes, sand transport flow regimes recognition, empirical and mechanistic correlations for predicting the minimum sand transport velocity in pipes. The chapter concludes with discussion of the implications of subsea pipeline inclination on prediction of critical sand transport velocity in multiphase pipelines and limitation of the existing correlations, which reveals the gap in knowledge addressed by the present study.

Chapter 3 presents a discussion of the methodology which includes a brief description of computational fluid dynamics (CFD) methods for multiphase flow systems modelling and a detailed description of the governing equations and closure models for modelling liquid-solids multiphase flow in pipes.

Chapter 4 presents the numerical solution procedures of the mathematical equations of the multiphase flow and describes all of the techniques used to obtain the realistic results of the flow quantities. The chapter covers detailed mesh independence study and validation of the numerical frameworks prediction for various sand flow regimes.

Chapter 5 presents the results of the numerical predictions of sand transport characteristics in pipe bends, which are analysed and discussed to reveal the implication of pipe bend on sand transport characteristics.

Chapter 6 presents the conclusions drawn from the findings of the present study and the recommendations for future work.

Chapter 2

Literature review

2.1 Solids transport applications

The transport of solids in pipeline systems is very useful in many industrial applications (Faraj, Wang and Jia 2015). Operators in petroleum industry transport undesired produced sand in multiphase flowlines as a form of flow assurance strategy known as sand management (King, Fairhurst and Hill 2001). Hydraulic transport of solids in pipelines is useful in mining and mineral processing industry to convey coal and other forms of raw solid materials to distant processing facilities. Pneumatic transport of solids is applied in pharmaceutical industry to transport drug particles and powders in tubes (Soepyan et al. 2014; Aziz and Mohammed 2013). The broad applications of solids transport has motivated considerable research in this area over the past years.

2.2 Experimental and Numerical Studies of Solids transport in Pipes

Experimental studies have been recently performed by Rice et al. (2015), Faraj, Wang and Jia (2015), Hashemi et al. (2014), Kesena et al. (2014, Matousek, Krupicka and Penik (2014), Chemioul, Chaib and Mostefa (2009) and Giguere et al. (2008) to investigate solids transport in pipes. Numerical simulation methods have also been used by Messa and Malavasi (2015), Jayaraju et al. (2015) Kaushal and Tomita (2013), Capacelatro and Desjardins (2013), Antaya, Adane and Sanders (2012) and Ekambara et al. (2009) to study solids transport in pipes. Although, majority of these studies are carried out for different purposes, but determination of the concentration distribution of the solids in the pipe is a common interest of the various studies. Therefore, the solids concentration distribution across pipes is an important parameter that needs to be determined in studies for solids transport in pipes, for all solids transport applications.

2.2.1 Solids concentration distribution across pipe

Solids distribution in pipes is usually quantified by means of its volume fraction across a pipe cross-section (Chemioul, Chaib and Mostefa 2009). Accurate measurement or prediction of the solids concentration is important to better understand solids transport characteristics and efficiency in pipes. The experimental study by Kesena et al. (2014) used an intrusive pitot-tube and non-intrusive fixed-sensors to measure sand distribution at different locations in horizontal and elbow pipes in order to better understand erosion mechanism in pipes. They observed significant difference in the sand concentration distribution at various sections of the pipes, particularly in the elbow pipe. The difference in the solids distribution at the various pipe sections indicates that various issues may occur at different sections of a pipe at a certain operating condition, depending on the concentration of the solids at a particular pipe section.

The shapes of profiles of measured solids distributions across the pipe in the experimental studies by Matousek, Krupicka and Penik (2014) and Hashemi et al. (2014) have been used to determine the transport mechanisms of solids and solids concentration fluctuations. The numerical studies by Capecelatro and Desjardin (2013) and Ekambara et al. (2009) also present predictions of solids concentration profiles in horizontal pipes. Although, both the experimental and numerical studies present considerable accurate measurements and predictions of solids distribution in the pipes centre region. However, discrepancy is observed in the measured data and predicted results near the pipe- wall. This discrepancy in results of solids concentration in pipe-wall region indicates that determination of solids concentration distribution across pipes is associated with considerable difficulties, particularly at pipe-wall region.

The challenges in obtaining accurate measurement of solids concentration near pipe-wall is attributed to the access limitation of most measurement instruments and sensors close to pipe-wall (Rice et al. 2015 and Kesena et al. 2014). The experimental studies by Matousek, Krupicka and Penik (2014) and Giguere et al. (2009) reveal that the thickness of a pipe-wall may hamper sufficient penetration of measurement sensor rays. Also, the interference of pipe-wall and measurement

probes is also a limitation in accurate measurements near the pipe-wall. These limitations of measurement instruments in pipe-wall region may reduce accuracy of experimental studies of solids transport. Considerable research is being carried out in recent years to develop robust and viable measurement techniques to improve measurement of solids concentration distribution in near pipe-wall region.

Numerical simulation method for the investigating solids transport in pipes is not without difficulties in predictions of solids concentration across pipes. The major difficulty lies in modelling the pipe near-wall region (Portela et al. 2002), which poses challenges in predicting solids concentration distribution accurately in pipes. A sudden drop in predicted solids concentration which appears as a kink near the pipe bottom wall is observed in certain profiles of solids concentration predicted by Ekambara et al. (2009). Capecelatro and Desjardin (2013) also attributed the disagreement observed between their predicted solids concentration profile and experimental data at the pipe wall region to issues of pipe wall region modelling. It should be noted that the accuracy of numerical simulation predictions depends on several factors, which include but not limited to the assumptions in which the models applied in the numerical simulation are developed.

The turbulent fluctuations in pipes near-wall region is strongly anisotropic (Jayaraju et al. 2015), unlike in pipes centre region where turbulent fluctuations may be characterised as being isotropic (Eskin 2012). However, most of the turbulence models applied in CFD codes are developed on the assumption that turbulence is isotropic in the entire pipe domain. This assumption may have some limitations near the pipe-wall, in which flow quantities may vary significantly. Although, modelling near-wall turbulence still poses challenges, but there are a number of various approaches such as near-wall functions that have been developed to improve predictions of near-wall turbulence in engineering applications. The detailed description of the various approaches for pipe-wall turbulence modelling can be found in Versteeg and Malalasekera (2007), Menter (1994), Speziale, Abid and Anderson (1992), Launder and Spalding (1974) and many others.

In effort to understand the near-wall behaviour of solid particles, Portela, Cota and Oliemans (2002) and Young and Leeming (1997) studied particles deposition in turbulent horizontal pipe flow. They point out that at certain flow conditions, the gradient of concentration of solids which develops across pipes may induce drift velocity in the pipe-wall region, in which high particles concentration is likely. However, the induced drift velocity is usually not accounted for by most models developed on the assumption of local-equilibrium between liquid and solids phase (Bartosik 2010). In addition, most closure models do not distinguish the difference between the liquid and solids phase velocity fluctuations in particle clustered region in liquid-solids flow (Xu and Subramanian 2010). The assumption of equilibrium between velocity fluctuations of liquid and solid particles in pipe-wall region may be inaccurate (Marchioli, Piciotto and Soldati 2006). The difference in fluid and particle phase velocity fluctuations is non-zero in particle clustered region (Capeceletro, Pepiot and Desjardin 2015).

In addition to the non-zero difference in the velocity fluctuations of liquid and solids phase which may occur in pipe wall region, the results in studies by Wilson et al. (2010), Pan and Banerjee (1996) and Gore and Crowe (1989) have also revealed that particle size have various effects on turbulence intensity in regions near pipe-wall. The Pan and Banerjee (1996) study shows that the size of computational mesh adjacent to pipe-wall relative to the dimensionless particle size (d_p^+), if not appropriately specified may introduce some inaccuracy in numerical predictions of liquid-solids flow in horizontal pipe wall region. This requirement suggests that specification of appropriate computational mesh size relative to particle size in pipe near-wall region can play an important role in accurate prediction of solids concentration distribution in solids transport modelling. Therefore, appropriate treatment of computational mesh and accurate representation of the dynamics of liquid-solids flow in pipe wall region presents additional challenges in near modelling of solids transport in pipes.

The need for accurate representation of the dynamics of flow turbulence and particles behaviour in horizontal pipe-wall region cannot be overemphasized in numerical modelling of solids transport in turbulent pipe flow. The sand produced during petroleum production is usually transported in turbulent hydrocarbon fluid stream in multiphase flowlines. Deposition of the sand particles in the turbulent fluids stream in the flowline bottom wall is of great concern in the petroleum industry. According to Oudeman (1992), sand deposition in flowlines is regarded as the main risk in some particular petroleum fields in the North Sea, UK Continental Shelf (UKCS). Matilda, Nishino and Torii (2000) and Young and Leeming (1997) have noted that precise modelling of pipe-wall conditions is important for predicting particle deposition. Therefore, accurate representation of pipe-wall boundary condition is important in order to numerically predict sand deposit in pipe bottom wall and the sand concentration distribution across the pipe. The transport mechanisms of solids in multiphase flow and the flow regimes in horizontal pipes can be inferred from the gradient and steepness of the profiles of solids concentration distribution across horizontal pipes (Matousek and Krupicka 2013; Giguere et al. 2009).

2.3 Solids transport flow regimes in pipes

The sand transport flow regime is a qualitative description of the solids-phase distribution in pipes (El-Sebakhy 2010). Accurate knowledge of sand flow regimes is of paramount importance in sizing and operations of petroleum flowlines (Salama 2000). Over the past years, researchers have attempted to develop various methods for recognition of solids transport flow regimes in pipelines without considerations for the solids concentration distribution across the pipe. In most cases the flow regimes are recognised by either visual observations, which is subjective to the operator's judgement, or by flow regime maps (Faraj, Wang and Jia 2015), as presented in Figure 2.1. The flow regime map in Figure 2.1 presents the various solids transport flow regimes as a function of the liquid phase superficial velocity (U_{LS}) against the solids phase superficial velocity (U_{SS}). The flow regime maps such as the Doron and Barnea (1996) flow regime map and many others are often dimensional and may be misleading when applied to different operational conditions. Therefore, a variety of names and classifications of solids transport flow regimes exist.

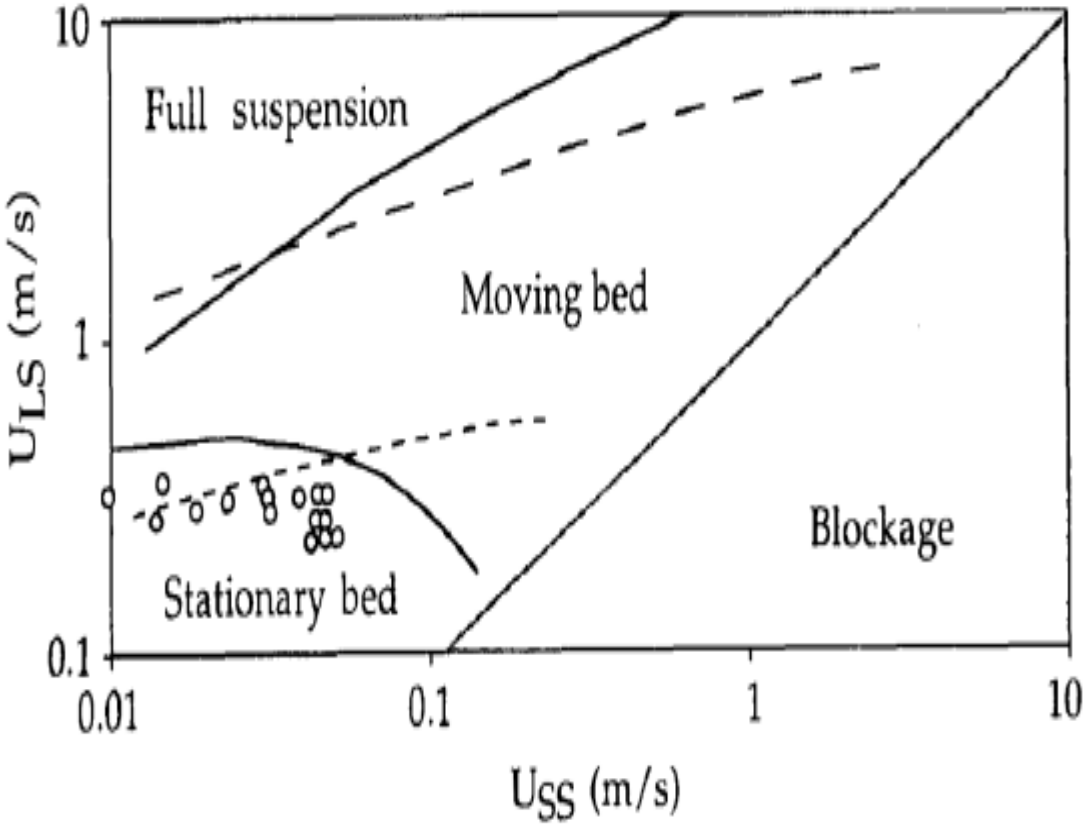

Figure 2.1: Solids transport flow regime map for horizontal pipe flow (Doron and Barnea 1996)

The most common classification of solids transport flow regimes as related to petroleum industry application is reported in study by (Oudeman 1993), in which the sand transport modes are classified as suspension, moving-bed and stationary-bed flow regimes. However, recently, Ibarra, Mohan and Shoham (2014) report in their sand transport study that the sand suspension flow regime can further be divided into pseudo-homogeneous suspension and heterogeneous suspension. However, the difference between these two flow regimes may be difficult to determine just by visually observation without the knowledge of the in-situ sand concentration distribution across the pipe. The heterogeneous flow regime may be referred to as partially-stratified flow regime, which is considered the most encountered flow regime in solids transport in pipes (Matousek and Krupicka 2013).

However, numerical modelling and recognition of the heterogeneous sand transport flow regime in pipes is quite difficult (Matousek, Krupicka and Charra 2014). The flow regime is characterised by somewhat solids-rich zone in the bottom-half region of a pipe cross-section and solids-lean zone in the top-half of a horizontal pipe (Pugh and Wilson 1999). Two different solids transport mechanisms may occur in the different pipe halves simultaneously in the entire pipe when heterogeneous sand flow regime exists in a pipe. The contact-load in the solids-rich zone is carried predominantly by inter-particle contact while turbulence suspension as a result of interactions between solids and the fluid phase turbulent eddies transport the solids in the top-half region, as described in Wilson and Pugh (1988). Heterogeneous suspension leads to the onset of moving solids bed and stationary-bed regimes when the stratified fraction of the solids increases to a certain threshold which persistent inter-particle contact dominates in the pipe bottom wall (Wilson and Sellgren 2008).

The unique characteristics of the transport mechanisms that exist in heterogeneous sand transport flow regime has motivated considerable research work over the past years such as those by Matousek, Krupicka and Charra (2014), Kaushal and Tomita (2013), Gillies, Shook and Xu (2004), Gillies and Shook (2000), Wilson and Sellgren (2008), Wilson and Pugh (1988), to study sand transport mechanisms and develop predictive models for solids concentration distribution and particle support mechanisms that exist in various sand transport flow regimes, in order to be better understand sand transport in pipes. The results in previous study by Shook et al. (1982) revealed that simultaneous measurement of local parameters in solids transport in pipes, such as the pressure gradient across pipe may be used to distinguish the zones supported by the various solids support mechanisms.

An interesting observation in the unique characteristics of heterogeneous flow is reported in studies by Matousek and Krupicka (2013), Matousek (2005) and Pugh and Wilson (1988), in which they reported that there is an interface between the zones supported exclusively by turbulent particles suspension and inter-particle contact in heterogeneous solids transport regime. Pugh and Wilson (1999) noted

that the interface between the two solids transport mechanism may be of several particle diameter in thickness. The two solids support mechanisms may be active simultaneously at the interface zone, as illustrated in the dispersive force analysis in study by Wilson and Pugh (1988). The presence of the combined solids support mechanisms may be responsible for the difficulty in predicting solids concentration distribution, particularly solids concentration distribution in heterogeneous solids transport flow regimes.

The study by MatouseK, Krupicka and Charra (2014) analysed the shapes of measured profiles of solids concentration in pipe and the solids stress distribution in the pipe, in order to develop quantitative methods to determine solids transport flow regime in pipes. Their analysis shows that the different solids transport mechanisms tend to produce different shapes of profiles of solids concentration distribution in pipes for the various solids transport flow regimes, as illustrated by the schematic in Figure 2.2. The previous studies by Savage (1984), Johnson and Jackson (1987) and Bagnold (1956) also present classic approach in which the stress distribution from collisional granular (solids) materials suspended in Newtonian fluids can be used to distinguish the different flow regimes in the transport of solids in pipes. The stress analysis presented in the various studies revealed that the transition zone supported by both the turbulent suspension and inter-particle contact mechanisms in solids transport in pipes can be determined by the fluids and solids phase stresses distribution across the pipes.

The transition zone in which the turbulent suspension and inter-particle-contact may coexist is also regarded to as shear-layer or transport-layer, particularly when there exist a stationary solids bed layer beneath a moving bed layer in pipe (Wilson and Pugh 1988). The pioneer work which studied the mechanisms in which solids is suspended in turbulent flow can be regarded as the works of Schmidt-Rouse (1937), in which the one dimensional Schmidt-Rouse turbulent diffusion model, as given in Equation 2.1 is developed for predicting solids concentration distribution across horizontal pipe. The diffusion model simply states that the downward flux of solids due to gravity is balanced by upward flux due to turbulent diffusion, as defined by Kaushal and Tomita (2013) and Karabela (1977).

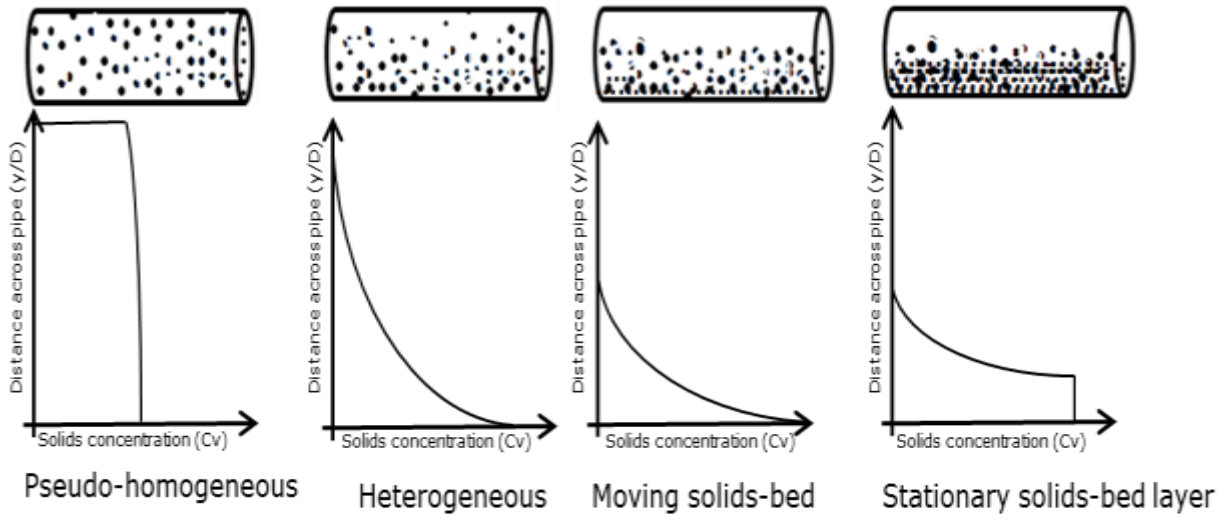

Figure 2.2: Profiles of solids distribution for solids transport flow regimes

$$\varepsilon_s \frac{\partial C}{\partial y} + wC = 0 \qquad (2.1)$$

Where ε_s is the solids diffusivity,w, is the solid particle settling velocity and C is the concentration of solids.

The turbulent diffusion models of the Schmidt-Rouse type have proved to be successful in predicting solids concentration profile of dilute suspension of fine particles (Matousek, Krupicka and Charra 2014), in which hindered settling velocity may be neglected (Gillies and Shook 1994). However, Hunt (1954) pointed out in his analytical study that the Schmidt-Rouse diffusion equation assumes uniform solids diffusivity and concentration across pipe and cannot be applied to predict solids concentration in flow in which solids concentration gradient is appreciable. Hunt (1954) suggested that the equation must be modified to account for the fall velocities of solid particles in the presence of other particles in order to be useful for predicting solids distribution in a wide range of solids transport flow regimes, such as the heterogeneous flow in which strong solids concentration gradient across pipe exist.

The need to provide predictive models such as the Schmidt-Rouse turbulent diffusion model for predicting solids concentration distribution across pipe for the various types of solids transport regimes led to various types of modification of the Schmidt-Rouse turbulent diffusion equation by several researchers. A typical modified diffusion model in which the hindered settling effect is incorporated is given in Equation 2.2, as expressed in study by Karabella (1977).

$$\varepsilon_s \frac{\partial C}{\partial y} + (1 - C) w C = 0 \qquad (2.2)$$

Where $(1 - C)wC$ account for the solid particles settling velocity in the presence of other particles.

Other similar forms of predictive models for predicting solids concentration distribution across pipe in which strong gradient of solids concentration may exist in the pipe are the two-layer models by Kaushal and Tomita (2002), Gillies et al. (1991), Wilson (1976), Doron Granica and Barnea (1987) and many others. However, the profiles of solids concentration distribution across pipe predicted by most two-layer models appear somewhat as superimposed profiles of fully suspended solids, in which the solids transport mechanism is exclusively by flow turbulent eddies and contact-load solids flow, in which the transport mechanism is exclusively by inter-particle collision (Gillies, McKibben and Shook 1996). Therefore, a sharp interface which demarcates the different transport mechanisms zone exists in profiles of solids concentration predicted by two-layer models, as depicted in Figure 2.3. However, Gillies et al. (1994) and Wilson and Pugh (1988) point out that the profiles predicted by most two-layer models do not represent a realistic profile of most solids transport flow regimes in pipes, as the gradients of solids concentration for most solids transport flow regimes do not shift sharply at a particular interface but changes gradually, as shown in the profile for heterogeneous solids transport regime in Figure 2.2. Most two-layer models are developed with the assumption that the turbulent suspension and inter-particle contact-load solids transport mechanisms do not coexist.

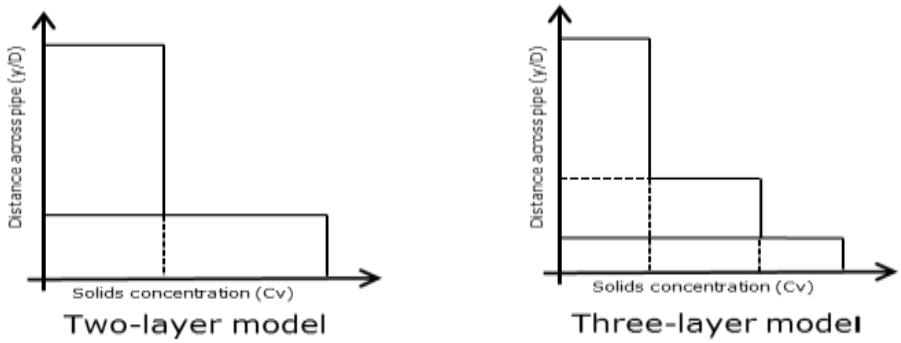

Figure 2.3: Step profile of solids distribution for two-layer and three-layer models

The limitation of the assumption of two-layer model has been revealed in experimental study by Doron and Barnea (1993), in which the two-layer model developed by Doron, Granica and Barnea (1987) failed to predict the presence of a stationary solids-deposit at low flow velocity. They reported that the two-layer model is mostly applicable for specific flow conditions without a stationary solids deposit. This observation prompt Doron and Barnea (1993) to develop a three-layer model using a force balance approach in order to address the shortcoming of the two-layer model, likewise Gillies et al. (1996) modified their two-layer model and developed three-layer model in order to predict stationary sand deposit in pipe flow. More recently, Kaushal and Tomita (2013) modified their two-layer model by taking into account the effects of particle size, solids concentration and pipe diameter in order to improve prediction for solids distribution across pipes.

The extensive research on development of predictive models for predicting solids concentration profile in multiphase pipe flows as observed in the literature shows the considerable importance of solids concentration profiles for flow regimes recognition in solids transport applications. The various solids transport flow regimes in pipes could pose different problems (Salama 2000; Oudeman 1993). Therefore, ability to identify the critical transition condition between the various solids transport flow regimes is useful for pipeline design purposes. Studies have shown that several parameters may be used to identify the transition conditions of the various solids transport flow regimes in horizontal pipelines. However, a straight forward and controllable parameter used to draw the transition condition of the different flow regimes is the flow velocity (Sambath et al. 2014).

2.4 Critical velocity for solids transport in pipelines

The critical velocity required to transport solids has been a famous topic of research over the past years but yet can be confusing (Aziz and Mohammed 2013). Consequently, the literature contain many correlations for predicting critical solids transport velocity. Also, the definition of the critical velocity has been taken as different meaning by various authors and has been a source of confusion in solids transport studies (Najmi, McLaury and Shirazi 2014). Therefore, it may be suggested that the specific sand transport flow regime which represents the sand transport condition at which correlations for predicting critical transport velocity are developed must be defined. However, the specific sand transport flow regime may differ in different solids transport studies depending on the application focus of the study (Hill et al. 2011).

The study by Soepyan et al. (2014) suggested that the critical fluid velocity must exceed the velocity for incipient stationary solids bed formation in pipes in order to successfully transport solids in multiphase pipelines. It can be said that the focus of Soepyan et al. (2014) study is prevention of stationary solids bed formation in pipelines. However, in study by Salama (2000) which focused on petroleum pipeline integrity management, the heterogeneous sand transport flow regime is regarded as scouring flow regime and reported to promote erosion of critical components of petroleum pipelines. Salama (2000) mentioned that the ability to predict the critical velocity for incipient heterogeneous sand flow regime in flowlines is crucial for pipe integrity management. The different focus of solids transport studies indicate that the transition velocity which leads to any of the flow regimes may be considered critical depending on the operation requirements.

One of the earliest empirical correlations for predicting critical velocity for solids transport in pipes was proposed by Durand (1953), as expressed in Equation 2.3. He conducted experimental study of sand and water in horizontal pipe and defined the critical velocity as the 'limit deposition velocity' which corresponds to the velocity below which a stationary sand deposit may form in pipes.

$$V_D = F_L \left[2gD\left(\frac{\rho_s - \rho_l}{\rho_l}\right)\right]^{1/2} \quad (2.3)$$

The term, F_L, in the correlation is the dimensionless Froude number, the value of F_L depends on the range of solid-particle size and the concentration, obtainable from a developed graph, which is limited to certain range of particle size and solids concentration. Therefore, the validity of the Durand (1953) correlation is limited to the range of particle parameters on the graph from which F_L is determined. Wasp, Kenney and Gandhi (1977) extended Durand's work by modifying the approach in which the Froude number is determined in order to develop correlation that accounts for a wider range of particle sizes and solids concentration. They renamed critical velocity as 'minimum transport velocity' (MTV).

Several correlations such as those of Oroskar and Turian (1980), Thomas (1962) and Davies (1987) and many others have been developed after the Durand's correlation in order to provide a more improved correlation for predicting critical solids transport velocity. Theoretical approach was incorporated in the development of most of the correlations such as the Oroskar and Turian (1980) and Davies (1987) semi-mechanistic MTV correlations to provide a correlation applicable for a broad spectrum of particle size, pipe size and fluid properties, which empirical MTV correlations may be inadequate (Gillies et al. 2000). A more detailed review of models for solids critical transport velocity can be found in recent study by Soepyan et al (2014), in which the models are classified and discussed based on the approaches used in development of the models.

The majority of the earlier models mentioned are developed specifically for slurry transport in mining industry where the particle size, solids concentration are considered larger than those of the sand produced during petroleum production (Najmi et al. 2014, Al-lababidi, Yan and Yeung 2012). The mean particle size of produced sand in petroleum fields is in the range of 105 μm-255 μm, as observed from two anonymous petroleum fields mentioned in the study by Stevenson and Thorpe (2002). This range of particle size represents the typical sand particles in petroleum flowlines. However, despite the difference in the properties of produced sand and slurry particles, some of the earlier correlations such as those of Oroskar and Turian (1980) and Thomas (1962) have been very useful for predicting sand critical transport velocity in petroleum application as noted in Yan et al. (2011).

Oroskar and Turian (1980) defined the critical transport velocity as the 'minimum velocity' which marks the transition between suspension of solids and settling of solids deposit at the bottom of pipes. Their MTV model as given in Equation 2.4 is developed based on turbulence energy balance, which corresponds to when the energy required to keep all solid particles in suspension just equals the dissipating energy of fluid turbulent eddies.

$$V_c = 1.85C^{0.1536}(1-C)^{0.3564}\left(\frac{d_p}{D}\right)^{-0.378} \times N_{Re} \times \varkappa^{0.30} \times \left[gd_p\left(\frac{\rho_s}{\rho_f}-1\right)\right]^{0.5} \qquad (2.4)$$

Where, $N_{Re} = D\rho_f \frac{\left[gd_p\left(\frac{\rho_s}{\rho_f}-1\right)\right]^{0.5}}{\mu}$, $\varkappa$, is the fraction of the turbulent eddies having velocity greater than or equal to the settling velocity, taken as $(\varkappa > 0.95)$ in the study. A similar concept is also adopted by Davies (1987), who analysed the balance between solids sediment force and the lift force provided by turbulent fluctuations, and develop a similar correlation as in Equation 2.4. Thomas (1962) defined critical velocity as the 'minimum transport condition', MTC, required to prevent the accumulation of a layer of stationary particles at the bottom of horizontal pipes. The Thomas (1962) approach is used by British Petroleum (BP)-Amoco to deal with solids transport issues, as mentioned in study by King, Fairhurst and Hill (2001).

The advantages of sand management strategy for managing produced sand in petroleum industry, which include economic production of hydrocarbon and reduced workover intervention operations have encouraged petroleum operators to seek improved predictive models for predicting critical sand transport velocity in pipelines (Dabirian et al. 2015). This need has motivated several researchers such as Danielson (2007), Stevenson and Thorpe (2002), Stevenson et al. (2001), Salama (2000), Oudeman (1999), Gillies et al. (1997) and many others to investigate sand transport in pipelines by considering typical fluids and particle properties that represent those of produced sand in petroleum production, in order to developed accurate predictive MTV correlations for predicting critical sand transport velocity specifically to address sand deposition issues in petroleum flowlines.

The correlation developed by Salama (2002) is based on extension of the earlier work done by Oroskar and Turian (1980) and Davies (1987). He reorganised their correlations and developed a correlation for predicting sand settling in liquid and gas-liquid horizontal pipe flows. The final form of the correlation is given in Equation 2.5, in which the ratio of liquid superficial velocity and mixture velocity, $\left(\frac{V_{sl}}{V_{mix}}\right) = 1$ for sand settling in liquid phase only, Δ_ρ is the density difference between the liquid and solid particles, ν, kinematic viscosity, d_p and D is particle and pipe size, respectively.

$$V_m = \left(\frac{V_{sl}}{V_{mix}}\right)^{0.53} {d_p}^{0.17} \nu^{0.19} \left(\frac{\Delta_\rho}{\rho_f}\right)^{0.55} D^{0.47} \tag{2.5}$$

The results presented in the study by Salama (2002) show that the sand settling velocity predicted by the correlation show a good agreement with measured data for horizontal pipe flow. Although, Salama (2002) claims that the correlation can be used for flow in near-horizontal inclined pipes. However, results of validation of the correlation for near-horizontal inclined pipe is not presented in the study. The majority of the sand transport studies intended for petroleum production application have investigated flow of liquid-gas and solids phase, in order to represent the typical multiphase flow often present in petroleum flowlines. It should be noted that the simultaneous flow of liquid and gas in pipes exhibit different liquid-gas flow regimes such as slug and stratified flow regimes due to the discontinuities in the spatial distribution of the fluids in pipelines (Shen and Nakamura 2014). The gas-liquid flow regimes complicate prediction of sand settling in petroleum flowlines.

However, most of the correlations for liquid-gas-solids flow are extension of correlations developed for sand-liquid two-phase flow, as performed by Salama (2002), but the correlations do not account for the effect of gas-liquid flow regime on sand settling. The other types of correlations for liquid-gas-solids are those developed for sand settling in a specific gas-liquid flow regime such as stratified flow. For example, the MTV correlations of Ibarra, Mohan and Shoham (2014) and Stevenson and Thorpe (1999) are developed specifically for sand settling in stratified gas-liquid flow only. Also, the Stevenson et al. (2001) MTV correlation is developed specifically for sand deposition in slug flow. These MTV correlations developed for different gas-liquid flow regime may have inherent limitation when applied for prediction of sand settling in long subsea petroleum flowlines.

The inherent limitations of the MTV correlations developed for predicting sand settling in specific gas-liquid flow regime may be attributed to the fact that the prevailing gas-liquid flow regime in flowlines is not known prior to production. Also, different gas-liquid flow regimes may occur simultaneously in long subsea flowlines, probably in the bend sections of the flowline. Therefore, issues of sand deposition may occur in various regions which different liquid-gas flow regimes occur in a pipeline, which the critical transport velocity for sand has been determined by a correlation developed for a specific gas-liquid flow regime. Recently, Ibarra, Mohan and Shoham (2014) reported that gas-liquid-sand flow characteristic in petroleum pipelines is yet not well understood. The transient nature of gas-liquid flow regimes may be one of the drawbacks of existing MTV correlations for accurately predicting the critical sand transport velocity pipelines.

Studies by Najmi et al. (2014) and Danielson (2007) have confirmed that sand particles reside in the liquid phase in gas-liquid-sand flows, as depicted in Figure 2.4, which shows that the sand particles reside in the liquid body of the slug and suspended by the liquid turbulence eddies in the turbulent diffusion region of the slug. The gas phase has little influence on critical carrying capacity of the liquid except that increased gas rate indirectly increases liquid velocity (Danielson 2007). Also, the results in Najmi et al. (2014) study show that the primary transport of sand is in the liquid phase for gas-liquid-sand flows. This observation suggested to the authors that the actual velocity of the liquid phase may be a way of defining critical sand transport velocity, regardless of the number of fluid phases present in the pipeline. Therefore, in order to improve the accuracy of the predictions of critical sand settling velocity for gas-liquid-sand flow, the interaction between the sand and liquid phase needs to be well understood.

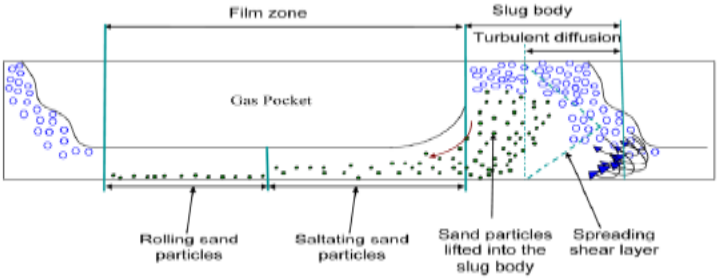

Figure 2.4: Sand transport mode in gas-liquid-sand flow pipes (Al-lababidi, Yan and Yeung 2012)

Improved understanding of the critical interaction mechanisms between liquid-sands phase in pipes may provide the platform for development of more accurate MTV correlations for sand transport in pipes. Therefore, more research work is still needed for sand transport in liquid-phase only with the particle properties that represent the typical produced sand in petroleum production. Correlations developed based on accurate knowledge of the local concentration distribution of the sand phase in the liquid and the dynamics of turbulence may significantly improve accuracy of predictions of sand settling in liquid, which in turn may effectively address issues of sand settling in multiphase flowlines. The fact that the sand phase reside in the liquid-phase as observed by Najmi et al (2014) suggests that when liquid carrying capacity is sufficient, sand settling is unlikely, regardless of the gas-liquid flow regime. This may be a reason some earlier semi-mechanistic MTV correlations such as the Oroskar and Turian (1980) and Thomas (1962) correlations developed for slurry transport are still very useful in petroleum industry over most correlations developed for gas-liquid-sand flow.

2.5 Subsea pipelines inclination effect on solids transport

The subsea pipelines (flowlines) unavoidably follow the seabed hilly terrain, which comprises of horizontal, slightly downhill and uphill landscape (Zheng, Brill and Shoham 1993). Therefore, majority of pipelines installed on the seabed are always undulated at various shallow angles caused by seabed topology (King, Fairhurst and Hill 2001). Consequently, in addition to the spatial distribution of gas-liquid flow regime issues which complicate predictions of sand settling in petroleum flowlines, the abrupt change in subsea pipeline inclination due to shallow pipe-dip adds to the complex nature of multiphase phase flow dynamics in the pipeline and in turn add to the difficulty in predicting sand settling in subsea pipelines. Understanding the flow mechanisms of multiphase mixture through pipe bends (dip) may play a crucial role in the economic transport of hydrocarbon fluids in pipelines. However, the flow in pipe bends of subsea undulating pipelines are seldom reported in literature compared to flow in horizontal and other forms of inclined pipes, due to the complexity of flow in pipe bends (Huang et al. 2013).

The studies by Huang et al. (2013), Al-Safran et al. (2005), Issa and Kwemf (2003), Taitel, Sarica and Brill (2000) have investigated flow in hilly terrain pipes, in which shallow angle pipe bend (dip) section exists. However, the studies focused on liquid-gas flow without solids phase. The Majority of the studies reported that the flow characteristics of liquid and gas at the dip of V-inclined pipe bend is coupled by those of the downhill and uphill sections of the pipe bend. Issa and Kwemf (2003) investigated liquid-gas flow in horizontal, downward inclined and shallow V-inclined pipes, as depicted in Figure 2.5 and reported that slug initiation mechanism in the V-inclined pipe downhill section is different from that in the uphill section of the pipe. They mentioned that the slugging in the horizontal and -1.5° downward inclined pipes was initiated by hydrodynamics instability, whereas the slug in the V-inclined pipe was initiated by both hydrodynamics instability and terrain induced due to the pipe curvature effect.

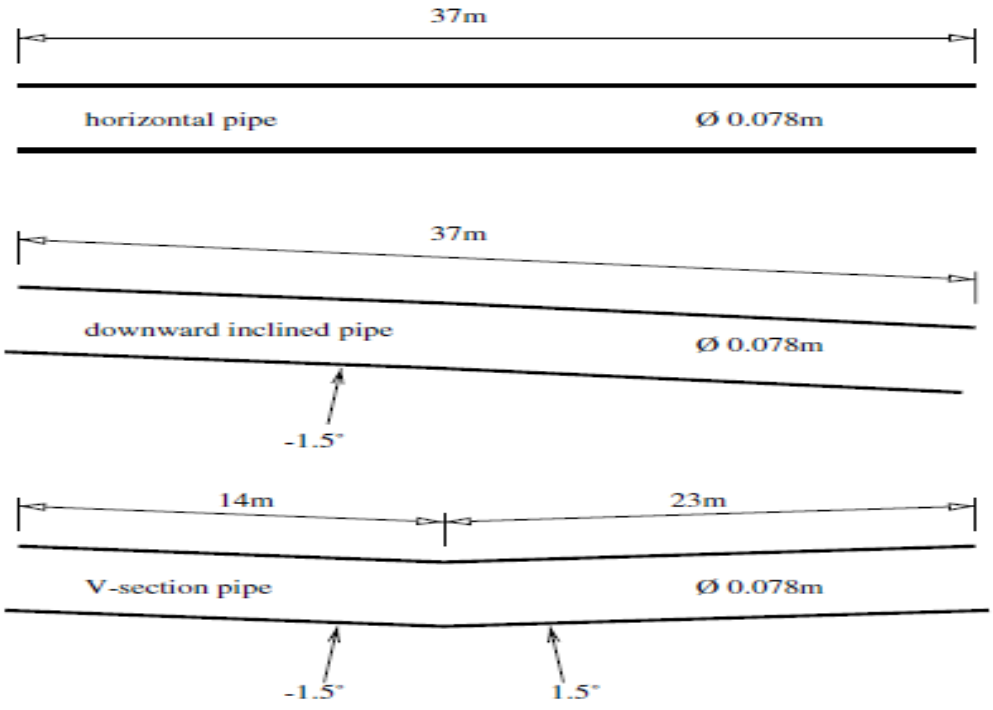

Figure 2.5: Pipe inclinations encountered in petroleum flowlines (Issa and Kwemf 2003)

Although, solids phase is not included in the gas-liquid flow investigated by Issa and Kwemf (2003), but the slug initiation mechanism in the $\pm 1.5^{o}$ V-inclined pipe suggests that the pipe curvature of the seemingly shallow angle pipe bend influenced the multiphase flow characteristics in modes which are not observed in the horizontal and -1.5^{o} downward inclined pipes. The pipe curvature effect on slug initiation mechanisms in the V-inclined pipe may also play a crucial role in sand transport characteristics in V-inclined pipe bends. However, the majority of the earlier MTV correlations for predicting solids transport velocity in pipes are developed from studies which focused on slurry transport in horizontal pipelines. Such MTV correlations are also applied in the petroleum industry for predicting critical sand transport velocity in pipelines on the assumption that offshore flowlines are absolutely horizontal (Albabidi, Yan and Yeung 2012; Stevenson and Thorpe 2002), without adequate consideration for the effect of pipe bend sections on hydrocarbon transport in pipelines. This assumption may be one of the reasons sand deposition still remains a reoccurring issue in the petroleum industry.

The literature is limited in studies on sand transport in shallow angle multiphase inclined pipes that represent the typical inclined pipe sections of subsea petroleum flowlines. Critical review of the available literature shows that majority of the studies which studied sand transport in low angle inclined pipes focused on a standalone section of the low angle downward inclined pipe or upward inclined pipes separately, and reported contrast findings of effects of the low angle inclined pipes on sand transport characteristics. The previous study by Al-lababidi, Yan and Yeung (2012) reported that the characteristics of sand-liquid transport in horizontal and $+5^{o}$ upward inclined pipe are similar. However, the more recent study by Goharzadeh, Rodger and Wang (2013) found that the transport characteristics of moving sand bed and sand dunes in +1 upward inclined pipe is different and more complex compared to that in horizontal pipe.

The study by Danileson (2007) investigated sand transport in liquid and liquid-gas flow in -1.35 and +4 upward inclined pipes concluded that the pipe inclinations do not have effect on sand transport in liquid, except for gas-liquid flows. Conversely, the experimental study by Nossair, Rodger and Goharzadeh (2012) of sand-liquid

transport in +3.6° upwind inclined pipe showed that higher flow rate is required to move stationary sand deposit in the seemingly small angle upward inclined pipe compared to a horizontal pipe. Stevenson and Thorpe (1999) also reported that downward inclined flowlines are more susceptible to sand deposition than upward inclined flowlines. This disparity in the findings reported by various author in the literature shows that sand transport characteristics in low angle inclined pipe is yet not well understood.

In addition to the disparity in reports by previous researchers on effect of low angle inclined pipes on sand transport characteristics in pipes, the investigation approach in which sand transport is investigated by flow in standalone downward and upward inclined pipe sections may not reveal the actual complexity of sand transport characteristics in V-inclined undulated pipe. This may be a reason for the assumption by previous researchers that shallow angle inclined petroleum flowline bends (pipe dips) do not have effect on sand transport characteristic and critical sand transport velocity in pipes. Consequently, there is paucity of published research studies on sand transport in shallow angle V-inclined pipe bends. The only available published studies on sand transport in multiphase bend pipes that represent the seemingly small gradient V-inclined pipe bend are the experimental studies by Kings, Fairhurst and Hill. (2001) and Tippet and Priestman (1997).

Although, Yan et al. (2011) also studied sand transport in pipe bend, but the curvature angle of $\pm 24^{o}$ of the V-inclined pipe investigated seems inordinate pipe curvature for a typical seabed undulation. Tippet and Priestman (1997) have previously pointed out that the typical gradient of seabed undulation is approximately $\pm 1\text{-}6^{o}$ and the results from their study show that pipe bends of such seemingly small gradient have significant effects on sand mobility in pipes. The more recent study on sand transport in pipe bend by Kesena et al. (2014) focused on sand transport in pipe-elbow, which gives a good representative of bend pipes at the riser junction between subsea flowlines and riser systems, but not for flowline dips. The seemingly small pipe dips may also cause problem during pigging operations, as the liquid and sand particles may accumulate at the dips of the flowline, which may lead to pigging spheres being trapped in pipelines (Jawaderna, Dykhno and Hudson 2002).

The effect of the seemingly small gradient $\pm$1-6° V-inclined pipe bend that represent subsea flowliine-dips on sand mobility as reported in the few available studies implies that flowline-dips may have effect on critical or minimum sand transport velocity differently from those of other inclined pipes. However, to the best of the knowledge of the present study, there is no existing published MTV correlation for predicting sand settling in V-inclined multiphase pipes. Therefore, more work is required on sand transport in multiphase flowlines which take into account the local sand concentration distribution and other hydrodynamics parameters of liquid-sand flow in V-inclined pipes in order to improve the understanding of sand transport in subsea multiphase flowlines and to develop correlation for predicting sand settling in multiphase flowline-dips.

Therefore, the purpose of this study is to develop a three-dimensional (3D) unified CFD model framework that accounts for the interactions between liquid-particle, particle-particle and pipe wall and numerically simulate sand transport characteristics and sand deposition in V-inclined bend pipe using particle parameters that represent the produced sand in petroleum production. The numerical investigation will provide improved understanding of sand transport characteristics in petroleum flowline-dips and predictions of the minimum transport velocity for sand suspension and stationary sand deposit regimes in pipe dips based on accurate knowledge of the local sand concentration distribution in the pipe. Correlations developed based on accurate knowledge of local sand concentration distribution in liquid is essential in order to improve the predictions of sand settling in gas-liquid-sand three-phase flow in multiphase bend pipes. The CFD approach if appropriately tuned offers the advantage of providing more detailed and accurate information of the local flow parameters rapidly which may be difficult to obtain experimentally.

Chapter 3

Computational Fluid Dynamics Methodology

3.1 Computational Fluid Dynamics (CFD) and Governing Equations

Computational fluid dynamics (CFD) is the analysis of engineering systems involving fluid flow, heat transfer and related phenomena, by means of computer based simulation (Versteeg and Malalasekera 2007). The process of obtaining numerical solutions in CFD generally comprises of two stages. The first stage involves formulation of the partial differential equations (PDE) that govern the flow based on the conservation laws. The second stage involves generating the geometry and mesh structure of the computational domain, including specification of the boundary conditions for the computational domain and then application of appropriate numerical method to obtain solutions of the conservation equations (Xu and Subramaniam 2010; Oliveira and Issa 2003).

The flow to be simulated may exist as single or multiphase flow depending on the number of phases present in the flow system. The word 'phase' in multiphase flow refers to the three physical state that a matter can exist and the prefix 'multi' means multiple, which implies two or more. Therefore, a flow that consists of a liquid-solid, gas-liquid, gas-solid or liquid-gas-solid phase mixture may be referred to as multiphase flow. The flow may be turbulent or laminar, depending on the degree of randomness of the flow properties. Most flows encountered in nature and engineering applications are turbulent, which is characterised by highly random and chaotic motion. However, laminar flows may also occur in certain conditions. The numerical solution of laminar flows is relatively easy to obtain, and the accuracy of the solutions are reliable (Anderson et al. 2012). However, the simulation of turbulent flow is very complex and accurate solution of the conservation equations still poses major difficulty to obtain. The major difficulty may be attributed to the intensity of the velocity fluctuations associated with turbulent flow, which manifest as highly random and chaotic motion of the flow.

The random and chaotic nature of turbulent flow may be resolved by various methods in CFD. The instantaneous equations that govern the flow can be solved directly by resolving the entire scales of the velocity fluctuations by a method known as direct numerical simulation (DNS) (Elghobashi 1991). However, this method is computationally expensive, in terms of simulation time, which may be responsible for the limitations in the usefulness of DNS approach for computation of practical engineering flow problems. The advancement of computers speed and numerical algorithms have made it possible to resolve turbulent flow as distinct large and small scale fluctuations. This method is known as large eddy simulation (LES), which involves direct solution of the large scale turbulent motion and the small scales are modelled accordingly (Crowe, Troutt and Chung 1996).

However, it is often not necessary to predict the detailed flow and instantaneous information of entire turbulence scale in most engineering applications (Drew 1983). The average of the instantaneous equations that describe the flow may be obtained by a suitable averaging procedure to obtain a solution of the flow mean properties. However, the averaging procedure introduces additional unknown variables in the equations, which require turbulence model for a solution to be feasible. This method is known as Reynolds-averaged Navier-Stokes (RANS) approach for modelling turbulent flows. The RANS method is computationally less expensive in terms of computer memory and time required to obtain a converged solution of the flow equations. It is possible to adopt a coarser mesh structure and a larger time step in the numerical simulation (Jakobsen 2014).

3.2 Multiphase flow modelling methods

The challenges with numerical modelling of turbulent multiphase flow is quite enormous than that of single-phase flow. Apart from the issues of resolving the flow turbulence as in single-phase flow, the interfacial interaction between the phases in multiphase flow poses additional difficulties in the mathematical formulation of the flow problem (Ishii and Hibiki 2011). Accurate solution of the full RANS equations and accounting for the interfacial interaction is a major problem in multiphase flow modelling (Tryggvason et al. 2001). No existing available general numerical framework applicable for modelling all types of

multiphase flows encountered in engineering applications (Van-Wachem and Almstedt 2003).

There are several numerical approaches for modelling multiphase flow. The numerical approaches are generally classified into two reference frames, in which numerical frameworks for multiphase flow may be developed. These model frameworks are the Euler-Lagrange model and the Euler-Euler model approach. A more detailed discussion on the various multiphase models approaches and formulation of the numerical frames can be found in Tryggvason et al. (2001), Enwald, Peirano and Almstedt (1997). The following sections present a brief discussion of the multiphase flow models in context of liquid-solids flow.

3.2.1 Euler-Lagrange Model Approach

In the Euler-Lagrange approach for liquid-solids flow modelling, the liquid phase is treated as a continuum by solving the Navier-Stokes equations, while the dispersed solids-phase is modelled by tracking a large number of solid particles as they move through the computational domain (Sommerfeld 2003). The solid particles trajectories are computed for each parcel of particles that follow the same trajectory by solving equation of motion. This approach is mainly applicable when the volume fraction of the solids phase is relatively low. The liquid phase can exchange momentum and energy with the solids phase, as in one-way or two-way coupling. However, the account of the particle-particle interaction as in four-way coupling may not be possible.

The computational time increases and the quality of the simulation reduces, as the number of solid particles increases, since particle trajectories are required to be solved for each particle. Therefore, this approach is limited to flow with low volume fraction of solids-phase, in which the flow is dominated by the liquid phase and the inter-particle interaction can be neglected (Hiltunen et al. 2009). Weber and Hrenya (2006) suggested that the Euler-Lagrange modelling approach is mostly appropriate for multiphase flow systems in which solid particles is less than 100 000.

3.2.2 Euler-Euler Approach

In the Euler-Euler model for liquid-solids flow modelling, the liquid and solid phases are treated as interpenetrating continuum. This multiphase model approach is often referred to as the two-fluid model. The model is derived by volume or ensemble averaging of the instantaneous continuity and momentum equations for each phase. Detailed description of the derivation is presented in Ishii and Hibiki (2011) and Drew (1983). The averaging introduces a volume fraction function which defines the probability of occurrence of a phase in a fixed control volume in space and time, and their sum is equal to one (Enwald, Peirano and Almstedt 1996).

The available multiphase models within the Euler-Euler framework are the volume of fluid (VOF) model, mixture model and Eulerian model. The mixture model is a simplification of the Euler-Euler model which assumes the phases interact strongly and a single momentum equation is used for the phases using mixture properties of the phases. The VOF model involves interface surface tracking technique where the interface between different phases is tracked. VOF model is suitable for separated flow of two immiscible fluids. The Eulerian model is applicable for a wide range of complex multiphase flows. It can be applied for modelling flow with multiple phases.

The closure equations for Eulerian model can be represented by empirical models in a non-granular approach or by models derived based on kinetic theory of dense gases in an approach known as Eulerian-granular modelling approach. The Eulerian-granular approach is computationally efficient for modelling liquid-solids flow where various interactions occur. In sand transport in pipes, various inter-phase forces dominate at different operating conditions. Hence, different forms of interactions between the liquid and sand phase may occur. Consequently, a wide range of sand flow regimes is expected in the pipe. Therefore, all possible interactions between liquid and solids-phase should be accounted for.

An additional advantage of Eulerian-granular modelling approach is that it allows for inclusion of models that are capable of accounting for enduring frictional contact between solids, which is not taken into account in kinetic theory of granular flow (KTGF) based models. The frictional inter-particles contact is likely to dominate in stationary sand bed flow regime, which is a critical flow regime in sand transport in pipes and of interest in the present study. For these reasons, Eulerian-granular multiphase flow modelling methodology is adopted for modelling sand transport in pipes in the present study.

3.3 Transport Equations and Closure models

This section presents the averaged conservation of equations of mass and momentum for isothermal incompressible liquid-solids flow and the closure models formulated in Eulerian-Eulerian granular multiphase model framework applied in the present study. The detailed descriptions of the derivation and the various averaging procedures of the conservation equations can be found in Jakobsen (2014), Ishii and Hibicki (2011), Enwald, Peirano and Almsted (1996), Ma and Ahmadi (1990), Banerjee and Chan (1980) and Drew (1983).

The mass conservation equation is given by:

$$\rho_i \left(\frac{\partial}{\partial t} \alpha_i + \nabla \cdot \alpha_i \vec{v}_i \right) = 0 \tag{3.1}$$

where, α represents volume fraction and i = (liquid or solid)

$$\sum_{i}^{n} \alpha_i = 1$$

The momentum equation for the liquid is given by:

$$\frac{\partial}{\partial t}(\alpha_l \rho_l \vec{v}_l) + \nabla \cdot (\alpha_l \rho_l \vec{v}_l \vec{v}_l) = -\alpha_l \nabla_P + \nabla \cdot \bar{\bar{\tau}}_l + \alpha_l \rho_l \vec{g} + \vec{M}_{ls} \tag{3.2}$$

Where $\bar{\bar{\tau}}_l$ is the liquid phase stress-strain tensor given by:

$$\bar{\bar{\tau}}_l = \alpha_l \mu_l \left(\nabla \vec{v}_l + \nabla \vec{v}_l^{\,T} \right) + \alpha_l \left(\lambda_l - \frac{2}{3} \mu_l \right) \nabla \cdot \vec{v}_l \bar{\bar{I}} \tag{3.3}$$

The momentum equation for the solids phase is given by:

$$\frac{\partial}{\partial t}(\alpha_s \rho_s \vec{v}_s) + \nabla \cdot (\alpha_s \rho_s \vec{v}_s \vec{v}_s) = -\alpha_s \nabla P + \nabla \cdot \bar{\bar{\tau}}_s - \nabla P_s + \alpha_s \rho_s \vec{g} + \overrightarrow{M}_{sl} \quad (3.4)$$

Where subscript l and s denote liquid and solids phase respectively, α is the phase volume fraction, P_s is the solid pressure, $\overrightarrow{M}_{ls} = \overrightarrow{M}_{sl}$ is the interfacial momentum exchange between liquid and solids-phase and $\bar{\bar{\tau}}_s$ is the solids-phase stress-strain tensor. The stress terms and the interfacial momentum exchange terms in the transport Equations (3.2) and (3.4) must be interpreted and closed by appropriate closure models before a solution of the equation can be obtained.

3.3.1 Interfacial momentum exchange

The mechanism responsible for solids acceleration due to the liquid-phase velocity fluctuations is that of interfacial momentum transfer, $\overrightarrow{M}_{ls}$ (Burns et al.2004). The term comprises the drag force, lift and virtual mass force, as expressed in Equation (3.5):

$$\overrightarrow{M}_{ls} = \vec{F}_D + \vec{F}_l + \vec{F}_{vm} \quad (3.5)$$

where, $\vec{F}_D$, $\vec{F}_l$, and $\vec{F}_{vm}$ represent drag, lift and virtual mass force respectively.

The lift force $\vec{F}_l$ may act on solids due to velocity gradient of the liquid phase. The virtual mass force $\vec{F}_{vm}$ arises from the acceleration of liquid surrounding accelerating solid particles (Sankaranarayanan et al. 2002). The effect of the lift and virtual mass forces on the solid particles are not considered in the present study. The effect of these forces is insignificant when the particle density is greater than the liquid density ($\frac{\rho_s}{\rho_l} > 1$) (Issa and Oliviera 1993). The predicted results in numerical study by Ekambara et al. (2009) confirmed the insignificant effect of the lift and virtual mass forces for the range of particle sizes considered in the present study. Therefore, the drag force $\vec{F}_D$ is the only inter-phase momentum exchange force considered in the numerical framework of the present study.

3.3.1.1 Drag Force Modelling

There are several drag force models developed to account for the interfacial interaction between phases in multiphase flows. The models include the drag force model by Symlal-O'Brien (1989), Wen and Yu (1966) and Gidaspow (1994) models, to mention a few. The general form of the drag force is given by Equation (3.6), where, K_{sl}, is the liquid-solids momentum exchange coefficient. The approach in the formulation of the momentum exchange coefficient, K_{ls} is the main difference in the various drag force models.

$$\vec{F}_D = K_{ls}(\vec{v}_l - \vec{v}_s) \tag{3.6}$$

Where, $(\vec{v}_l - \vec{v}_s)$ is the relative velocity, which represents the difference between the liquid and the solids-phase velocity. The Gidaspow drag force model incorporates a combination of Ergun (1952) model and Wen and Yun (1996) model in the formulation of the momentum exchange coefficient, K_{ls}, as given by Equation (3.7). The Ergun model is effective when the solids–phase volume fraction, $\alpha_s > 0.2$ and then Wen and Yun model when $\alpha_s < 0.2$. The in-situ sand volume fraction of the various sand transport flow regimes that may exist in pipes varies over a wide range. Therefore, the drag force in the present study is computed from the Gidaspow (1994) model, in order to account for a wide range of sand concentration. The smooth switch provided by the volume fraction function when solids volume fraction (α_s) changes within the defined limit is what makes the Gidaspow (1994) drag force model approach suitable for a wider range of applications.

$$K_{sl} = \begin{cases} 150\frac{\alpha_s(1-\alpha_l)\mu_l}{\alpha_l {d_s}^2} + 1.75\frac{\rho_l \alpha_s |\vec{v_s} - \vec{v_l}|}{d_s} & \text{if } \alpha_s > 0.2 \\ \frac{3}{4}C_D\frac{\alpha_s \alpha_l \rho_l |\vec{v_s} - \vec{v_l}|}{d_s}\alpha_l^{-2.65} & \text{if } \alpha_s < 0.2 \end{cases} \tag{3.7}$$

Where C_D is the drag coefficient given by Equation (3.8).

$$C_D = \begin{cases} \frac{24}{\alpha_l Re_s}[1 + 0.15(\alpha_l Re_s)^{0.687}] & \text{if } \alpha_l \cdot Re < 1000 \\ 0.44 & \text{if } \alpha_l \cdot Re \geq 1000 \end{cases} \tag{3.8}$$

Where Re_s is the Reynolds number of the solids phase given by:

$$\mathrm{Re_s} = \frac{\rho_l d_s |\vec{v_s} - \vec{v_l}|}{\mu_l} \tag{3.9}$$

Where d_s is the diameter of the solid particles.

3.3.1.2 Turbulent Dispersion Force

The concentration of solids in liquid-solids transport in pipes may vary across the cross-section of the pipe under certain conditions. The uneven distribution of solids across pipes will result in a local solids concentration gradient in the pipe. The solid particles in the high concentration region of the pipe may be entrained in the turbulent eddies of the liquid phase as the liquid phase drifts away from the high concentration region to low concentration region (Lee and Weisler 1987). Turbulent dispersion force transfers the suspended-load of solids to the liquid phase when solids is being transported from the regions of high concentration to low concentration (Burns et al. 2004; Wilson and Pugh 1988).

The drag force expressed in Equation (3.6) represents the interfacial momentum transfer between the liquid and solids phase. However, the turbulent dispersion that may arise due to interface interaction is not represented in the expression in Equation (3.6). Burns et al. (2004) have shown that the choice of averaging process has a significant effect on the modelling of turbulent dispersion in turbulent liquid-solids multiphase flow. The results from their study show that it may be necessary to apply a double time-averaging process on the conservation equations in order to account for the drift velocity, which may arise due to liquid and solids phase interaction at certain conditions. The double-averaged conservation equations are essentially unchanged from those given by Equations (3.2) and (3.4) except for the additional term, $\vec{v}_{dr}$, as presented in Equation (3.10) for the drag force , $\vec{F}_D$ which accounts for the turbulent dispersion force.

$$K_{ls}(\vec{v}_l - \vec{v}_s) = K_{ls}\left(\vec{U}_l - \vec{U}_s\right) - K_{ls}\vec{v}_{dr} \tag{3.10}$$

The first term on the right-hand side, $K_{ls}(\vec{U}_l - \vec{U}_s)$, is the mean drag, the $\vec{v}_{dr}$ is the drift velocity which arises from liquid phase turbulent fluctuations in the volume fraction. The product of the $\vec{v}_{dr}$ and K_{ls} as given by the last term of Equation (3.10) represents the turbulent dispersion force, $\vec{F}_{td}$. The turbulent dispersion force serves as a correction to the drag force and provides a complete account of particle dispersion in liquid-solids turbulent flow (Issa and Oliviera 1997). The drift velocity, $\vec{v}_{dr}$ in the present study is modelled by the model proposed by Simonin and Viollet (1990), as given by Equation (3.11).

$$\vec{v}_{dr} = \frac{D_{t,sl}}{\sigma_{sl}}\left(\frac{\nabla\alpha_s}{\alpha_s} - \frac{\nabla\alpha_l}{\alpha_l}\right) \tag{3.11}$$

Where, $D_{t,sl}$, is the binary diffusivity, $\nabla\alpha_s$ and $\nabla\alpha_l$ account for the concentration fluctuations of solids and liquid, σ_{sl} is the dispersion Prandtl number taken as 0.75. Therefore, the turbulent dispersion force, $\vec{F}_{td}$ is expressed as given by Equation (3.12):

$$\vec{F}_{td} = K_{sl}\frac{D_{t,sl}}{\sigma_{sl}}\left(\frac{\nabla\alpha_s}{\alpha_s} - \frac{\nabla\alpha_l}{\alpha_l}\right) \tag{3.12}$$

3.3.2 Solids-Phase Stresses Closure Models

The solids phase momentum equation (3.4) contains the solids stress term, $\bar{\bar{\tau}}_s$. In the present study, the solids stress is modelled based on the kinetic theory of granular flow (KTGF) closure models. The granular model approach involves application of models developed based on concepts from the kinetic theory of dense gases as described in Chapman and Cowling (1970). Detailed descriptions of the KTGF models are given by Savage and Jeffrey (1981) and Jenkins and Savage (1983). The solids phase stress is expressed as given in Equation (3.13).

$$\bar{\bar{\tau}}_s = (-P_s + \lambda_s\nabla\cdot\mu_s)\,I + \mu_s\left\{[\nabla\mu_s + (\nabla\mu_s)^T] - \frac{2}{3}(\nabla\cdot\mu_s)I\right\} \tag{3.13}$$

Where, P_s is the solids-phase pressure, λ_s is the solids-phase bulk viscosity and μ_s is the solids-phase dynamic viscosity. A key parameter in the KTGF closure models for solids phase stress is a parameter known as granular temperature, Θ_s.

3.3.2.1 Granular Temperature

All the closure models for the solids-phase stress based on KTGF approach contain the granular temperature, Θ_s term. The granular temperature provides a measure of the energy associated with solid particles fluctuations. The intensity of the particle velocity fluctuations determines the pressure and viscosity of the solids-phase. Therefore, the granular temperature is a key parameter in modelling liquid-solids flow. The granular temperature is given as the specific kinetic energy of the random fluctuating component of the particle velocity, as expressed in Equation (3.14).

$$\Theta_s = \frac{1}{3} < {\nu_s}^2 > \tag{3.14}$$

Where ν_s is the fluctuation velocity of the solid phase.

The solids-phase stress depends on the magnitude of the granular energy ($\frac{3}{2}\,\Theta_s$). The transport of the granular energy in the solids-phase is given by the relation in Equation (3.15).

$$\frac{3}{2}\left[\frac{\partial}{\partial t}(\varepsilon_s \rho_s \Theta_s) + \nabla \cdot (\varepsilon_s \rho_s \Theta_s)\vec{v}_s\right] = \left(-P_s\bar{\bar{I}} + \bar{\bar{\tau}}_s\right): \nabla \vec{v}_s + \nabla \cdot \left(k_{\Theta_s} \nabla \Theta_s\right) - \gamma_{\Theta_s} \phi_{ls} \tag{3.15}$$

Where the first term on the right hand side represents the creation of fluctuating energy due to shear in the particle phase, the second term represents the diffusion of fluctuating energy along gradient in Θ_s, γ_{Θ_s} is the rate of granular energy dissipation due to inelastic collision and ϕ_{ls} accounts for the transfer of granular energy between the liquid and solids-phase.

The granular temperature may be evaluated by solving the complete transport equation (3.15). Alternatively, instead of solving the detailed transport granular energy equation, an algebraic expression for the granular temperature can be obtained from the transport equation by assuming the granular energy is in a steady state and dissipates locally, where the convection and diffusion contribution

may be neglected, keeping only the generation and dissipation as demonstrated in Van Wachem et al. (2001) and Syamlal, Roger and O'Brien (1993). The resulting algebraic expression for the granular temperature is given by Equation (3.16).

$$0 = \left(-P_s\bar{\bar{I}} + \bar{\bar{\tau}}_s\right): \nabla\vec{v}_s : -\gamma_{\Theta_s}\phi_{ls} \tag{3.16}$$

3.3.2.2 Solids Pressure Closure

The solids pressure P_s corresponds to the solids-phase normal force due to particles motion. Both the kinetic and the collisional contributions are accounted for in the KTGF model. The kinetic contribution is caused by particle velocity fluctuations while the collisional contribution is as a result of particles collisions. The solids pressure in the present study is modelled by the model proposed by Lun et al. (1984), as given in Equation (3.17).

$$P_s = \rho_s\alpha_s\Theta_s + 2\rho_s\alpha_s^2\Theta_s(1+e_{ss})g_{0,ss} \tag{3.17}$$

Where, e_{ss} , is the coefficient of restitution for particles collision, which represents the change of kinetic energy upon particles collision. The restitution coefficient of a perfectly elastic collision is given by, $e_{ss} = 1$, and $e_{ss} = 0$ for a perfectly inelastic collision. The particles collision in this study is assumed to be inelastic, and the $e_{ss} = 0.9$, is specified. $g_{0,ss}$, is the radial distribution function, which accounts for the probability of a particle contacting another particle. The model proposed by Lun et al. (1984) as given by Equation (3.18) is applied for the solids radial distribution function.

$$g_{0,ss} = \left[1 - \left(\frac{\alpha_s}{\alpha_{s,max}}\right)^{\frac{1}{3}}\right]^{-1} \tag{3.18}$$

Where, $\alpha_{s,max}$ is the maximum packing limit for solids, specified as 0.63 for mono-dispersed solids.

3.3.2.3 Solids-Phase Bulk Viscosity

The solids-phase bulk viscosity, λ_s accounts for the resistance of the solids against compression. The solids bulk viscosity is given by Lun et al. (1984) as expressed in Equation (3.19):

$$\lambda_s = \frac{4}{3}\alpha_s \rho_s d_s g_{0,ss}(1+e_{ss})\left(\frac{\Theta_s}{\pi}\right)^{\frac{1}{2}} \tag{3.19}$$

3.3.2.4 Solids-Phase Shear Viscosity

The solids-phase shear viscosity plays a critical role in the mechanisms influencing the various sand transport flow regimes in pipes. For homogeneous and heterogeneous sand transport flow regimes, the solids may undergo an instantaneous motion with wide distance between particles and particles may rebound away from each other rapidly upon collision. The solids viscosity in these regimes depends primarily on the fluctuation and collisional motions of the solid particles. Therefore, the solids viscosity for the homogeneous and heterogeneous regimes is modelled as a sum of the kinetic and collisional particles viscosity, as expressed in Equation (3.20).

$$\mu_s = \mu_{s,kin} + \mu_{s,col} \tag{3.20}$$

Where, $\mu_{s,kin}$ and $\mu_{s,col}$ are the solids-phase kinetic and collisional viscosities respectively. The model by Syamlal et al. (1993) given in Equation (3.21) is applied to account for the kinetic viscosity contribution, whereas the model by Gidaspow et al. (1992) given in Equation (3.22) is applied for the collisional viscosity.

$$\mu_{s,kin} = \frac{\alpha_s \rho_s d_s \sqrt{\Theta_s \pi}}{6(3-e_{ss})}\left[1+\frac{2}{5}(1+e_{ss})(3e_{ss}-1)\alpha_s g_{0,ss}\right] \tag{3.21}$$

$$\mu_{s,col} = \frac{4}{5}\alpha_s \rho_s d_s g_{0,ss}(1+e_{ss})\left(\frac{\Theta_s}{\pi}\right)^{\frac{1}{2}} \tag{3.22}$$

The terms in the models above are as previously defined.

However, at certain sand transport conditions the solid particles may become significantly stratified and flow less rapidly in the liquid phase. The inter-particle interaction at these conditions may be persistent contact or enduring static contact between particles at the pipe bottom. These phenomena are likely in the moving sand-bed and stationary sand-bed flow regimes in pipes. The persistent and static particles contact will result in additional viscosity known as frictional viscosity. The account of the solids frictional interaction is not provided by the KTGF based models. The frictional viscosity stress may be modelled simultaneously with the kinetic and collisional stresses, as expressed in Equation (3.23), to provide a model that can predict the whole range of sand transport flow regimes in a single numerical framework.

$$\mu_s = \mu_{s,kin} + \mu_{s,col} + \mu_{s,fr} \tag{3.23}$$

where, $\mu_{s,fr}$, is the frictional viscosity, which becomes effective in pipe regions where in-situ solids volume fraction approaches the friction packing limit.

The packing limit for mono-dispersed particles which solids friction viscosity becomes effective is approximately 0.5 (Makkawi, Wright and Ocone 2006; Wachem and Almstedt 2003). The solids frictional stress in the present study is modelled by the model proposed by Schaeffer (1987), as given in Equation (3.24).

$$\mu_{s,fr} = \frac{P_{sf} \sin\phi}{2\sqrt{I_{2D}}} \tag{3.24}$$

Where ϕ is internal friction angle specified as 30^0 in this study, I_{2D} is the second invariant of the deviatoric strain rate tensor for solid phase and P_{sf} is the solid frictional pressure which becomes effective when solids fraction approaches 0.5. The friction pressure is calculated by the model proposed by Johnson and Jackson (1987), as given in Equation (3.25).

$$P_{sf} = F_r \frac{(\alpha_s - \alpha_{s,min})^n}{(\alpha_{s,max} - \alpha_s)^p} \tag{3.25}$$

where, coefficients $F_r = 0.1\alpha_s$, n=2 and p=5, $\alpha_{s,min}$ is the solids fraction at which frictional stress becomes effective and $\alpha_{s,max}$ is the maximum packing limit.

3.4 Turbulence modelling

Turbulence is a crucial aspect of liquid-solids transport in pipes. Therefore, it is important to account for the turbulence stress in the multiphase flow investigated in the present study. There are various turbulence models available in CFD codes for closure of the RANS equation. The turbulence models include the mixing length model, Spalart-Allmaras model, the two-equation models ($k-\varepsilon$, $k-\omega$ and $k-kl$), and Reynolds stress model (RSM). These models are classified based on the number of additional transport equations to be solved, where the RSM has the highest number of additional transport equations (Versteeg and Malalasekera 2007).

The majority of the turbulence models are originally developed based on single-phase turbulence flow. However, considerable efforts have been made by previous researchers to extend the models for multiphase flow turbulence modelling. It should be noted that a good turbulence closure model should have extensive applicability and not too complex to apply (Launder and Spalding 1974). The standard $k-\varepsilon$ turbulence model originally developed by Launder and Spalding (1974) has been applied successfully for numerous practical engineering purposes. The turbulence model is reported as the most validated turbulence model and its strengths and weaknesses are well known. Various modifications of the $k-\varepsilon$ turbulence model have been developed to improve its performance and applications to more wide range of turbulent flows, including solids-fluids turbulence modelling (Issa and Oliveira 1997). The present study investigated two different approaches based on the $k-\varepsilon$ turbulence model for modelling the multiphase turbulence of liquid-solids pipe flow.

3.4.1 Two-equation turbulence model for multiphase flows

The first approach in which the turbulence of the liquid-solids flow is investigated is in the context of the $k-\varepsilon$ mixture multiphase turbulence model. The approach uses the mixture properties such as densities and velocities of the liquid and solids phases in the computation of the turbulent viscosity, $\mu_{t,}$ as given by Equation (3.26). The transport equations for the turbulence kinetic energy k and the dissipation rate, ε are given by Equations (3.27) and (3.28), respectively.

$$\mu_{t,m} = \rho_m C_\mu \frac{k^2}{\varepsilon} \tag{3.26}$$

where $\mu_{t,m}$ is the mixture turbulence viscosity.

$$\frac{\partial}{\partial_t}(\rho_m k) + \nabla \cdot (\rho_m \vec{v}_m k) = \nabla \cdot \left(\frac{\mu_{t,m}}{\sigma_k} \nabla k\right) + G_{k,m} - \rho_m \varepsilon \tag{3.27}$$

$$\frac{\partial}{\partial_t}(\rho_m \varepsilon) + \nabla \cdot (\rho_m \vec{v}_m \varepsilon) = \nabla \cdot \left(\frac{\mu_{t,m}}{\sigma_\varepsilon} \nabla \varepsilon\right) + \frac{\varepsilon}{k}\left(C_{1\varepsilon} G_{k,m} - C_{2\varepsilon} \rho_m \varepsilon\right) \tag{3.28}$$

where ρ_m and $\vec{v}_m$ are the mixture density and velocity respectively, computed as given below:

$$\rho_m = \sum_{i=1}^{N} \alpha_i \rho_i \tag{3.29}$$

The production of kinetic energy, $G_{k,m}$, is given by Equation (3.30).

$$G_{k,m} = \mu_{t,m}\left(\nabla \vec{v}_m + (\nabla \vec{v}_m)^T\right) : \nabla \vec{v}_m \tag{3.30}$$

The $C_{1\varepsilon}$, $C_{2\varepsilon}$, C_μ, σ_k and σ_ε are the model constants

The second approach in modelling the liquid-solids flow turbulence incorporates additional terms, Π_{kl} and $\Pi_{\varepsilon l}$, in the transport equations of the liquid phase turbulent kinetic energy k_l and dissipation ε_l, which account for the solids-phase turbulence effect. The turbulence viscosity of the liquid phase, $\mu_{t,l}$ is defined in terms of the liquid phase turbulence kinetic energy, k_l and computed as given in Equation (3.31).

$$\mu_{t,l} = \rho_l C_\mu \frac{k^2}{\varepsilon} \tag{3.31}$$

The characteristic time of the turbulent eddies is defined as given in Equation (3.32)

$$\tau_{t,l} = \frac{3}{2} C_\mu \frac{k_l}{\varepsilon_l} \tag{3.32}$$

The length scale of the turbulent eddies is defined as given in Equation (3.33)

$$L_{t,l} = \sqrt{\frac{3}{2}}\, C_\mu \frac{{k_l}^{3/2}}{\varepsilon_l} \tag{3.33}$$

The transport equation for k_l and ε_l with the additional terms are given in Equations (3.34) and (3.35), respectively.

$$\frac{\partial}{\partial_t}(\alpha_l \rho_l k_l) + \nabla \cdot (\alpha_l \rho_l \overrightarrow{U_l} k_l) = \nabla \cdot \left(\alpha_l \frac{\mu_{t,l}}{\sigma_k} \nabla k_l\right) + \alpha_l G_{k,,l} - \alpha_l \rho_l \varepsilon_l + \alpha_l \rho_l \Pi_{kl} \tag{3.34}$$

$$\frac{\partial}{\partial_t}(\alpha_l \rho_l \varepsilon_l) + \nabla \cdot (\alpha_l \rho_l \overrightarrow{U_l} \varepsilon_l) = \nabla \cdot \left(\alpha_l \frac{\mu_{t,l}}{\sigma_k} \nabla \varepsilon_l\right) + \alpha_l \frac{\varepsilon_l}{k_l}\left(C_1 G_{k,l} - C_{2\varepsilon} \rho_l \varepsilon_l\right) + \alpha_l \rho_l \Pi_{\varepsilon l} \tag{3.35}$$

where, Π_{kl} and $\Pi_{\varepsilon l}$ represent the influence of the solids phase on the liquid phase turbulence and are computed as given by Equations (3.36) and (3.37).

$$\Pi_{kl} = \sum_{P=1}^{M} \frac{K_{sl}}{\alpha_l \rho_l} (k_{sl} - 2k_l + \vec{v}_{sl} \cdot \vec{v}_{dr}) \tag{3.36}$$

$$\Pi_{\varepsilon l} = C_{3\varepsilon} \frac{\alpha_l}{k_l} \Pi_{kl} \tag{3.37}$$

where, k_{sl} is the covariance of velocities of the liquid-phase l and solids-phase s, $\vec{v}_{sl}$ is the relative velocity and $\vec{v}_{dr}$ is the drift velocity.

The turbulence in the solids phase is computed as follows:

The characteristic particle relaxation time connected with the inertial effect acting on the solids phase is defined as given in Equation (3.38).

$$\tau_{F,sl} = \alpha_l \rho_l {k_{sl}}^{-1} \left(\frac{\rho_s}{\rho_l} + C_V \right) \tag{3.38}$$

The Lagragian integral time scale calculated along the particle trajectories, mainly affected by the crossing trajectory effect is defined as given in Equation

$$\tau_{t,sl} = \frac{\tau_{t,l}}{\sqrt{(1 + c_\beta \xi^2)}} \tag{3.39}$$

where

$$\xi = \frac{|\vec{v}_{sl}| \tau_{t,sl}}{L_{t,l}} \tag{3.40}$$

and

$$c_\beta = 1.8 - 1.35 \cos^2 \theta \tag{3.41}$$

where, θ is the angle between the mean particle velocity and the mean relative velocity.

The terms $\tau_{t,sl}$ and $\tau_{F,sl}$, represent the time of interaction between solid-particle motion and the liquid-phase fluctuations, and the entrainment of the solid particles by the continuous phase, respectively. The ratio between the two characteristic

time, η_{sl} as given in Equation (3.42) provides a measure of the efficiency of turbulence to entrain solid particles (Peirano and Leckner 1998).

$$\eta_{sl} = \frac{\tau_{t,sl}}{\tau_{F,sl}} \tag{3.42}$$

The turbulence quantities for the solids-phase are given in Equation (3.43) – (3.47).

$$k_s = k_l \left(\frac{b^2+\eta_{sl}}{1+\eta_{sl}}\right) \tag{3.43}$$

$$k_{sl} = 2k_l \left(\frac{b+\eta_{sl}}{1+\eta_{sl}}\right) \tag{3.44}$$

$$D_{t,sl} = \frac{3}{2} C_\mu \frac{k_l}{\epsilon_l} \tag{3.45}$$

$$D_s = D_{t,sl} + \left(\frac{2}{3}k_s - b\frac{1}{3}k_{sl}\right)\tau_{F,sl} \tag{3.46}$$

$$b = (1 + C_V)\left(\frac{\rho_s}{\rho_l} + C_V\right)^{-1} \tag{3.47}$$

C_V=0.5 is the added mass coefficient.

where $D_{t,sl}$ is the binary diffusivity which appears in the drift velocity, $\vec{v}_{dr}$ as given Equation (3.11).

The drift velocity is computed from Equation (3.11) when the diffusivities in the liquid and solids phase are assumed to be equal. However, when there exists a significant difference in the diffusivities of the liquid and solids phase, the drift velocity is computed as given in Equation (3.48).

$$\vec{v}_{dr} = \left(\frac{D_s}{\sigma_{sl}\alpha_s}\nabla\alpha_s - \frac{D_l}{\sigma_{sl}\alpha_s}\nabla\alpha_l\right) \tag{3.48}$$

where D_s is solids-phase diffusivity as given in Equation (3.46).

Chapter 4

Solution Procedure and Validation

This chapter presents the solution procedure of the Eulerian-granular multiphase model and validation study of the model predictions. The validation involves comparing the predictions of the numerical frames investigated in the present study to published experimental data. An ideal validation test case should have pipe geometry and solids parameters similar to the case of interest of the present study. However, published measured data obtained from inclined pipes similar to the pipe geometry investigated are scarce. Therefore, the data of the experimental study on sand-liquid transport in horizontal pipe by Gillies and Shook (1994) and Roco and Balakrishnam (1985) have been identified as most suitable for validation purpose. In addition, the results of numerical simulations by Capecelatro and Desjardins (2013) have been used to validate predictions in pipe regions where experimental data is insufficient. The critical solids transport velocity correlation of Oroskar and Turian (1987), Equation (2.4) has been used to analytically estimate the critical transport velocity for the simulation conditions.

4.1 Solution procedure

The governing equations and closure models for the multiphase flow have been numerically solved using the finite volume discretization method in a CFD solver, FLUENT 14.0. The transport of sand in pipes is considered turbulent in nature. Therefore, specific types of closure equations and modelling approaches for the liquid and solids phase stresses and the interfacial momentum transfer between the phases have been investigated. The FLUENT code provides three different multiphase turbulence model options in the context of the $k-\varepsilon$ turbulence model. The turbulence models include the mixture, dispersed and per-phase models (FLUENT 14.0 theory documentation). The computation of k and ε is treated differently in the various turbulence models. The numerical frameworks investigated in the present study are in the context of the $k-\varepsilon$ mixture and $k-\varepsilon$ dispersed multiphase turbulence models for the liquid-solids flow turbulence.

4.1.1 CFD Model Frameworks Investigated

The CFD model frameworks investigated are classified based on the treatment of the multiphase turbulence, interfacial force and solids stress closure within each framework. The numerical frames with the flow quantities solved are enumerated below:

1. Frame-I: k_m- ε_m-F_D- τ_s-Θ_c
2. Frame-II: k_m-ε_m-F_D−$K_{ls}.\nu_{dr}$ − τ_s+μ_f-Θ_c
3. Frame-III: k_l- ε_l-Π_{kl}-$\Pi_{\varepsilon l}$-F_D−$K_{ls}.\nu_{dr}$- τ_s+μ_f - Θ_c
4. Frame-IV: k_l- ε_l-Π_{kl}-$\Pi_{\varepsilon l}$- F_D- $K_{ls}.\nu_{dr}$- τ_s+μ_f - Θ_T

Where, k_m is the mixture turbulent kinetic energy, ε_m, dissipation of the mixture turbulent kinetic, k_l is the liquid turbulent kinetic energy, ε_l, dissipation of the liquid turbulent kinetic energy and F_D is the drag force. The terms Π_{kl}, and $\Pi_{\varepsilon l}$, represent the effect of the solids phase on the liquid phase turbulent kinetic energy and dissipation, which provide the account of the covariance of velocities of the liquid and solids phase, k_{ls} and the solids phase turbulence k_s; τ_s, represents the solids stress, Θ_c, algebraic form of granular temperature, $K_{ls}.\nu_{dr}$, turbulent dispersion force, μ_f, solids frictional viscosity and Θ_T, is the transport equation form of the granular temperature.

4.1.1.1 The Frame-I: k_m- ε_m-F_D- τ_s-Θ_c

The Frame-I treats the multiphase turbulence in the context of the $k-\varepsilon$ mixture turbulence model in which the mixture properties and mixture viscosities of the liquid and sand phase are used in the calculation of the turbulent kinetic energy production, k and the dissipation rate, ε. The fundamental assumption in this Frame is that the turbulence in the liquid phase is taken as same for the solids phase. The transport equations for the production of turbulence kinetic energy (k) and the dissipation rate (ε) are calculated by Equations (3.27) and (3.28), respectively. The algebraic form of granular temperature (θ_c), Equation (3.16) is solved for the solids stress KTGF closure models.

4.1.1.2 The Frame-II: k_m-ε_m-$F_D - K_{ls}.\nu_{dr} - \tau_s + \mu_f$-$\Theta_c$

The Frame-II treats the multiphase turbulence as same as that of the Frame-I with the addition of turbulent dispersion force ($K_{ls}.\nu_{dr}$), calculated from Equation (3.12). The turbulent dispersion force accounts for the dispersion of solids due to the effect of liquid drift velocity. The algebraic equation form of granular temperature (Θ_c), as in the Frame-I is solved for the solids stress KTGF closure models.

4.1.1.3 The Frame-III: k_l- ε_l-Π_{kl}-$\Pi_{\varepsilon l}$-$F_D - K_{ls}.\nu_{dr}$- $\tau_s + \mu_f$ - Θ_c

The Frame-III treats the multiphase turbulence in the context of the $k-\varepsilon$ dispersed turbulence model in which the liquid phase turbulent kinetic energy (k_l) and the dissipation rate (ε_l) are calculated from Equations (3.32) and (3.33). The terms, Π_{kl} and $\Pi_{\varepsilon l}$ are solved by Equations (3.34) and (3.35), respectively. It should be noted that the Π_{kl} and $\Pi_{\varepsilon l}$ provide the account of covariance of velocities of the liquid and solids, k_{sl} and the solids phase turbulence, k_s calculated from Equations (3.43) and (3.44), respectively. The turbulent dispersion force ($K_{ls}.\nu_{dr}$) is calculated as in the Frame-II. The algebraic equation form of granular temperature (θ_c) is solved for in the solids-stress KTGF closure models.

4.1.1.4 The Frame-IV: k_l- ε_l-Π_{kl}-$\Pi_{\varepsilon l}$- F_D- $K_{ls}.\nu_{dr}$- $\tau_s + \mu_f$ - Θ_T

The Frame-IV treats the multiphase turbulence in the context of the $k-\varepsilon$ dispersed turbulence model, and the other parameters are calculated as in the Frame-III, except the granular temperature, Θ. The full transport equation form of the granular temperature, Θ, Equation (3.15) is solved for the solids-phase stress KTGF closure models.

The model constants used in the computation of the transport equations for the turbulent kinetic energy, k and dissipation rate, ε in the $k-\varepsilon$ mixture and $k-\varepsilon$ dispersed multiphase turbulence model are presented in Table 4.1. The dispersion Prandtl number is specified as 0.75.

Table 4.1: Constants for $\mathrm{k}-\varepsilon$ multiphase turbulence models

Model Parameters	Values	
	$\mathrm{k}-\varepsilon$ mixture	$\mathrm{k}-\varepsilon$ dispersed
C_μ	0.09	0.09
σ_k	1	1
σ_ε	1.30	1.30
$\mathrm{C}_{1-\varepsilon}$	1.44	1.44
$\mathrm{C}_{2-\varepsilon}$	1.92	1.92
$\mathrm{C}_{3-\varepsilon}$	-	1.30

4.1.2 Boundary Conditions

The specification of boundary conditions of a computational domain is a necessary component of numerical simulation in order to direct the motion of flow and prescribe information of flow variables at the domain boundaries. In the present study, inlet, outlet and wall boundaries are specified for the pipe computational domain. The boundaries are shown in the 3-D sketch of a horizontal pipe in Figure 4.1.

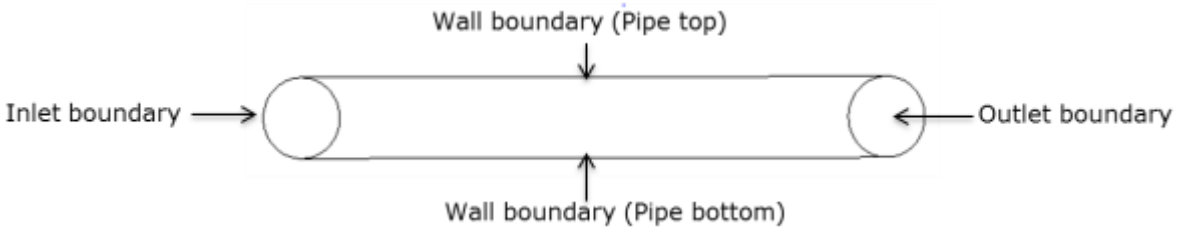

Figure 4.1: Boundaries of the computational domain

4.1.2.1 Inlet and Outlet boundary conditions

The pipe inlet boundary condition is defined as velocity-inlet and the initial velocities of the liquid and sand-phases are specified by assuming a no-slip between the phases at the inlet. The volume fraction of the sand phase is also specified at the inlet. The pipe outlet boundary condition is defined as pressure-outlet and zero value is specified as the pressure at the pipe outlet. The acceleration due to gravity is specified as -9.81 m/s^2 in the vertical (Y) plane of the geometry in order to account for gravitational effect on the flow. The inlet turbulent parameters for the liquid phase turbulent kinetic energy, k and the dissipation rate, ε are defined as given by Equations (4.1) and (4.2), respectively.

$$k_{in} = \frac{3}{2} I^2 {U_{in}}^2 \tag{4.1}$$

Where:

$$I = \frac{0.16}{Re^{1/8}}$$

$$\varepsilon_{in} = \frac{2{k_{in}}^{3/2}}{D} \tag{4.2}$$

4.1.2.2 Wall boundary condition

The flow may be affected by the conditions near the pipe wall. The viscous effect is dominant in the pipe wall region, which may result in larger gradient of flow properties in the region. Therefore, appropriate treatment of the wall boundary condition is necessary to provide a realistic solution of the flow in the pipe-wall region. The two-equation turbulence model is mostly valid in the pipe-core region, in which turbulent effect is dominant. The near wall viscous effect may be resolved by modelling the entire flow boundary layers using appropriate turbulence model. However, this approach requires high number of mesh cells in the vicinity of the pipe wall, and may result in much slower solution convergence and divergence issue due to high aspect ratio mesh cells. Alternatively, the flow at the near wall may be resolved by applying semi-empirical model functions known as wall-functions to bridge the vicinity of the pipe wall dominated by viscous effect. The wall-function approach requires a relatively low number of mesh cells to resolve the flow.

The present study applied the standard wall-function originally proposed by Launder and Spalding (1974) to resolve the flow in the pipe wall region, in order to obtain converged solution of the flow at a relatively faster computational time considering the high number of simulation cases to be performed. The underlying mesh requirement for the standard wall-function is to place the first computational mesh node adjacent to wall outside the viscous sub-layer region. The standard wall function formulation uses a logarithmic relation for the liquid phase in the near-wall region, which requires $30 < y^* < 200$, where y^* represents the dimensionless distance of the adjacent mesh node from the wall. The mean velocity in the near wall region for the law-of-the-wall is defined as given below:

$$U^* = \frac{1}{\kappa}\ln(Ey^*) \tag{4.3}$$

$$U^* \equiv \frac{U_P C_\mu{}^{1/4} k_p{}^{1/2}}{\tau_w/\rho} \tag{4.4}$$

$$y^* = \frac{\rho C_\mu{}^{1/4} k_p{}^{1/2} y_P}{\mu} \tag{4.5}$$

Where subscript P refers to the first node point from the wall, μ, is the dynamic viscosity of the liquid, U_p, is the mean velocity at the near-wall node distance y_p, E is the log-layer constant given as 9.743, κ, is the von-karman constant given as 0.4187 and k_p is the turbulent kinetic energy at the near wall node P. The k_p and ε_p of the liquid-phase at the near-wall node, P are defined and calculated as given by Equations (4.6) and (4.7).

$$k_p = \frac{U^{*2}}{\sqrt{C_\mu}} \tag{4.6}$$

$$\varepsilon_p = \frac{U^{*2}}{\kappa y_P} \tag{4.7}$$

The wall boundary condition for the solids-phase poses additional complications in modelling the near-wall physical behaviour of liquid-solids flow in pipes, due to certain parameters that need to be specified for the solids-phase. The coefficient of specularity, ϕ which represents the momentum and energy exchange between the solid particles and the pipe wall, and the particle-wall restitution coefficient, e_w which represents the dissipation of the solids phase kinetic energy upon collision with the pipe wall are the most important parameters reported in studies by Benyahia et al. (2005) and Johnson, Nott and Jackson (1990), which need to be defined in specifying the wall boundary conditions for the solids-phase.

The present study investigated the effect of defining the solids-phase wall boundary condition in the numerical Frame-IV, in which the transport equation for solids granular temperature is calculated. The solids-phase wall boundary condition for granular temperature at the wall is calculated from model proposed by Johnson and Jackson (1987), as given by Equation (4.8), in which values in the range of 0.008-0.06 and 0.2-06 are investigated for the specularity coefficient and particle-wall restitution coefficient, respectively. It is expected that the ϕ and e_w need to be calibrated for a specific liquid-solids flow (Benyahia et al. 2005), in order to determine the actual values of the parameters, particularly the specularity coefficient which is reported to be more difficult to measure (Johnson and Jackson 1990). The time taken to obtain a converged solution in investigating the actual values for these parameters for solids-phase wall boundary condition for the present study is quite enormous. The actual values of these parameters may vary over a wide range depending on the particle and pipe properties. The need to calibrate these parameters for specific liquid-solids flow is evident in the time taken to investigate the values of the parameters for the particles.

$$q_s = \frac{\pi}{6}\sqrt{3\phi}\frac{\alpha_s}{\alpha_{s,max}}\rho_s g_o \sqrt{\Theta_s}\overrightarrow{U_{s,\parallel}}\cdot\overrightarrow{U_{s,\parallel}} - \frac{\pi}{4}\sqrt{3}\frac{\alpha_s}{\alpha_{s,max}}(1-e_w{}^2)\rho_s g_o \Theta_s^{\frac{3}{2}} \qquad (4.8)$$

Where, ϕ and e_w are the coefficient of specularity and particle-wall restitution coefficient, respectively. The other parameters are as defined in section 3.2.2, except for $U_{s,\parallel}$, which represents the particle slip velocity parallel to the pipe wall.

The summary of the boundary conditions prescribed at the pipe boundaries are presented in Table 4.2.

Table 4.2: Summary of boundary conditions prescribed for each variable at the pipe boundaries

Variables	Inlet	Outlet	Wall
$\overline{U}_l$	Dirichlet	Zero Gradient	Dirichlet
$\overline{U}_s$	Dirichlet	Zero Gradient	Dirichlet
α_s	Dirichlet	Zero Gradient	Zero Gradient
P	Zero Gradient	Dirichlet	Zero Gradient
k	Dirichlet	Zero Gradient	Dirichlet
ε	Dirichlet	Zero Gradient	Dirichlet

4.1.3 Solver control

The numerical simulations performed in the present study have been carried out in time dependent (transient) conditions. The time-step size in time dependent solution scheme is one of the critical controlling factors needed to avoid divergence problem in transient simulations. It is important to adjust and specify a time-step size as small as possible in order to maintain a smoothly converging simulation solution. The time-step size (s) has been adjusted to 0.001 (s) such that it is sufficiently small in order to ensure stability of the numerical solution within optimum simulation time. The under-relaxation factor is also used to control the stability and convergence rate of numerical simulation. Appropriate values of under-relaxation factor in the range of 0.3-0.7 have been specified for pressure, momentum, turbulent kinetic energy and dissipation rate, and turbulent viscosity in the solver. The summary of the simulation solution scheme settings is presented in Table 4.3.

Table 4.3: Summary of simulation solution scheme

Variable	Scheme
Solver	Pressure based
Pressure-velocity coupling	Phase Coupled Simple
Momentum	Second Order Upwind
Volume fraction	First Order Upwind
Turbulence kinetic energy	Second Order Upwind
Turbulence dissipation rate	Second Order Upwind
Residual convergence criteria	1×10^{-6}
Transient formulation	Second Order Implicit

4.2 Test Case of the Solution Procedure and Mesh Independence Study

This section presents the numerical simulation of the solution procedure discussed in the preceding section. The summary of the experimental condition for the test case taken from Gillies and Shook (1994) is presented in Table 4.4.

Table 4.4: Experimental test case (Gillies and Shook 1994)

Pipe Diameter (m)	Velocity (m/s)	Sand-phase fraction	Particle size (um)	Particle density kg/m^3	Liquid density kg/m^3	Liquid viscosity (pa.s)
0.1	3	0.19	90	2650	1000	0.001

4.2.1 Computational Geometry and Mesh Generation

A 3-dimensional horizontal pipe geometry has been created using ANSYS Design-Modeller. The pipe geometry length is 10 m, which provides sufficient length to obtain a fully developed turbulent flow in the pipe. The entrance length for fully developed turbulent flow has been estimated by Equation (4.9).

$$\frac{L_e}{D} = 4.4 R_e^{1/6} \tag{4.9}$$

Where, L_e is the entrance length required for fully developed turbulent flow in a pipe and D represents the pipe diameter.

The pipe geometry has been exported to ICEM CFD 14.0 meshing software, in which a structured hexahedral mesh as shown in Figure 4.2 has been generated using the O-grid type method to enable a smooth refinement of the mesh spacing and clustering in the pipe wall-region. The computational mesh is then imported to FLUENT solver, version 14.0, in which all the simulation calculations have been performed. It should be noted that application of the built in models in FLUENT code requires careful extensive parameter tuning and validations in order to obtain realistic results of sand transport modelling.

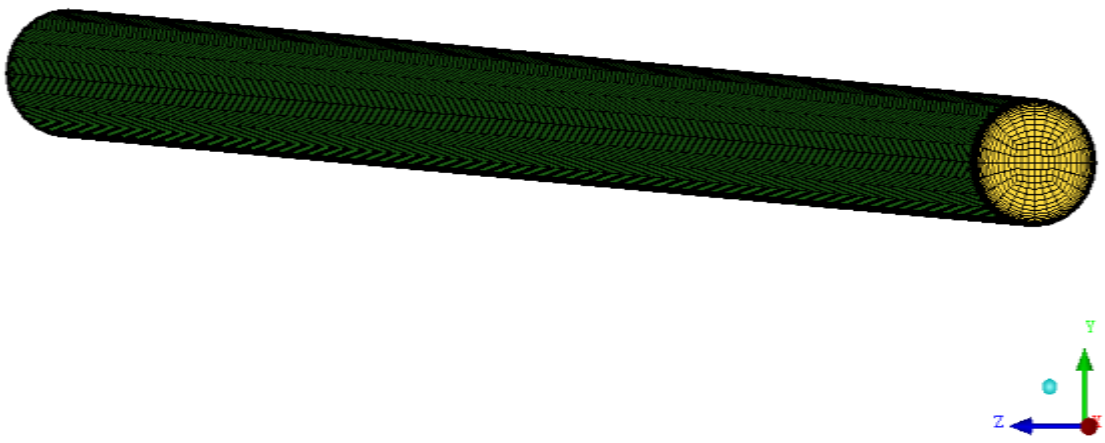

Figure 4.2: 3-D hexahedral mesh pipe geometry

4.2.2 Mesh independence study and refinement

The cross-sectional views of the four hexahedral mesh structures of 183540, 258588, 289538 and 345538 cells investigated in the present mesh independence study are presented in Figure 4.3. It should be noted that particular attention is given to the height of the mesh cell adjacent to the pipe wall relative to the dimensionless sand particle size, $\Delta y/(d_P/D)$, where d_P and D are the particle size and pipe diameter, respectively as presented in Table 4.5. The optimum mesh that produced the most realistic results is determined by comparing the predicted liquid velocity and sand concentration profiles using the different mesh structures in the simulations. In the present study, the predicted profiles of sand concentration provided an indication of the sand transport flow regimes in the pipe. Therefore, particular attention is given to the sand concentration profiles during the duration of the simulations performed in order to determine when a numerical solution is converged.

Table 4.5: Mesh refinement parameters

Mesh cells	**Height (Δy)**	**Height ratio**	d_P/D	$\Delta y/(D_P/D)$
183540	0.0003	1.24	0.0009	0.33
258588	0.0005	1.22	0.0009	0.55
288932	0.0006	1.20	0.0009	0.66
345384	0.0008	1.20	0.0009	0.88

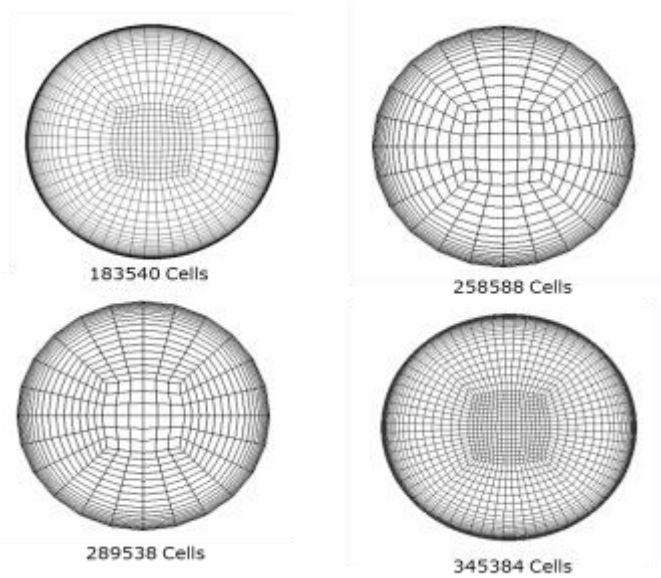

Figure 4.3: Cross-sectional view of the computational mesh structures

4.2.3 Preliminary Simulation

Preliminary simulations have been performed using the mesh of 183540 cells to verify the flow entrance length and the significance of the turbulent dispersion force in the numerical frameworks investigated in the present study by comparing predictions by the Frames I and II. The Frame-I is the only numerical Frame in which the turbulent dispersion force is not considered in the four numerical frames investigated. Figure 4.4 shows how the liquid velocity magnitude developed in the 10 m length horizontal pipe. It can be seen that the predicted velocity magnitude attained a steady state at an entrance length of ≈ 4 m where the velocity magnitude becomes uniform. Therefore, it can be concluded that the 10 m pipe length is sufficient to achieve a fully developed flow in the present study. The results presented here are obtained at 8 m pipe length region to ensure the results are completely independent of the inlet conditions.

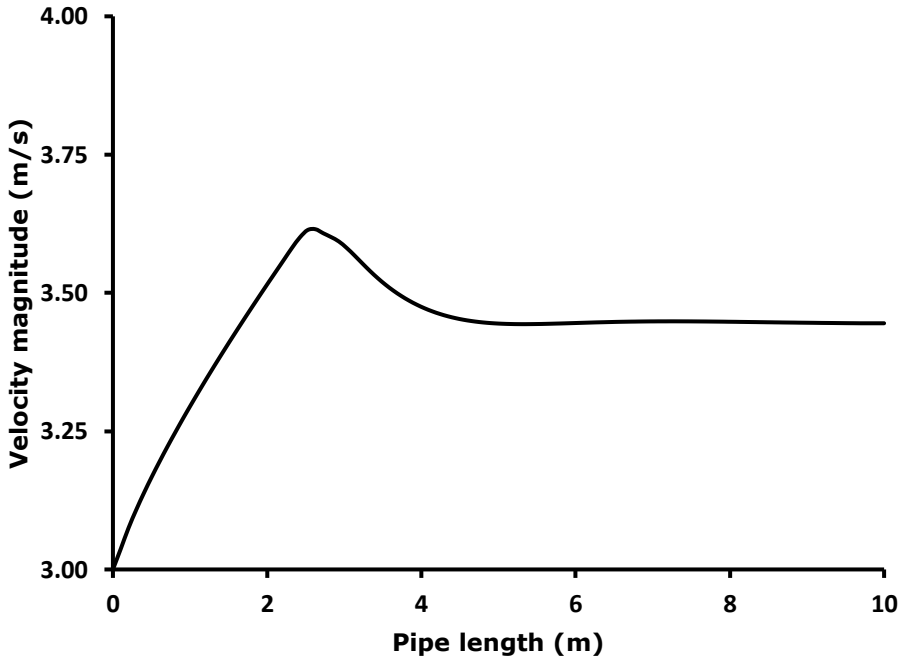

Figure 4.4: Liquid-phase velocity magnitude development in pipe

Figure 4.5 shows a comparison of the profiles of sand concentration in the pipe predicted by the Frames-I and II with experimental data of Gillies and Shook (1994). It can be seen that the profile predicted by Frame-I exhibits significant drop in sand concentration at the pipe-top region and abnormally high sand concentration at the pipe bottom region when compared with the other profiles. However, the profile predicted by Frame-II is in good agreement with the experimental data in the entire pipe region, but shows a kink in the pipe bottom wall. The flow velocity of 3m/s is expected to provide sufficient flow turbulence energy to keep the sand particles nearly uniformly distributed across the pipe, as exhibited by the profiles of Frame-II and the experimental data. The comparison clearly shows that turbulence dispersion force provides a balance in the interaction force between liquid-phase and sand particles when liquid turbulence is primarily responsible for the sand transport. Therefore, it may be concluded that inclusion of the turbulence dispersion force in the numerical framework for the simulations in the present study will produce more accurate predictions. For this reason, the Frame-I is not considered further in the subsequent simulations. The predictions by the Frame-II are further used in the mesh sensitivity study.

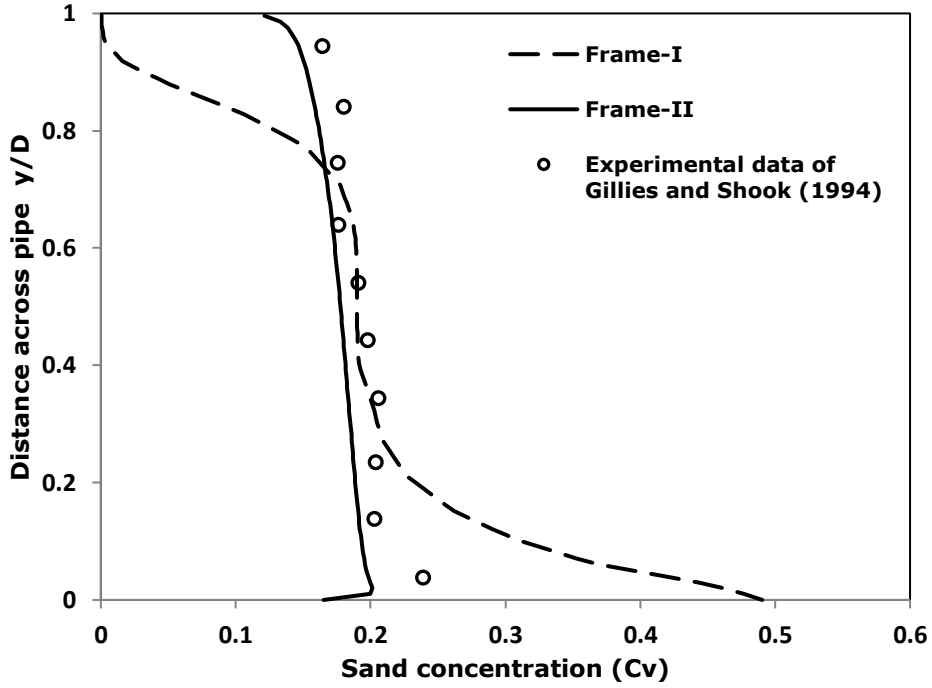

Figure 4.5: Validation of sand concentration profiles predicted by numerical Frames II and III for significance of turbulent dispersion force.

4.2.4 Results and Discussion of Mesh Independence Study

Figure 4.6 shows a comparison of the predicted liquid velocity profiles using the various mesh structures with the experimental data. It can be seen that the predicted profiles using the mesh structures of 258588, 288932 and 345384 cells are in good agreement with the experimental data. However, the profile predicted using the mesh of 183540 cells is not in agreement with the experimental data and those of the other mesh structures, particularly at the pipe top-half region. It should be noted that a typical velocity profile of turbulent flow in pipes is expected to be nearly uniform and full across the pipe. However, the profile predicted using mesh 183540 cells is not as full as those predicted using the other mesh structures. The comparison in Figure 4.6 shows that the predicted result using the mesh structure of 183540 cells is mesh size dependent. This observation of dependence of the predictions using the mesh structure of 183540 on mesh size provides an indication of the possible reason for the kink observed in the predicted sand concentration profile in the pipe wall, as observed in Figure 4.5, in which the mesh of 183540 cells has been used.

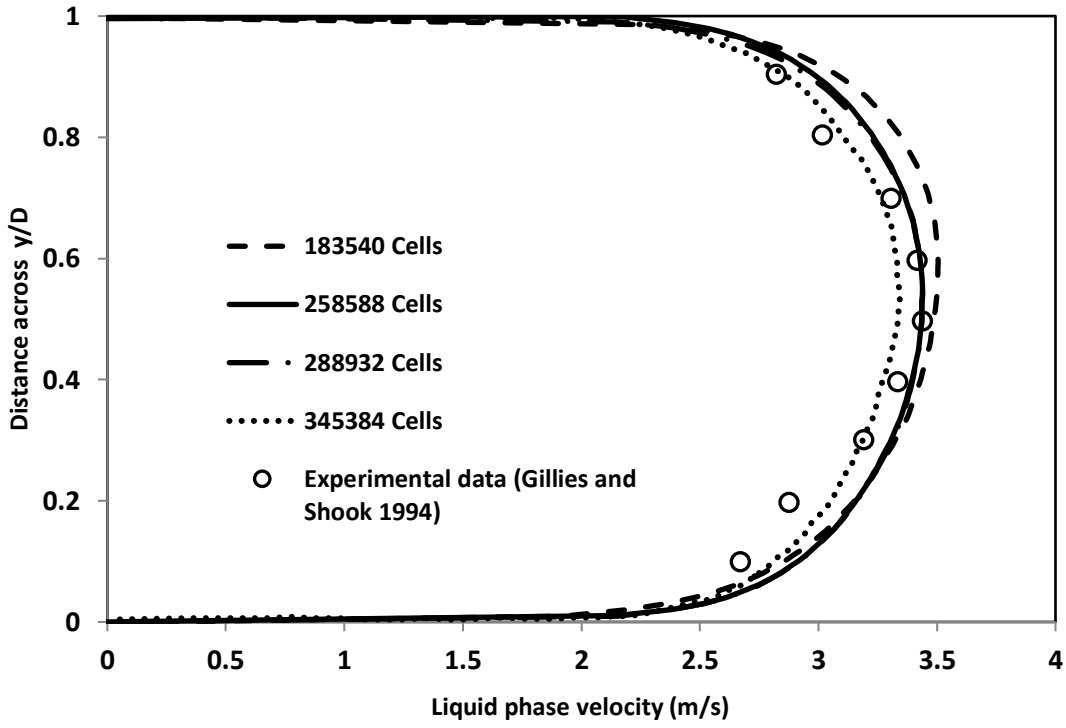

Figure 4.6: Comparison of predicted liquid velocity profiles for mesh independent prediction.

Figure 4.7 presents the sand concentration profiles predicted using the mesh structures of 258588, 288932 and 345384 cells. It can be seen that the profile predicted using the mesh structure of 258588 cells has a kink in the pipe bottom region, similar to that observed for the mesh structure of 183540 cells in Figure 4.5. However, excellent agreement is observed between the profiles predicted using the mesh structures of 288932 and 345384 cells with the experimental data in the entire pipe region. The profiles are smooth at the pipe-bottom where a kink has been observed in the predicted profiles using the mesh structures of 183540 and 258588. It should be noted that the ratio, $\Delta y/(d_P/D)$ plays a significant role in mesh generation for modelling liquid-solids flow in pipes. The values of the ratio, $\Delta y/(d_P/D)$ specified in generating the mesh structures of 288932 and 345384 cells are higher compared to those of the mesh structures of 183540 and 258588 cells, as presented in Table 4.4. This observation indicates that appropriate refinement of pipe wall-adjacent mesh cells improves the quality of numerical predictions for solids concentration profiles in liquid-solids transport modelling, as evident in the results of the present mesh independence study.

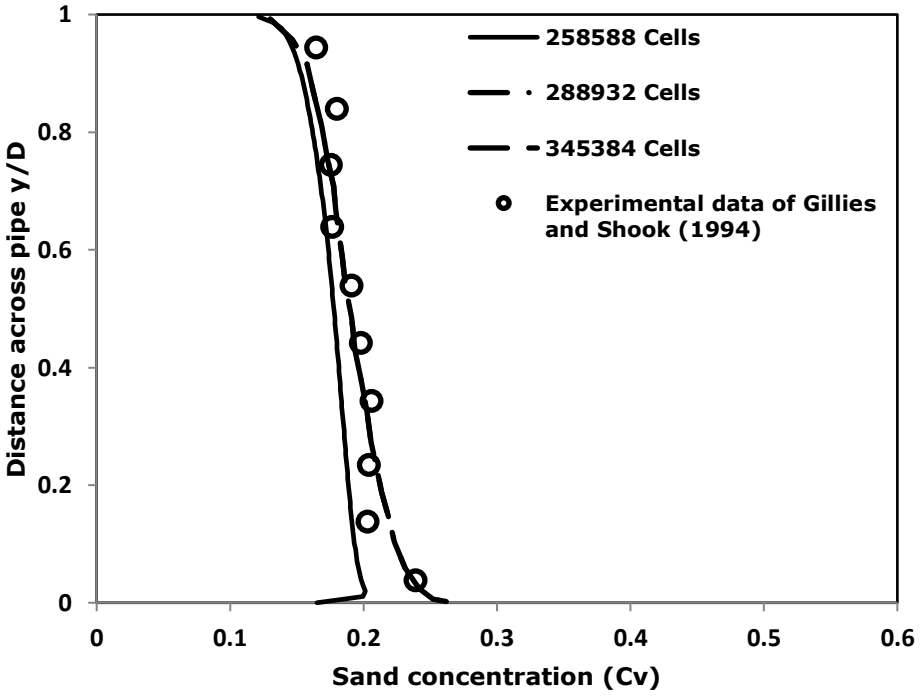

Figure 4.7: Comparison of predicted profiles of sand concentration for mesh independent prediction.

The present mesh independence study has revealed that a particular mesh size may produce mesh independent results in terms of liquid velocity profile, but may be insufficient to obtain the desired smooth profiles of sand concentration, as noticed in the predictions using the mesh structure of 258588 cells. Therefore, it can be concluded that mesh independence study required for modelling liquid-solids flow in pipe is not as straightforward compared to that required for single-phase liquid flow. It may require the refinement of both the mesh size and height of the first cells from pipe wall relative to the solid particle size in order to obtain grid independent results. The result of the mesh independency study indicates that the mesh of 288932 cells is the optimum mesh size and structure required to produce the most desirable results for the liquid-sand transport modelling. Therefore, the subsequent simulations have been performed using the mesh structures of 288932 cells.

4.3 Test cases for validation of the numerical model frames predictions

The case of interest of the present study is the transport of liquid-sand with relatively low sand volume fraction and medium particle size. Therefore, the solids-phase volume fraction, α_s in the numerical model validation is within, $\alpha_s < 10\%$ and the particle size is $< 260\ \mu m$. The summary of the liquid-solids phase parameters for the validation cases taken from published experimental data of Gillies and Shook (1994) and Roco and Balakrishnam (1985), and numerical data of Capecelatro and Desjardin (2003) used in the present numerical simulation is presented in Table (4.6). The expected minimum solids transport velocities (MTV) required to limit formation of sand deposit in the pipe for the different test cases are presented in Table (4.6), estimated from the MTV model of Oroskar and Turian (1980), Equation (2.4). The extent of the sand segregation in the direction of the bottom-wall of the horizontal pipe is inferred from the pattern of the predicted profiles of sand concentration in the pipe, which gives an indication of the different sand transport flow regimes.

Table 4.6: Simulation Conditions for Numerical Model Validation Cases

Parameters	Study type and Author		
	Experimental study		Numerical
	Gillies and Shook (1994)	Roco and Balakrishnam (1985)	Capecelatro and Desjardin(2003)
Pipe diameter (m)	0.159	0.0512	0.0512
Flow velocity (m/s)	3.7, 2.5	1.6	1.6, 0.83
Particle size (μm)	190	165	165
Liquid density ($\mathrm{kgm_3}^{-1}$)	998.9	998.9	998.9
Liquid viscosity (Pa.s)	0.00103	0.00103	0.00103
Sand density ($\mathrm{kgm_3}^{-1}$)	2650	2650	2650
Input sand fraction	0.06	0.08	0.08
Estimated MTV (m/s)	1.8	1.1	1.1

4.4 Results and Discussion of Validation Study

Figures 4.8 and 4.9 present the sand concentration profiles predicted by the numerical Frame-II at 3.7 m/s velocity and the Frames II, III and IV at 2.5 m/s velocity, respectively. The profiles are compared with the corresponding experimental data of Gillies and Shook (1994), as can be seen in the figures. The critical transport velocity at which sand deposit may form in the pipe is estimated as 1.8 m/s. The estimated value of MTV indicates that the 3.7 m/s and 2.5 m/s used in the simulations in which the profiles in Figures 4.8 and 4.9 have been obtained are well above the velocity below which sand deposit is expected to form in the pipe. Therefore, it is expected that the sand transport condition in the pipe should be pseudo-homogeneous sand transport flow regime. It can be seen from the shape of the profiles in the figures that the sand is distributed in the entire pipe cross-section with varying sand concentration. This distribution pattern indicates that the sand is in full suspension in the pipe, with the sand particles segregating towards the pipe bottom, as expected in horizontal pipe flows. The Figure 4.8 clearly shows that the profile predicted by Frame-II is in excellent agreement with the experimental data of Gillies and Shook (1994) in the entire pipe region at the 3.7 m/s flow velocity.

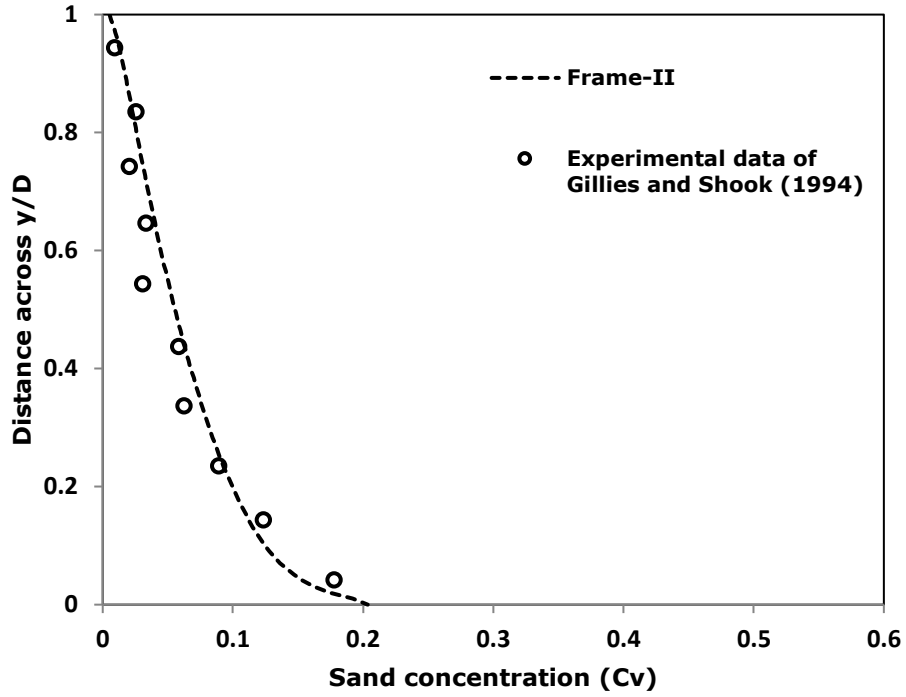

Figure 4.8: Sand concentration profiles predicted at 3.7m/s for 0.159 m pipe size

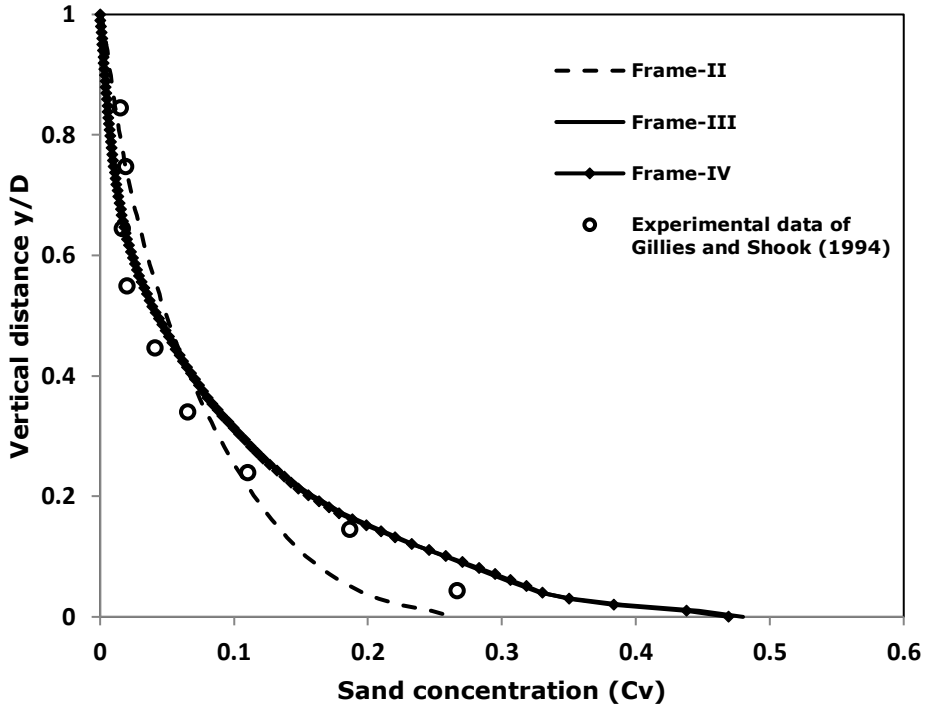

Figure 4.9: Sand concentration profiles predicted at 2.5m/s for 0.159 m pipe size

However, a noticeable disagreement is observed between the profiles predicted by the Frame-II and the experimental data at the reduced 2.5 m/s velocity, particularly at the pipe centre, $0.4 < {}^{y}/_{D} < 0.7$ and bottom, ${}^{y}/_{D} < 0.2$ regions, as can be seen in Figure 4.9. Whereas, the profiles predicted by the Frames III and IV exhibit good agreement with the experimental data of Gillies and Shook (1994) in most of the pipe region, except at the pipe wall region. It can be seen from the predicted profiles and the experimental data that the extent of sand segregation is more significant in Figure 4.9 compared to Figure 4.8. The sand segregation pattern indicates that the flow turbulence energy may be significantly higher at 3.7 m/s velocity than that at 2.5 m/s, which is expected. Consequently, the sand particles in the flow at 3.7m/s velocity are likely in more rapid and translational motion compared to those in the flow at 2.5 m/s velocity.

The inter-particle collision of the flow at 2.5 m/s velocity, which exhibits higher sand segregation is expected to be more frequent than that of the 3.7 m/s, particularly at the pipe lower half region, ${}^{y}/_{D} < 0.4$**.** The frequent collision expected between the solid particles at the 2.5 m/s velocity may have resulted in increased sand concentration at the pipe bottom region, ${}^{y}/_{D} < 0.2$, as can be seen in the experimental data and the profiles predicted by Frames III and IV in Figure 4.9. However, the Frame II failed to predict the increase in sand concentration at the pipe bottom as predicted by the other numerical frames at 2.5 m/s velocity. This observation in the sand concentration at the pipe bottom in Figure 4.9 indicates that the numerical Frame-II may have over-predicted the flow turbulence kinetic energy (TKE) at the pipe bottom region, ${}^{y}/_{D} < 0.4$. This is evident in Figure 4.10, which presents a comparison of the profiles of TKE predicted by the numerical Frames II and III. The Figure 4.10 shows that the magnitude of TKE in the entire pipe predicted by the Frame II is significantly higher compared to that predicted by Frame III, particularly at the pipe lower-half region. It should be noted that the treatment of TKE in the numerical Frame II is different from those of frame III and IV, whereas the TKE is treated in similar approach in Frames III and IV.

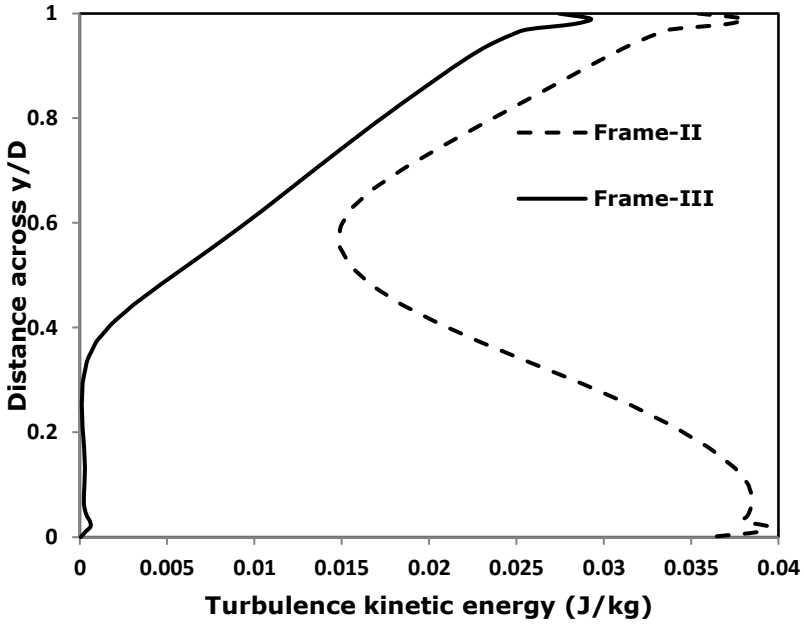

Figure 4.10: Predicted profiles of turbulence kinetic energy (TKE) at 1.6 m/s.

Figure 4.11 presents a comparison between the sand concentration profiles predicted by the numerical Frames II, III and IV, Capecelatro and Desjardin (2013) numerical prediction and experimental data of Roco and Balakrishnam (1985) at velocity of 1.6 m/s. The critical sand transport velocity for the flow condition is estimated as 1.1 m/s. Therefore, the 1.6 m/s velocity is above, but tends close to the estimated critical velocity below which sand deposit will likely form in the pipe. The expected sand transport condition in the pipe at the 1.6 m/s is heterogeneous sand suspension regime, considering the close margin between the 1.6 m/s simulation velocity and the estimated MTV of 1.1 m/s. Significant sand segregation is likely in heterogeneous suspension flow regime, due to the expected frequent inter-particles collision, particularly as the velocity approaches the critical transport velocity. It can be seen in the Figure 4.11 that all the numerically predicted profiles are in good agreement with the experimental data in the pipe top half region, $({}^{y}/_{D} > 0.5)$, except that of Frame II. The profile predicted by Frame-II significantly deviates from the experimental data of Roco and Balakrishnam (1985) in the pipe core region, $(0.4 < {}^{y}/_{D} < 0.8)$, in which the onset of sand segregation is noticeable. Whereas, the profiles predicted by the Frames III and IV maintain good agreement with the experimental data and the profile predicted by Capecelatro and Desjardin (2013) in the pipe-core region.

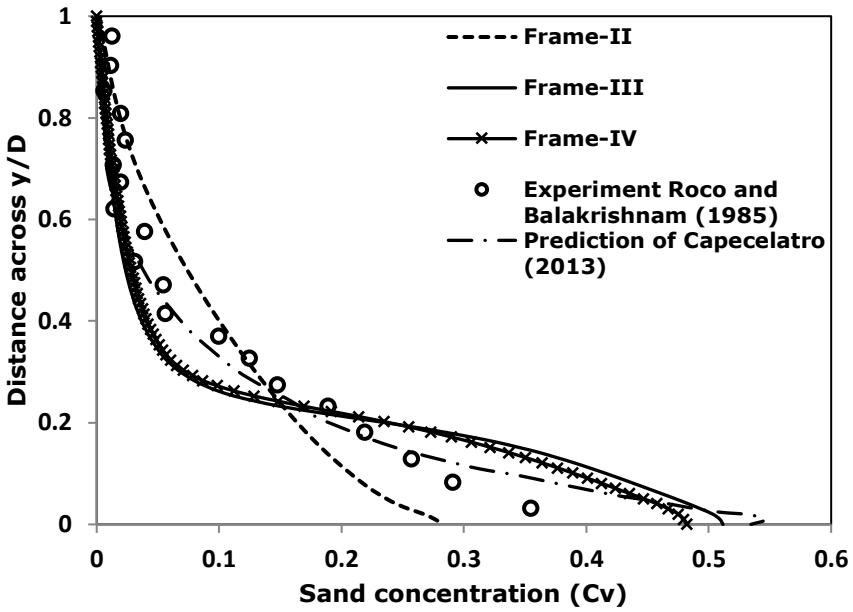

Figure 4.11: Sand concentration profiles predicted at 1.6 m/s for 0.051 m pipe

The Figure 4.11 also shows that the sand concentration profiles in the pipe bottom region, $^{y}/_{D} < 0.2$ predicted by the Frames III and IV are in fairly good agreement with the experimental data of Roco and Balakrishnam (1985) and the profile predicted by Capecelatro and Desjardin (2013). However, significant disagreement is observed between the profile predicted by Frame-II and all other profiles in the pipe bottom region. In addition, it can be observed from the Figure 4.11 that the local sand concentration, ($Cv \cong 0.28$) predicted by the Frame-II at the pipe wall is the lowest when compared to that predicted by the other numerical frames. The significant difference in the concentration at the pipe bottom predicted by the Frame-II and those of the Frames III and IV is evident in the contour plots in Figure 4.12., which clearly shows that the numerical Frame-II under-predicted sand concentration at the pipe-bottom.

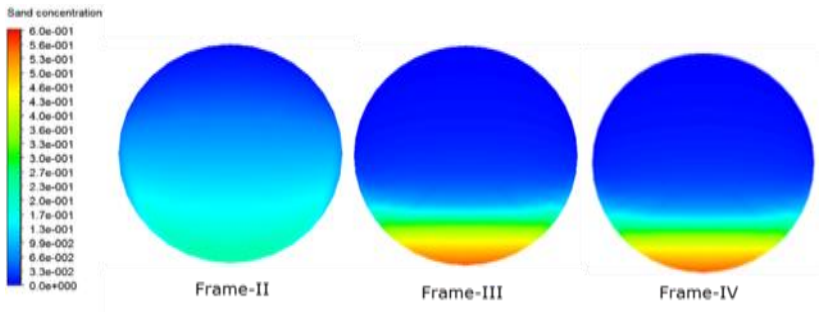

Figure 4.12: Contours of sand concentration at 1.6 m/s velocity in 0.051 m pipe

It is imperative to mention that the Roco and Balakrishnam (1985) experimental data point closest to the pipe-wall in Figure 4.11 is not sufficient to ascertain the exact sand concentration at the pipe wall. The data point is some distance away from the pipe-wall as can be seen in the Figure 4.11, in which the sand concentration may not represent the actual concentration at the pipe-wall in the experiment performed by Roco and Balakrishnam (1985). This insufficient data at the pipe-wall may be attributed to the difficulty in obtaining exact data of sand concentration at pipe-wall in experimental methods for investigating solids transport in pipes. However, it is expected that the concentration at the wall of horizontal pipe flows should be higher than that in other regions of the pipe. For this reason, it can be inferred that the exact sand concentration (Cv.) of the experimental data of Roco and Balakrishnam (1985) at the pipe wall should be $\mathrm{Cv} \geq 0.4$, or tend to those predicted by the Frames III and IV, and Capecelatro and Desjardin (2013), which show good agreement at the pipe wall. Therefore, it can be concluded from the comparison in Figure 4.11 and the contour plots in Figure 4.12 that the Frames III and IV predict a more realistic sand deposit in the pipe bottom compared to the Frame-II.

Figure 4.13 presents the comparison of the sand concentration profiles predicted by the numerical Frames II, III and IV with the profile of Capecelatro and Desjardin (2013) at 0.83 m/s flow velocity. The simulation velocity of 0.83 m/s is well below the estimated 1.1 m/s critical transport velocity for the flow condition. Therefore, stationary sand deposit is expected at the bottom wall of the horizontal pipe. It can be seen from the steepness of the profiles in the Figure 4.13 that the profiles predicted by the Frames III and IV, and Capecelatro and Desjardin (2013) exhibit the presence of a stationary sand bed deposit with significant bed height at the pipe bottom, $^{\mathrm{y}}/_{\mathrm{D}} < 0.2$. The profiles in Figure 4.13 also show that the sand concentration in the pipe top half region, $^{\mathrm{y}}/_{\mathrm{D}} > 0.7$ is $\cong 0$, as predicted by the Frames III and IV, and Capecelatro and Desjardin (2013). This observation indicates that the sand is fully stratified towards the pipe bottom, which may have resulted in the build-up of a significant sand bed deposit in the pipe bottom, as displayed by the profiles of Frames III, IV and Capecelatro and Desjardin (2013).

The nature of the stratification of sand in the pipe as observed from the profiles in Figure 4.13 suggests that the flow turbulence kinetic energy (TKE) dissipates towards the pipe wall, where $\mathrm{TKE} = 0$ is expected. This inference is evident in the profile of TKE predicted by Frame III in Figure 4.14, which presents the TKE predicted by Frames II and III. However, the Frame-II has not shown similar trend inferred, as shown in the magnitude of TKE at the pipe bottom.

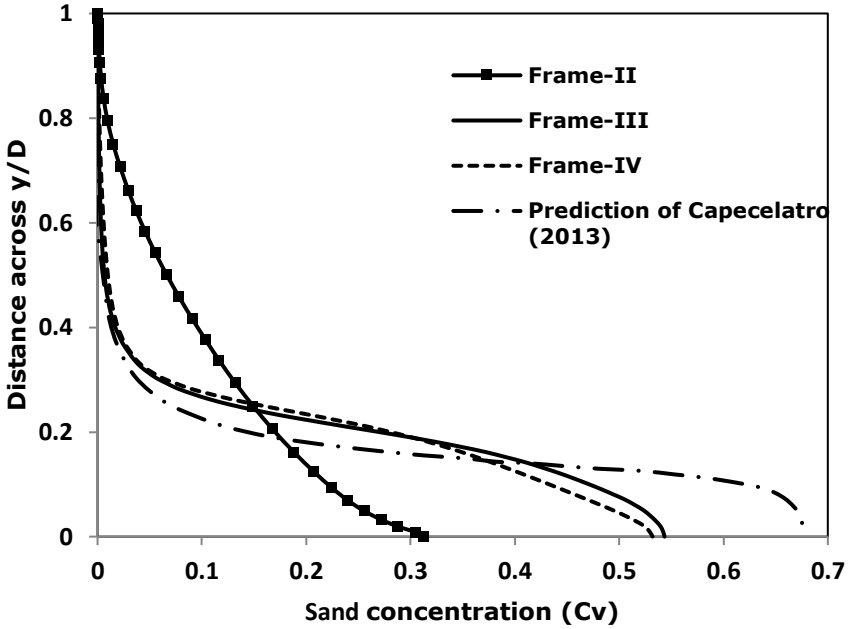

Figure 4.13: Sand concentration profiles predicted at 0.83 m/s in 0.051 m pipe.

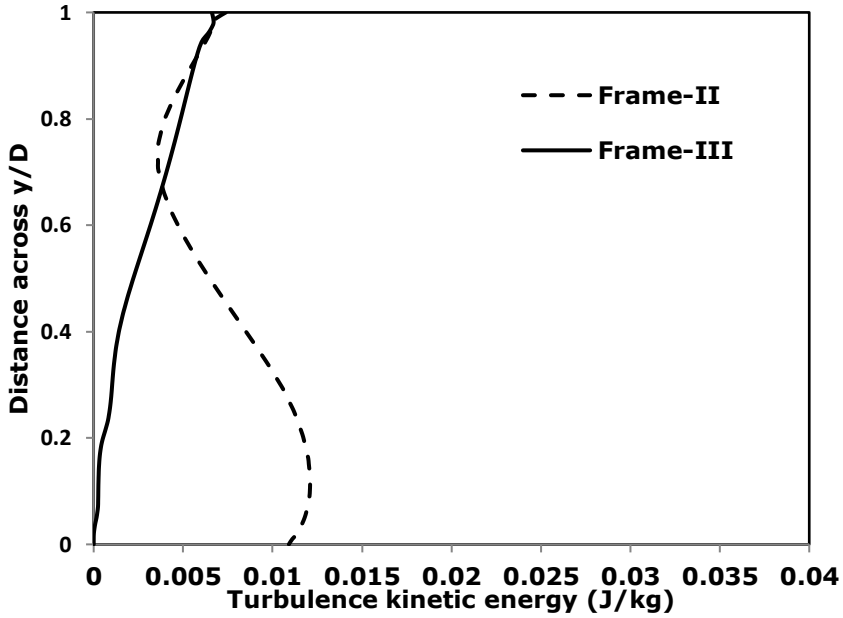

Figure 4.14: Predicted profiles of turbulence kinetic energy at 0.83 m/s velocity

The presence of the stationary sand bed in the pipe at velocity of 0.83 m/s as predicted by Frames III and IV is also evident in the contour plots in Figure 4.15, which shows that the sand concentration at the pipe bottom predicted by Frames III and IV significantly exceed the concentration packing limit for sand particles, $Cv = 0.5$ in which frictional enduring contact between particles will dominate the flow behaviour. However, the contour of the Frame-II displays a relatively uniform concentration across the pipe with $Cv \ll 0.5$ at the pipe bottom, as can be seen in Figure 4.15. It is expected that the particle fluctuation as a result of the collision of sand particles at the pipe bottom should become very small or negligible when enduring contact between particles persists. Figure 4.16 presents the profiles of granular temperature (GT) predicted by Frame II and III, which is a measure of the fluctuation from collision of solid particles. The figure shows that the magnitude of GT at the pipe bottom predicted by Frame-II is significantly higher than that predicted by Frame-III, which predicted GT $\cong 0$ at the pipe-wall region.

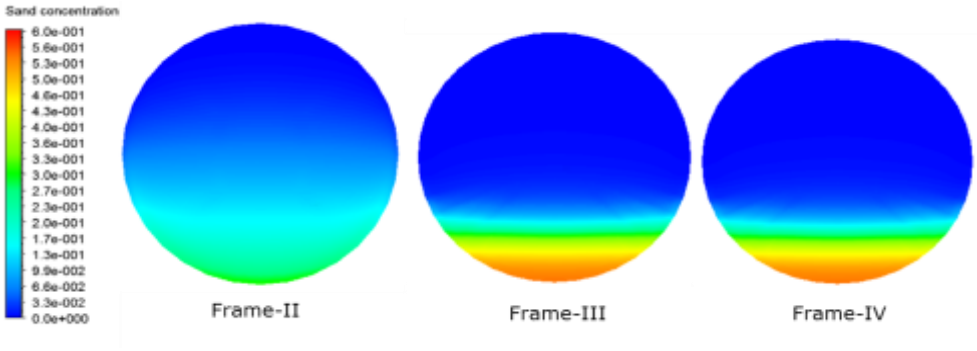

Figure 4.15: Contour plots of sand concentration distribution at 0.83 m/s

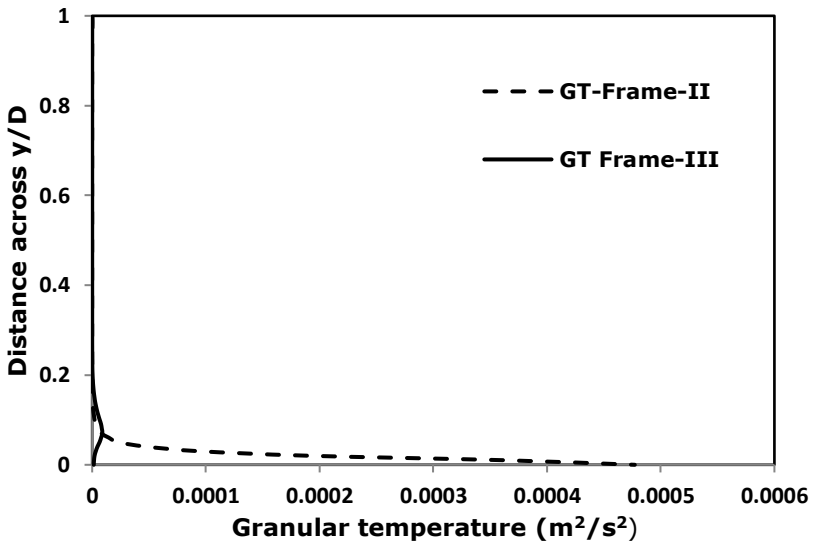

Figure 4.16: Predicted profiles of sand-phase granular temperature

It can be said that the strong sand segregation in the pipe at 0.83 m/s is accurately predicted by the Frames III and IV, as shown in Figure 4.13, in which the profiles of the Frames III and IV agree with the prediction of Capecelatro and Desjardin (2013) in the majority of the pipe, except at the pipe bottom region, $^{y}/_{D} < 0.2$ in which the concentration of sand at the wall predicted by Capecelatro and Desjardin (2013) exceed those of the Frames III and IV. It is imperative to mention that the difference observed between the sand concentration at the pipe-wall and thickness of the stationary deposit predicted by the Frames III and IV and that of Capecelatro and Desjardin (2013) in Figure 4.13 may be attributed to the treatment of the size distribution (PSD) of the solid particles in the study by Capecelatro and Desjardin (2013) and that of the present study.

The sand in the present study is treated as mono-size particles, whereas the simulation by Capecelatro and Desjardin considered poly-size particles. It should be noted that the maximum packing density for poly-size particles is usually higher compared to that of mono-size particles (Sohn and Moreland 1968), because smaller particles in poly-size particles have the tendency to occupy the voids between larger particles in stationary deposit of poly-size solids, which will eventually increase the solids packing density. Therefore, the sand concentration at pipe bottom is expected to be higher in deposit of poly-size particles than mono-size deposit, as observed in predictions by the Frames III and IV of the present study and Capecelatro and Desjardin in the Figure 4.13.

The profiles of solids and liquid phase stress, and solids-phase velocity may also provide indications of the mobility of sand phase at the bottom of pipes, as presented in Figures 4.17 (a) and (b). Figure 4.17 (a) shows that the value of sand and liquid phase stresses is zero at the pipe bottom region, $^{y}/_{D} < 0.1$ which may be regarded as the height of the stationary sand deposit zone in the pipe. The profiles of the sand phase velocity in Figure 4.17 (b) also suggest that the sand phase is immobile at the pipe bottom, as the velocity magnitude is $= 0$ at the pipe bottom. The good agreement in the velocity magnitude predicted by Frame III and Capecelatro and Desjardin (2013) at the pipe wall suggests that the Frame-III predicts realistic results of sand transport characteristics in pipe.

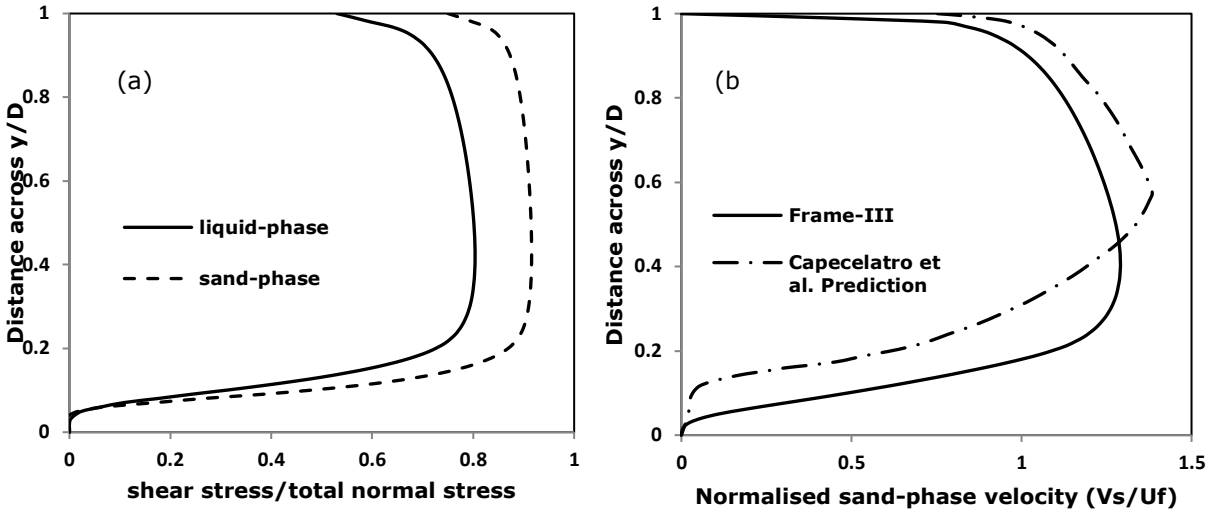

Figure 4.17: Predicted profiles of sand and liquid phase stress (b) Predicted profiles of sand phase velocity.

4.5 Summary of CFD Models Validation Study

The results of the present validation study have revealed that the treatment of the multiphase turbulence quantities and the phase interactions have significant effects on numerical predictions of sand concentration distribution and deposition in pipes. The numerical Frames III and IV investigated have accurately predicted a more realistic sand concentration distribution of the different sand transport flow regimes. However, the numerical Frame-II is only capable of predicting the sand suspension flow regime, in which the sand particles are in random translational motion with nearly fully elastic inter-particles interaction, but fails to predict a realistic sand segregation when inter-particle collision becomes frequent and inelastic, particularly when the flow velocity reduced well below the estimated critical transport velocity as can be seen in Figures 4.9, 4.11 and 4.13. It should be noted that a flow feature that is not accounted for in the Frame-II are the covariance of velocities of liquid and solids, k_{sl} and the presence of the sand particle-phase turbulence, k_s.

The sand-phase induced turbulence k_s resulted from the interaction of collisional sand particles and the interstitial liquid in the flow. Therefore, the inter-particle translation-collisional interaction and the intra-phase hydrodynamic interaction are the sources of sand-phase stress which contribute to sand segregation towards the pipe bottom. The granular temperature, Θ in the KTGF model represents a measure of the inter-particles interactions. However, the particle-phase induced turbulence k_s requires additional modelling, as the KTGF models do not account for it. The predicted results show that the, Θ and the flow TKE, k_l in which the effect of k_{sl} and k_s are accounted, dissipate towards the pipe wall, as evident in the predictions by the numerical Frame-III in Figures 4.10, 4.14 and 4.16. The magnitude of k_l and Θ at the pipe lower-half depends on the dominant interaction mechanism and the sand concentration at the pipe wall region. Therefore, a CFD model framework developed for predicting sand transport in pipes, which strong sand segregation due to inter-particle translational and collisional interaction may occur simultaneously must account for the granular temperature, Θ, k_{sl} and the particle-phase induced turbulence, k_s simultaneously, as provided by the numerical Frames III and IV of the present study.

Although the profiles predicted by the Frames III and IV are generally identical and the multiphase turbulence in the two frames is treated in a similar manner. However, the granular temperature is treated differently in the two frames. The Frame-III employs the algebraic form of the granular temperature, in which the production and dissipation of granular energy are treated as equal. Whereas, the Frame-IV employs the differential transport equation form of the granular temperature. The similarity in the profiles of sand concentration predicted by the two Frames indicates that the different forms of granular temperature do not have significant effect on the predictions. It should be noted the that the Frame-IV requires more computational time to obtain a converged solution due to the additional equations that have to be solved in the differential equation form of the granular temperature. The average simulation time for the calculations per simulation case on a PC at 3.20 GHz is significantly higher for the Frame-IV compared to Frame-III. Therefore, based on accuracy and computational time, the numerical Frame-III is adopted as the optimum CFD model framework for predicting sand transport in V-inclined pipe bend in the present research study.

Chapter 5

Sand transport in Pipe Bends

5.1 Description of pipe bend geometry and flow conditions

The schematic of the V-inclined pipe bend investigated in the present study is shown in Figure 5.1. The sections denoted P1, P2, P3 and P4 on the bend pipe as shown in the figure are the pipe sections where the predicted data have been obtained for analysis. The pipe sections have been identified as the critical sections of the bend pipe where significant variations in sand deposit have been observed after a thorough visualization of the contour plots of sand concentration in the pipe across the range of flow velocities investigated. The section denoted P2 represents the pipe-dip and the other pipe sections P1, P3 and P4 are located at distance 10D, 2.5D and 15D away from the pipe dip, respectively, where D represents pipe diameter. The data obtained at sections P1, P3 and P4 represent the flow conditions at the upstream before entering the dip, dip-exit and further downstream of the dip, respectively.

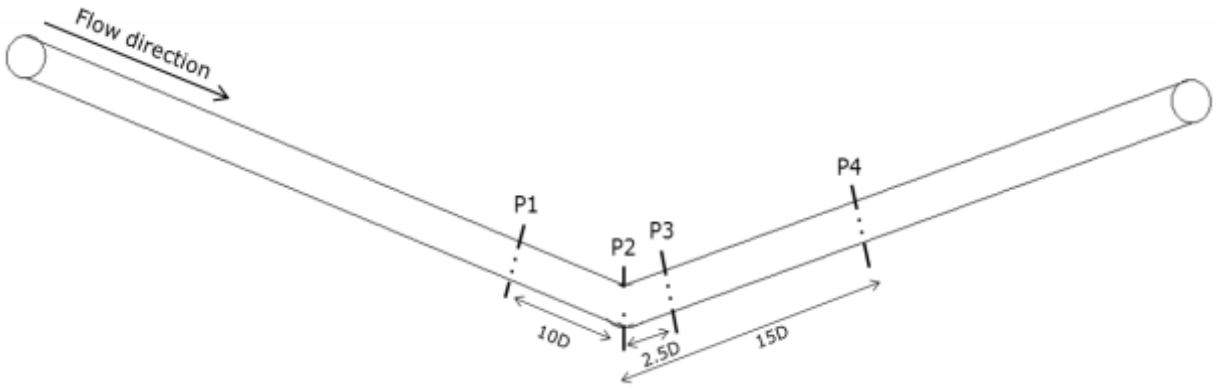

Figure 5.1: Schematic of V-inclined pipe bend

Figure 5.2 presents the computational mesh structures of the ±6° and ±4° V-inclined pipe bend geometry. Table 5.1 presents the simulation conditions and the estimated minimum sand transport velocity (MTV) for an equivalent horizontal pipe flow. The MTV has been estimated from the Oroskar and Turian (1987) MTV correlation, Equation (2.4). The solution procedures of the CFD model framework-III used in the calculation are described in chapter 4.

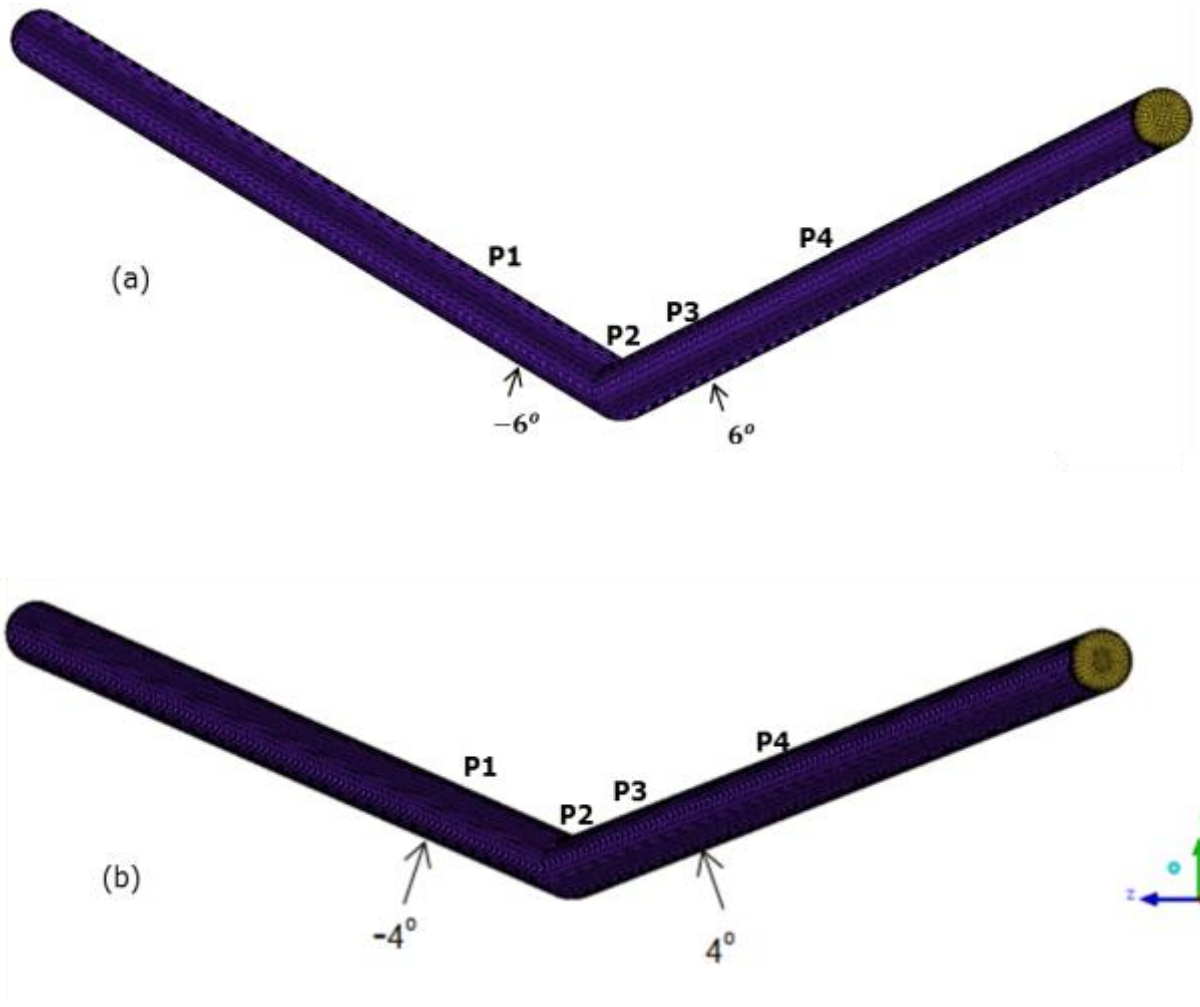

Figure 5.2: Hexahedral mesh structures of 3D bend pipes: (a) ±6° V bend pipe (b) ±4° V bend pipe

Table 5.1: Simulation condition for flow in bend pipe

Parameters	Pipe inclination	
	±6° V-pipe	±4° V-pipe
Pipe diameter (m)	0.1, 0.05	
Velocity range (ms^{-1})	3.7 - 0.3	
Liquid density (kgm_3^{-1})	998	
Liquid viscosity (pa.s)	0.001	
sand density (kgm_3^{-1})	2650	
Particle size (μm)	255, 180, 120	
Sand fraction	0.04	
MTV (ms^{-1}) estimated for 0.1m diameter horizontal pipe and 255 μm particle size	1.48	

5.2 Results analysis

5.2.1 Profiles of sand concentration in pipe bend

Figure 5.3 shows a comparison of the predicted sand concentration profiles at the pipe sections of the ±6° pipe bend for various flow velocities and sand particle size of 255μm. An asymmetric distribution of sand concentration across the pipe sections is displayed by the profiles and the particles segregated towards the pipe bottom at all the flow velocities as shown in Figure 5.3. The sand concentration at the bottom-wall of all the pipe sections at 3.7 m/s is less than the concentration limit for loose-packed particles (Cv=0.5), beyond which particles may undergo enduring contact with each other. The MTV estimated for sand transport in an equivalent horizontal pipe flow is 1.48 m/s ≈ 1.5 m/s, as presented in Table 5.1. It is observed that the concentration at the bottom of the sections P1, before the dip, P2, dip, and P4, downstream of the bend pipe exceeded the loose-packed particles limit well before the velocity approached the 1.5 m/s, MTV estimated for horizontal pipe flow. At the 1.5 m/s velocity, the concentration at the pipe bottom of all the pipe sections has exceeded the limit for loose-packed particles.

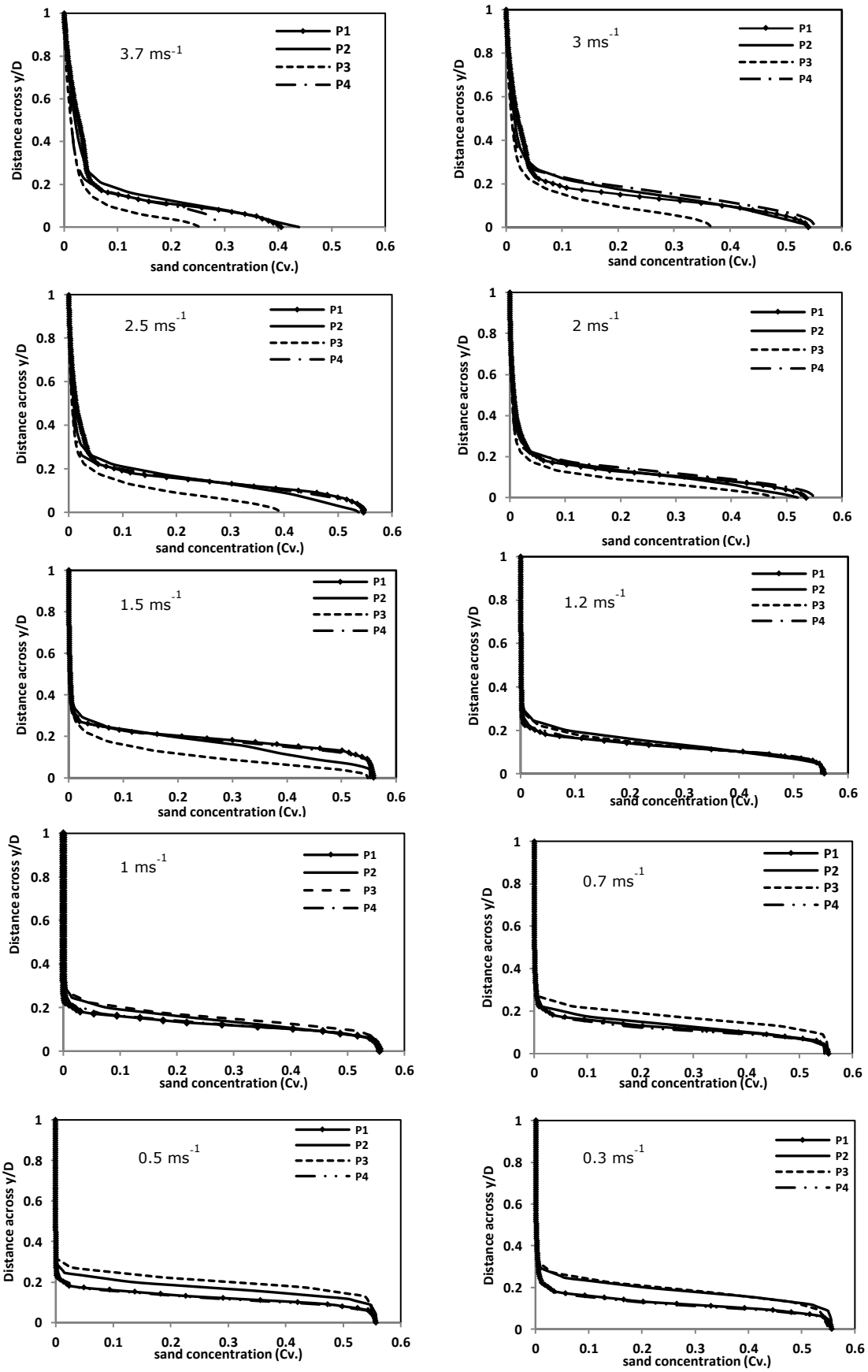

Figure 5.3: Profiles of predicted sand concentration in ±6° V inclined pipe bend at velocity range of 3.7 m/s-0.3 m/s

The degree of sand stratification in the bend pipe varies at all the flow velocities as can be seen in Figure 5.3. The steepness of the profiles closest to the pipe bottom-wall $^{y}/_{D} \leq 0.05$ started to develop at 3 m/s at sections P1, P2 and P4, and developed into an appreciable thickness at sections P1 and P4 as the velocity reduced to 2.5 m/s. The thickness of the steepness of profiles at sections P1 and P4 developed to $^{y}/_{D} = 0.15$ at 1.5 m/s and became uniform at all the pipe sections at 1 m/s. The concentration at the pipe bottom and the degree of sand stratification suggested several critical conditions in the pipe bend at certain velocities such as the 3 m/s and 2.5 m/s, in which the profiles steepness at the pipe bottom developed at certain sections of the pipe bend. Also, the 1.5m/s and 1 m/s velocities in which the sand concentration at all the pipe sections exceeded the limit of loose-packed particles and the steepness of the profiles at the pipe bottom became uniform at all the pipe bend sections. These observations in the profiles of Figure 5.3 provided indications of the transport mechanism. However, more data of other relevant flow properties may be required to aid a less subjective recognition of the actual sand transport regime in the pipe bend.

5.2.2 Contour of sand concentration and liquid-phase velocity magnitude in bend pipe at velocities above MTV estimated for horizontal pipe flow

Figures 5.4 and 5.5 present contour plots of sand concentration and liquid velocity magnitude in the bend pipe sections with the equivalent horizontal pipe case at the 3m/s and 2.5 m/s velocity, respectively, which are above the 1.5 m/s MTV estimated for the horizontal pipe flow. Qualitative observations of the contours in Figure 5.4 (b) show that the maximum point of the liquid-phase velocity magnitude is located close to the bottom of the bend pipe at section P3, which represents the pipe-dip exit, while those of the other bend pipe sections and the horizontal pipe are in the pipes centre region. Also, the velocity magnitude is fullest at section P3 compared to the other bend pipe sections and the horizontal pipe cross-section. The fullness of the velocity magnitude at section P4 diminished substantially in the pipe lower-half region towards the pipe bottom, whereas those of sections P1 and P2 are similar to that of the horizontal pipe. Consequently, the highest sand concentration is noticeable at the bottom of section P4 and the least concentration at section P3 where the velocity magnitude is fullest, as can be seen when the contours in Figures 5.4 (a) and (b) are observed simultaneously.

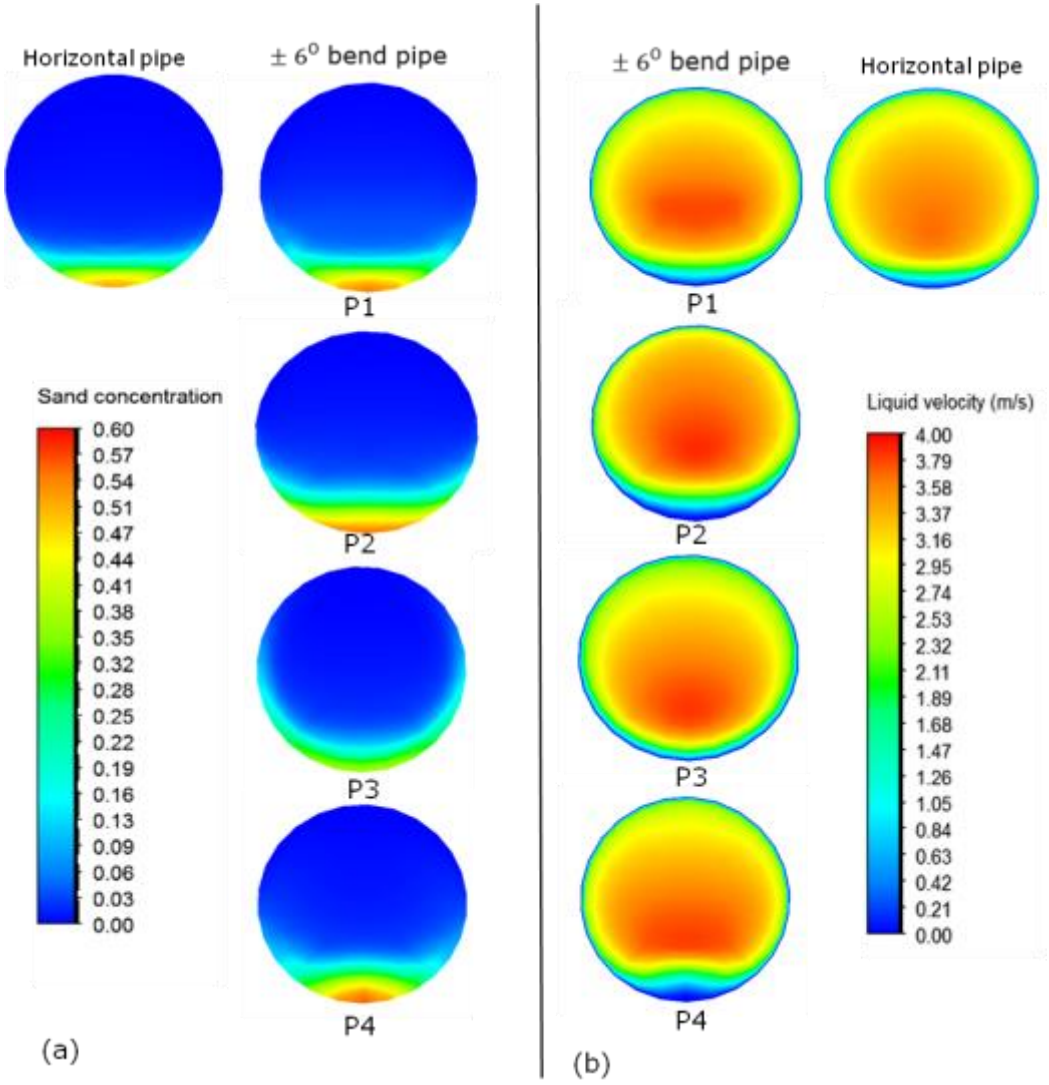

Figure 5.4: Contour plots at 3 m/s flow velocity: (a) sand concentration (b) liquid velocity magnitude.

The contours of sand concentration and velocity magnitude at 3 m/s in Figure 5.4 and those obtained at 2.5 m/s have similar trend, as shown in Figure 5.5, which shows the contour plots of sand concentration and velocity magnitude at 2.5 m/s. However, the thickness of the sand concentration at the pipe bottom at sections P1 and P4 at the 2.5 m/s velocity has substantially exceeded that of the equivalent horizontal pipe. The sand concentration at section P3 became more appreciable at 2.5 m/s compared to that at 3 m/s, as can be seen in Figures 5.5 (a) and 5.4 (a), respectively. The estimated Reynolds number (Re $= \mathbf{DV\rho_L/\mu_L}$) of the flow at the 3 m/s and 2.5 m/s are $\approx 2.99 \times 10^5$ and 2.49×10^5, respectively. The magnitude of the estimated Re at the 3m/s and 2.5 m/s velocity indicated that the flow is highly turbulent. The magnitude of the flow turbulence reduced by 17% between velocity range of 3 m/s and 2.5 m/s.

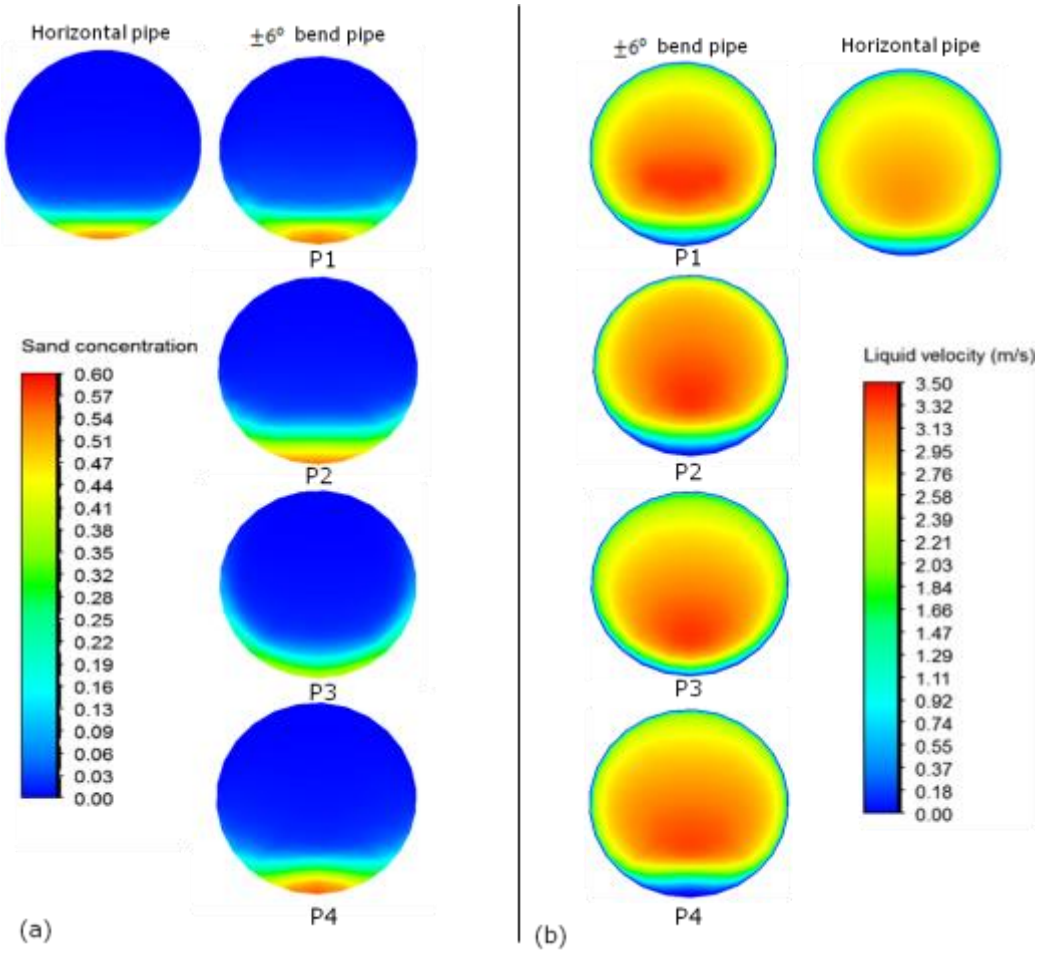

Figure 5.5: Contour plots at 2.5 m/s flow velocity: (a) sand concentration (b) liquid velocity magnitude.

5.2.3 Contours of pressure in bend pipe

Figure 5.6 presents predicted contours of pressure at the pipe sections as the flow-stream travels through the ±6° bend pipe. A pressure gradient is noticed across the pipe radial direction at section P2, at the various flow velocities. However, uniform pressure is observed across the other pipe sections P1, P3 and P4, as evident in the contours in Figure 5.6. Consequently, a positive pressure gradient is observed between sections P2 and P3 in the direction of flow in the pipe top-half region, whereas in the pipe lower-half region a negative pressure gradient is observed between the two sections. The pressure imbalance between the sections P2 and P3 is obvious in the contours at 3 m/s velocity in Figure 5.6 (a). The contours of pressure in the Figure 5.6 qualitatively suggested the presence of localized imbalance flow phenomena as the flow travels through the dip of bend pipe, particularly between sections P2 and P3, which represent the pipe-dip and the vicinity of the dip-exit, respectively.

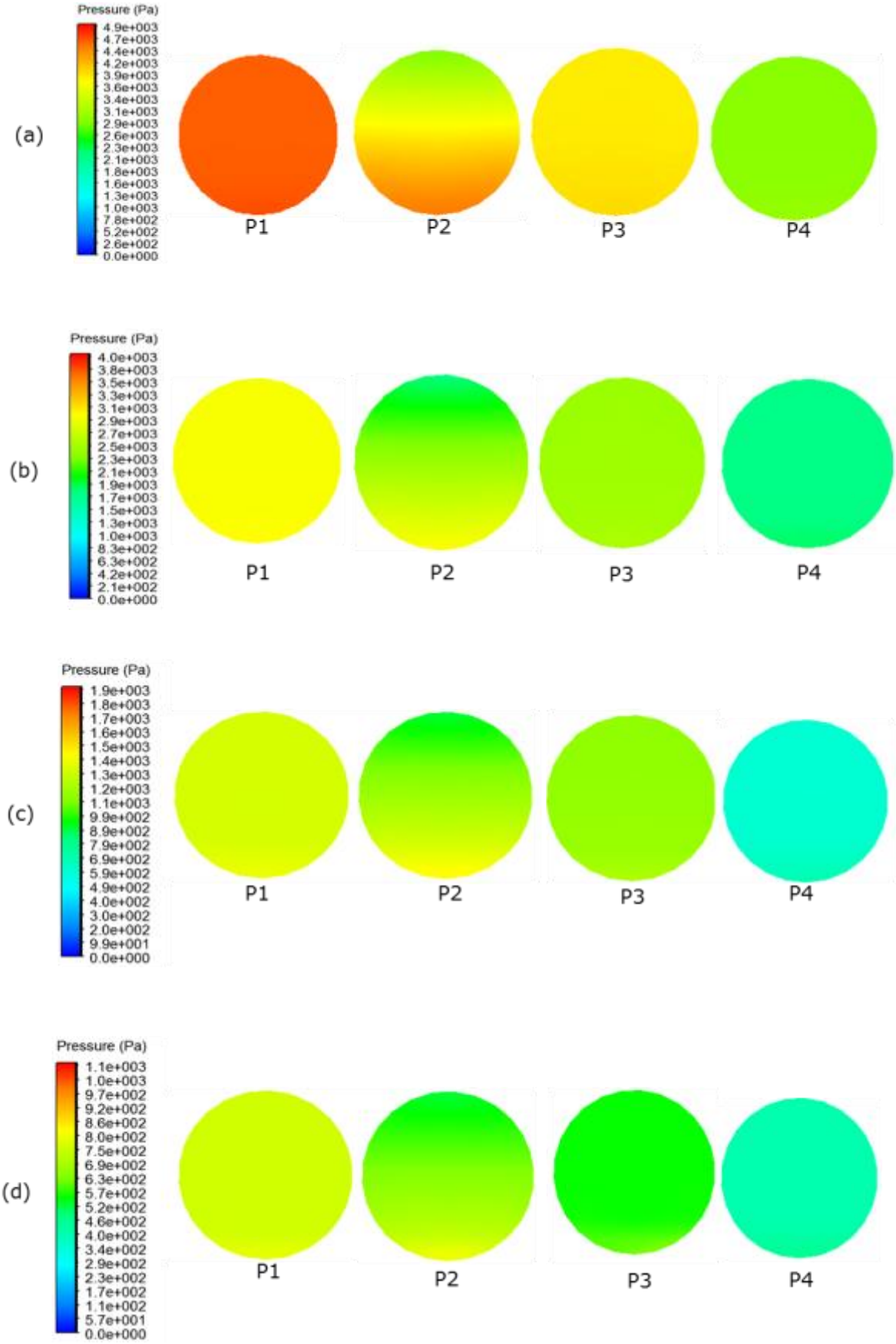

Figure 5.6: Contour plots of pressure at bend pipe sections (a) 3 m/s velocity (b) 2.5 m/s velocity (c) 1.5 m/s velocity (d) 1 m/s velocity.

5.2.4 Characteristics of in-plane velocity vectors of liquid phase in bend pipe

Figure 5.7 presents the in-plane velocity vectors of the liquid phase at the cross-sections of the pipe-dip and dip-exit at the 3 m/s and 1.5 m/s velocities. At the pipe-dip, section P2, the orientation of the velocity vectors around the pipe circumferential wall and those in the pipe core region are in opposite direction. Also, the velocity vectors around the pipe wall at section P2 drifted inward towards the pipe centre region, where the velocity vectors are all pointed downwards towards the pipe bottom and then separated in opposite direction at the pipe bottom wall, where the vectors recirculated to merge at the pipe top. However, at the dip-exit, section P3, the arrowheads of the velocity vectors are all aligned upward towards the pipe-top wall across section P3. It should be noted that the pipe-top and bottom walls at section P2 correspond to the inner-bend and outer-bend of the bend pipe curvature, respectively. The helical orientation of the liquid velocity vectors in the vertical halves of section P2 suggested that the flow is subjected to a localised vortex-type secondary motion at the vicinity of the pipe dip, as can be seen in Figures 5.7 (a) and (b).

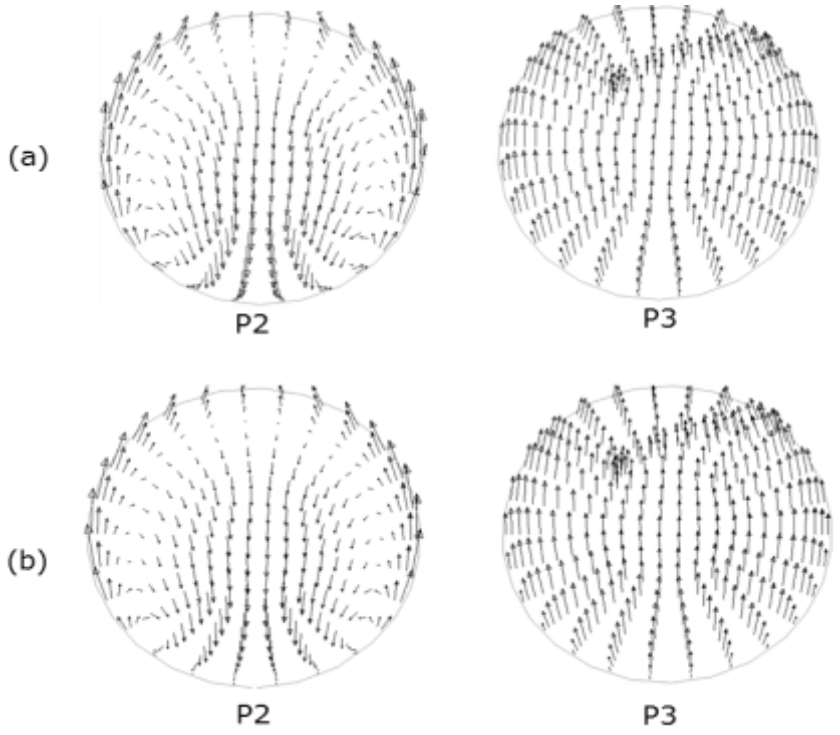

Figure 5.7: Characteristics of the in-plane velocity vectors of liquid-phase. (a) 3 m/s flow velocity (b) 1.5 m/s flow velocity.

5.2.5 Contour of sand concentration and liquid-phase velocity magnitude in bend pipe at velocity below MTV estimated for horizontal pipe flow

Figures 5.8 and 5.9 show the predicted contours of sand concentration and liquid-phase velocity magnitude in the bend pipe at 1.5 m/s and 1 m/s, which corresponds to the velocities at the MTV estimated for the horizontal pipe flow and below the estimated MTV, respectively. Figure 5.8 (b) shows that the velocity magnitude is fullest at section P3 of the bend pipe at 1.5 m/s as previously observed in Figures 5.4 (b) and 5.5 (b) at the velocities above the MTV estimated for horizontal pipe flow. However, at 1 m/s the fullness of the velocity magnitude at section 3 diminished significantly compared to those of the other pipe sections at the same velocity as can be seen in Figure 5.9 (b). Consequently, the highest sand concentration at the bend pipe bottom at the 1 m/s velocity is observed at section 3 compared to the other bend pipe sections and the horizontal pipe case.

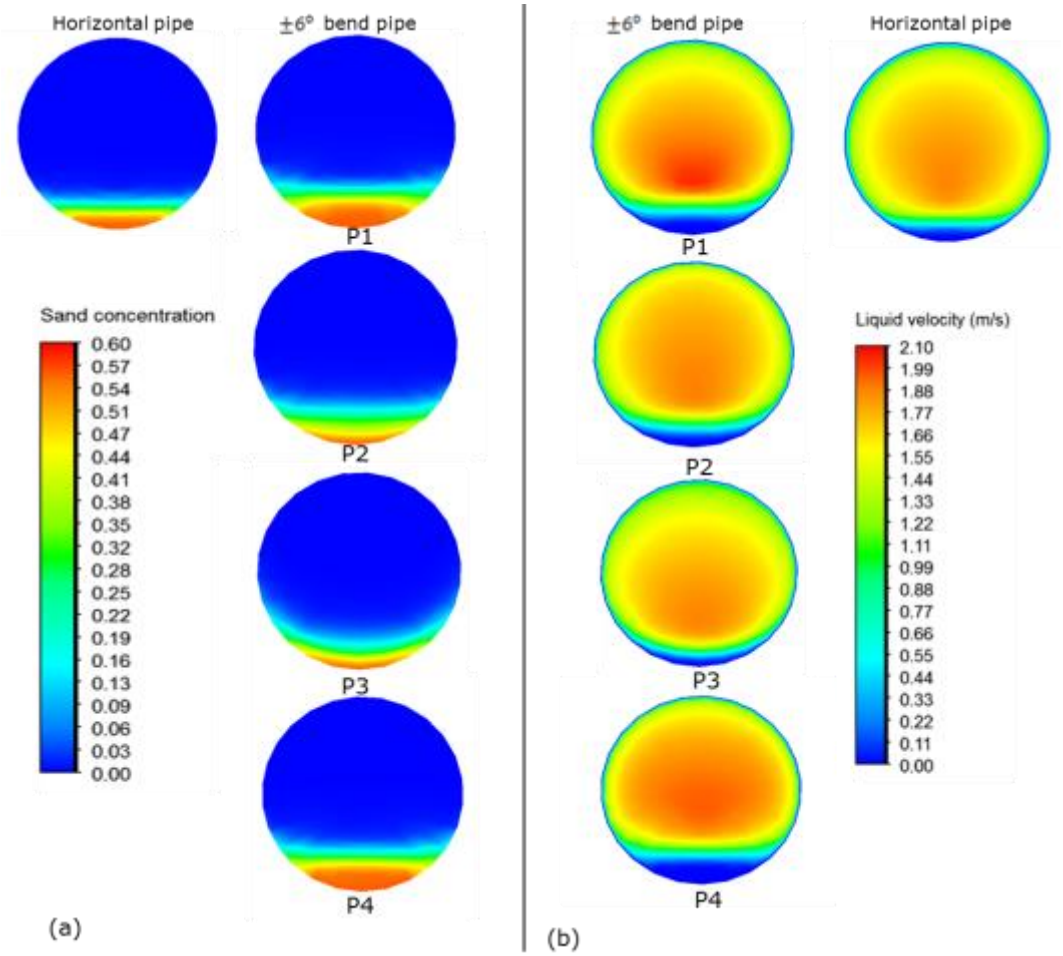

Figure 5.8: Contour plots at 1.5 m/s flow velocity: (a) sand concentration (b) liquid velocity magnitude.

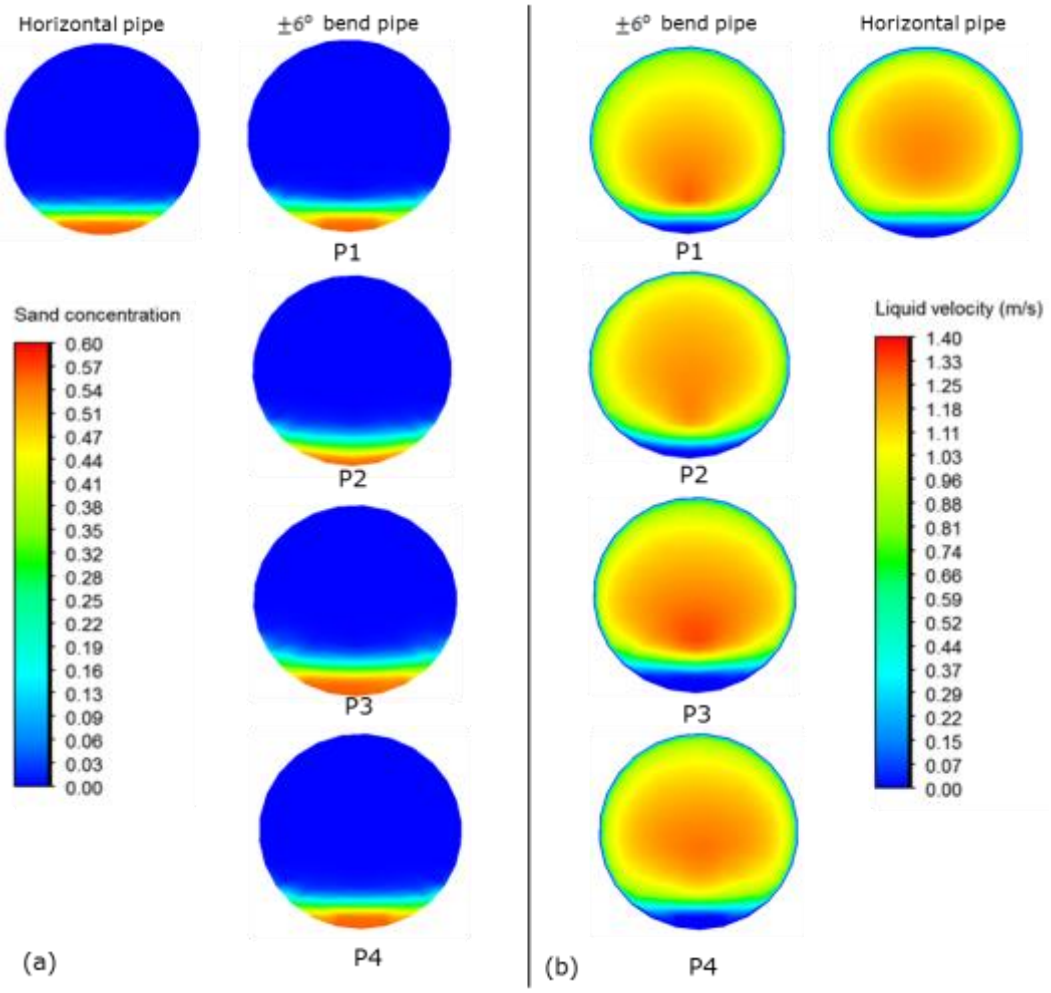

Figure 5.9: Contour plots at 1 m/s flow velocity: (a) sand concentration (b) liquid velocity magnitude.

The contour plots of Figures 5.4, 5.5, 5.8 and 5.9 show that the maximum sand concentration is located at section P4 and the least at section P3 at the velocities above the MTV estimated for an equivalent horizontal pipe. However, at velocities below the MTV estimated for the horizontal pipe flow the maximum sand concentration is located at section P3 and the least at section P2. The Re estimated at the 1.5 m/s and 1 m/s are $\approx 1.5 \times 10^5$ and 1.0×10^5, respectively. The estimated Re indicated that the flow turbulent intensity reduced by 33% between velocity range of 1.5 m/s and 1 m/s, and a significant reduction of 67% is indicated between the 3 m/s and 1 m/s velocity range. The Re provided preliminary estimate of the magnitude of the flow turbulence based on the liquid-phase properties, but the sand-phase effect on turbulence intensity magnitude is not accounted for by the Re. The knowledge of the multiphase turbulence intensity characteristics may be helpful to better understand the sand transport characteristics in the pipe.

5.2.6 Multiphase turbulence kinetic energy in bend pipe

Figure 5.10 shows the predicted profiles of the liquid-phase turbulence kinetic energy, in which the effect of the sand-phase on the multiphase turbulence has been accounted. The profiles are asymmetric at high velocities and then became gradually symmetric at certain pipe sections as the velocity varied from 3.7 m/s – 0.3 m/s. The figure shows that the turbulence intensity dissipated towards the bottom wall of the bend pipe, in the direction where the sand particles accumulated as the velocity reduced as seen in the concentration profiles in previous Figure 5.1. The comparison of the profiles at the pipe sections in Figure 5.10 shows that the multiphase turbulent kinetic energy varies at the various sections of the bend pipe.

It can be seen in Figure 5.10 that at 3.7 m/s and 2.5 m/s the peak of turbulent kinetic is located at sections P3 and P4 in the pipe-core region ($0.3 < {}^{y}/_{D} < 0.8$), compared to sections P1 and P2. However, this trend shifted to the pipe lower-half region ${}^{y}/_{D} < 0.4$ as the velocity dropped below 2.5 m/s. Also, at the 3.7 m/s and 2.5 m/s, significant difference in turbulence intensity is observed between sections P2 and P3, the sections where an imbalance pressure gradient across the bend pipe is observed in the previous pressure contours in Figure 5.6. It should be recalled that the sections P3 and P4 represent the dip-exit and upstream sections of the bend pipe, whereas sections P1 and P2 represent the upstream and dip sections of the pipe.

It can also be seen in Figure 5.10 that at the velocities below the estimated MTV of 1.5 m/s, all the profiles of turbulence intensity are similar in the pipe top half. However, in certain region of the pipe lower half, $0.1 < {}^{y}/_{D} < 0.3$, the profiles of sections P1 and P4 showed a peak, which is more noticeable in the profile of section P4. The characteristics of the turbulent kinetic energy profiles in Figure 5.10 appeared very complex, which posed significant difficulty in establishing a coherent pattern of turbulence modulation in the bend pipe at the various flow velocities. This complexity in the turbulence intensity characteristics may be attributed to the dynamic nature of turbulence kinetic energy in various solids transport mechanisms and the pipe curvature effect. This observation suggested

that the pipe curvature may have effect on turbulent modulation differently from that of the sand phase.

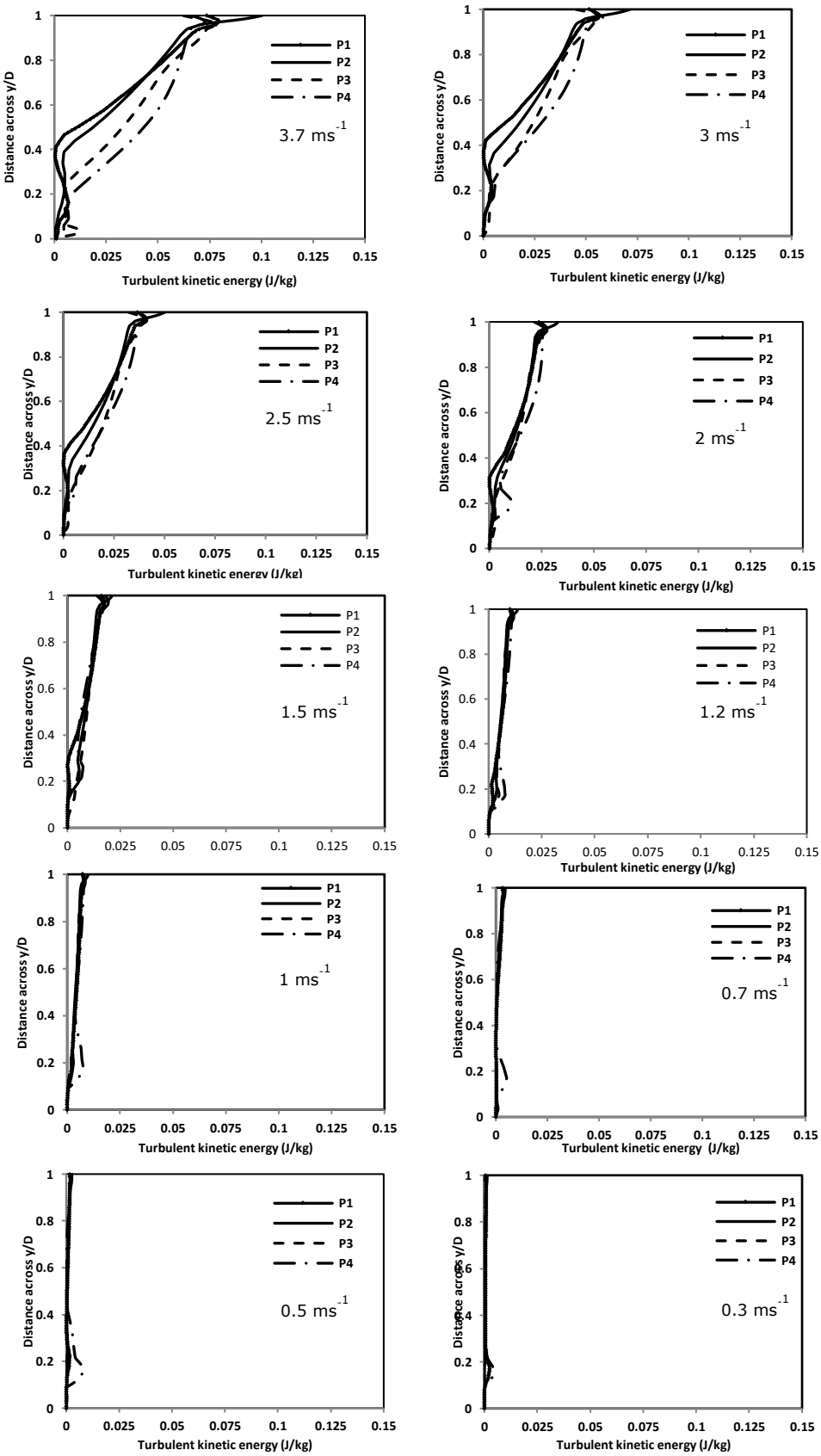

Figure 5.10: Comparison of predicted profiles of multiphase turbulence kinetic energy at ±6° bend pipe sections

5.2.7 Modulation of multiphase turbulence kinetic energy in bend pipe

Figure 5.11 shows the profiles of turbulence kinetic energy modulation in the ±6° bend pipe. The turbulence modulation (TM) has been evaluated as a percentage change in turbulence kinetic energy in the bend pipe $(\mathrm{K_b})$ compared to that of the equivalent horizontal pipe $(\mathrm{K_h})$, given as $(\mathrm{TM} = (\mathrm{K_b}/\mathrm{K_h} - 1)\times 100)$. The profiles at the various bend pipe sections P1-P4 show that the ±6° bend pipe curvature suppressed and enhanced turbulence kinetic energy simultaneously as the flow travels through the bend pipe. The modulation of turbulence kinetic energy in the bend pipe is significant in the pipe lower half region, $^{y}/_{D} < 0.5$, as can be seen in Figure 5.11. The sections P3 and P4 enhanced the turbulence intensity significantly at 3.7m/s, which is more noticeable at section P3. However, the profile of sections P1 and P2 indicated a suppression of turbulence kinetic energy at the velocities above the estimated MTV of 1.5 m/s for the horizontal pipe.

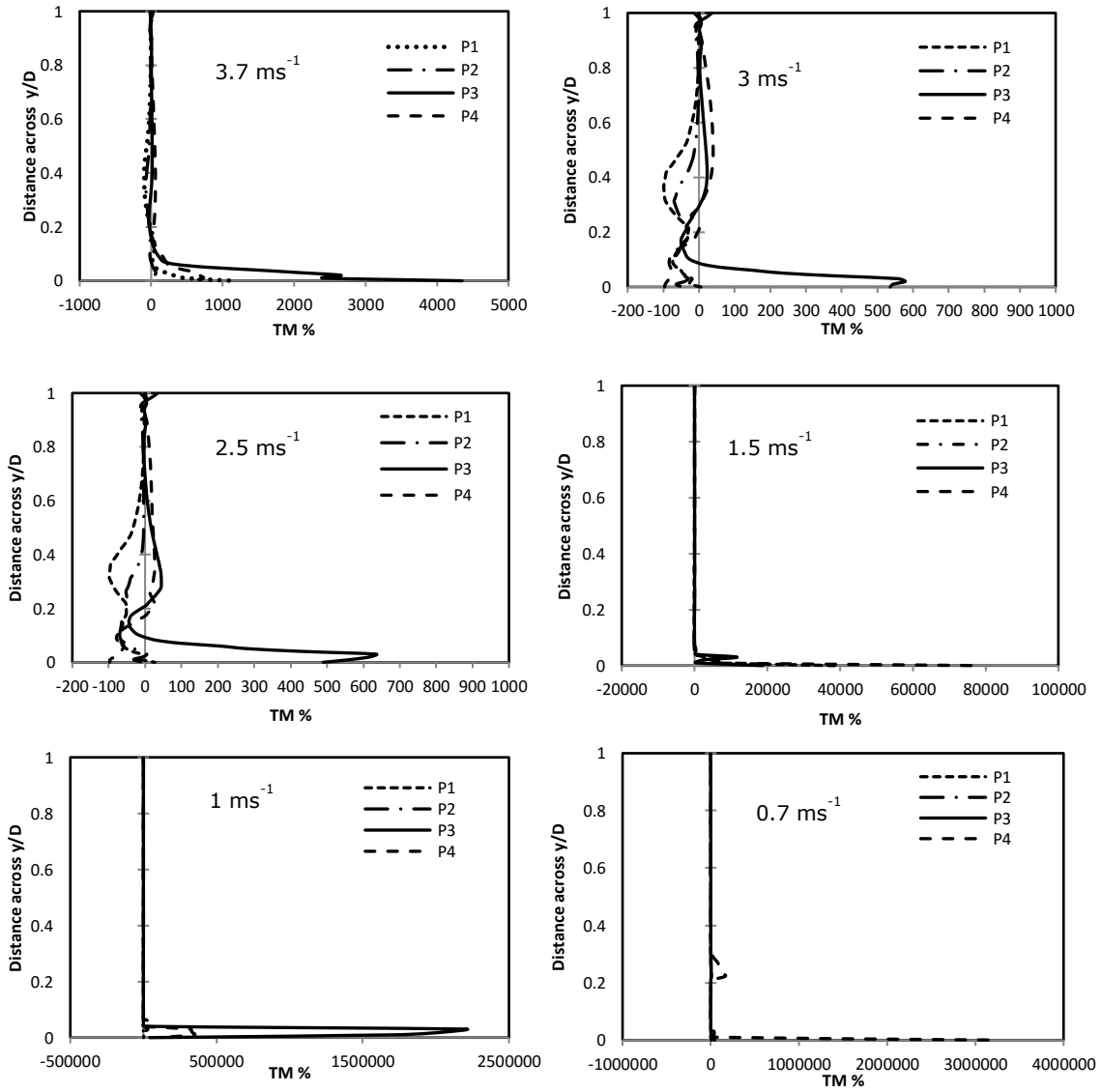

Figure 5.11: Turbulence modulation in ±6° bend pipe

The profiles at the various bend pipe sections in Figure 5.11 revealed that at the velocities above 1.5 m/s, the downward and dip sections of the bend pipe suppressed turbulence energy, whereas the turbulence kinetic energy regenerated at the vicinity of the dip-exit, P3, where the profiles show the peak of change in turbulence energy. However, the turbulent kinetic energy is modulated uniformly across the majority of the pipe sections at the velocities below 1.5 m/s, except at section P3 where the profile maintained a peak near the pipe wall. The regenerated turbulent intensity observed between sections P2 and P3 of the bend pipe suggested that the imbalance pressure gradient between the two sections and the vortex-type motion at the pipe dip, which are evident in the contours in Figure 5.6 and velocity vectors in Figure 5.7 may have introduced perturbations favourable to the turbulence intensity in the vicinity of the dip-exit of the bend pipe.

5.3 Sand transport flow regimes recognition in pipe bend

The mobility of the sand phase at the bottom-wall region of the bend pipe is an essential factor that indicated the various sand transport flow regimes in the pipe. Savage (1984), Johnson and Jackson (1987) and Bagnold (1956) have previously demonstrated in their studies the relationship between solid particles stresses and the total normal stresses to the mobility of cohesion-less solid particles in fluids. In the present study, the rate of the sand mobility is evaluated as proportional to the ratio of the sand phase stresses, which include the particles translational and collisional stresses to the total normal stresses in the pipe, denoted **R**. The frictional component of the inter-particles interactions dissipated the sand and liquid phase shear stress and contributed to the total normal stress at certain conditions in the pipe when sand particles cluster may roll, maintain sliding enduring contacts or become stationary on the pipe bottom wall. Figures 5.12, 5.13 and 5.14 present the curves of the evaluated ratio of the predicted translational-collisional stresses to the total normal stress for the sand and liquid phase, at the various bend pipe sections at velocities above 1.5 m/s.

It is observed from the curves that at 3.7 m/s the ratio $\mathbf{R}$ is nonzero at the pipe bottom at all the pipe sections, P1-P4, particularly at section P3 where, $\mathbf{R} > 0.2$, as can be seen in the Figure 5.12. However, in the curve of section P2, which represents the pipe dip, $\mathbf{R}$ is close to zero at the pipe bottom wall. The point of vanishing shear stress, where $\mathbf{R} \to 0$ in the curves corresponds to the transition point below which collisional and friction stresses due to enduring contact between sand particles may coexist simultaneously in the pipe. The shear stress vanishing point in Figure 5.12 is located well close to the pipe bottom wall region, $^{y}/_{D} < 0.1$, of the bend pipe at the 3.7 m/s, particularly at sections P3 and P4. The fullness of the curves of the sand and liquid phase across the pipe indicated that most of the load in the pipe at 3.7 m/s is mainly carried by the liquid turbulence energy and the sand particles translational-collisional interactions mechanisms. The mobility of the sand phase at all the pipe sections at the 3.7 m/s is confirmed by the profiles of sand concentration in previous Figure 5.3, in which the sand concentration at the pipe bottom of the pipe sections is well below the loose-packed limit at 3.7 m/s. From the features of the curves in Figure 5.12 and the predicted sand concentration at the pipe bottom in Figure 5.3, the sand transport flow regime at the 3.7 m/s can be described as heterogeneous sand suspension in the majority of the bend pipe sections.

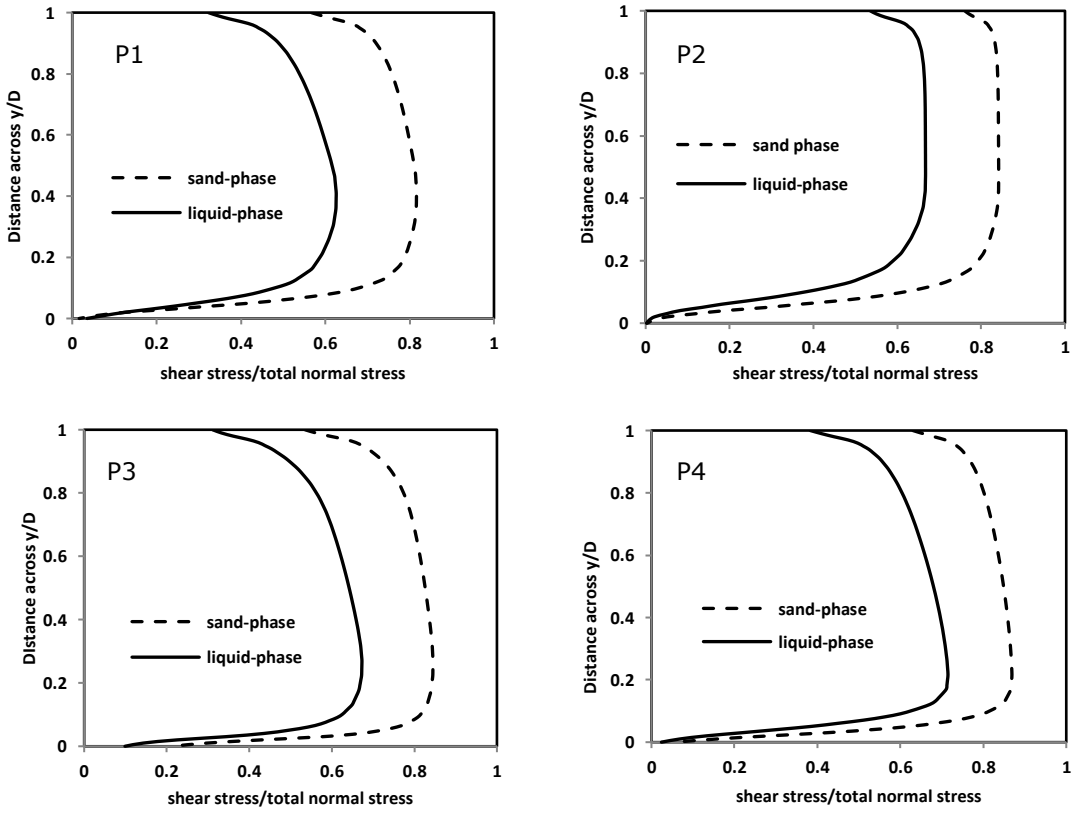

Figure 5.12: Curves of ratio of predicted sand and liquid phase stresses to the total stress in ±6° bend pipe sections at 3.7 m/s.

Figure 5.13 presents the curves of the **R** at the various bend pipe sections at 3 m/s velocity. It is observed from Figure 5.13 that the **R**-value at sections P2 and P4 is zero at the pipe bottom region $^{y}/_{D} < 0.1$, but those of sections P1 and P3 are nearly zero and non-zero ($\mathbf{R} > 0.05$), respectively. The $\mathbf{R} = 0$ observed at the pipe bottom region $^{y}/_{D} \leq 0.1$ at sections P1 and P4 indicated that the sand-phase is immobile at the bottom of bend pipe sections at the 3 m/s velocity. It should be noted that the critical condition that identifies the minimum transport velocity to avoid sand deposit at the pipe bottom is that in which $\mathbf{R} = 0$ at $^{y}/_{D}$ =0 (pipe bottom-wall). The critical velocity corresponds to the condition at the onset of non-shearing sand particles and formation of enduring contact sand-particles clusters at the pipe bottom wall, $^{y}/_{D}$ =0. The sand-particles clusters may roll, agglomerate to form moving or stationary sand bed, depending on the degree of compaction of the sand particles in the bed which mainly depends on the thickness of the non-shearing zone, where $\mathbf{R} = 0$ in the pipe region $0 < ^{y}/_{D} < 1$ and the interstitial liquid-phase shear stress in the non-shearing region.

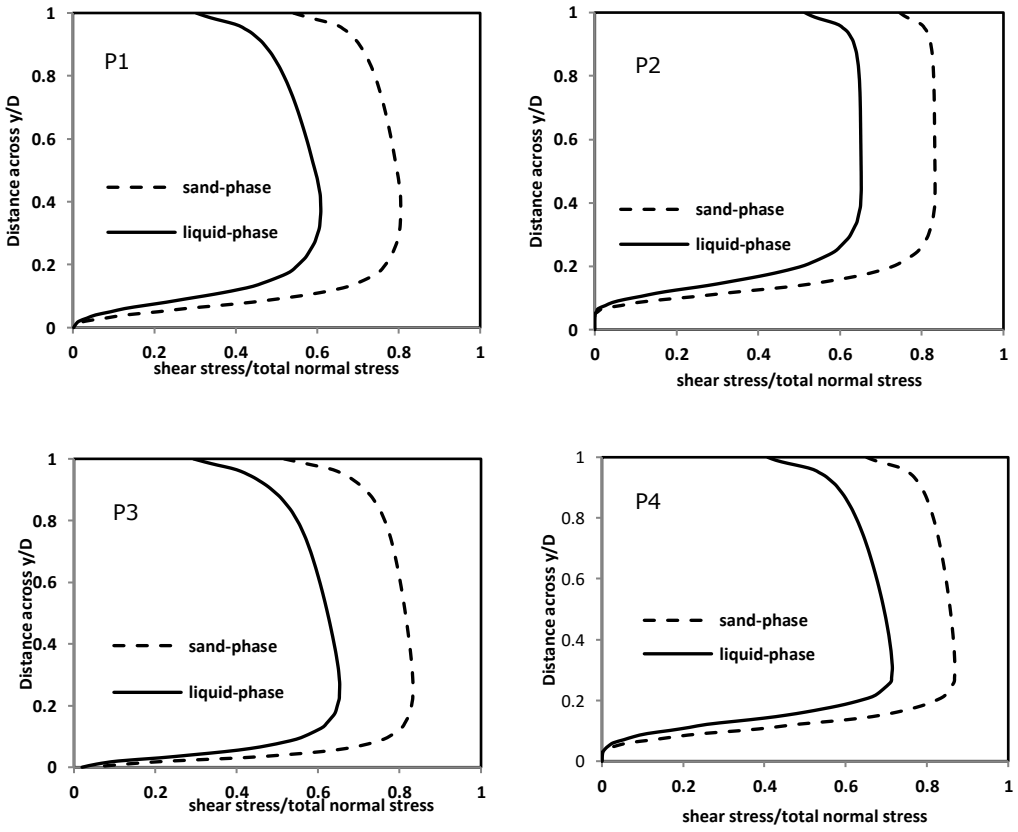

Figure 5.13: Curves of ratio of predicted sand and liquid phase stresses to the total stress in ±6° bend pipe sections at 3 m/s.

The concentration of sand at the pipe bottom of the pipe sections at 3 m/s observed in Figure 5.3 and the features of the curves of the pipe sections in Figure 5.13 indicated that various sand transport regimes existed in the ±6° bend pipe simultaneously at 3 m/s velocity. It should be noted that the critical features of the curves mentioned include the **R**-value, the non-shearing zone thickness and fullness of the curves. At sections P3 and P4, the curves indicated heterogeneous sand suspension and rolling sand-deposit regimes, respectively, whereas those of sections P2 and P4 indicated stationary and moving sand bed regimes, respectively. Also, the features of the curves of **R** at 2.5 m/s as can be seen in Figure 5.14 and the profiles of sand concentration in Figure 5.3 indicated that the sand phase is heterogeneously suspended at section 3 of the bend pipe, whereas stationary sand bed existed at sections P2 and P4 of the bend pipe.

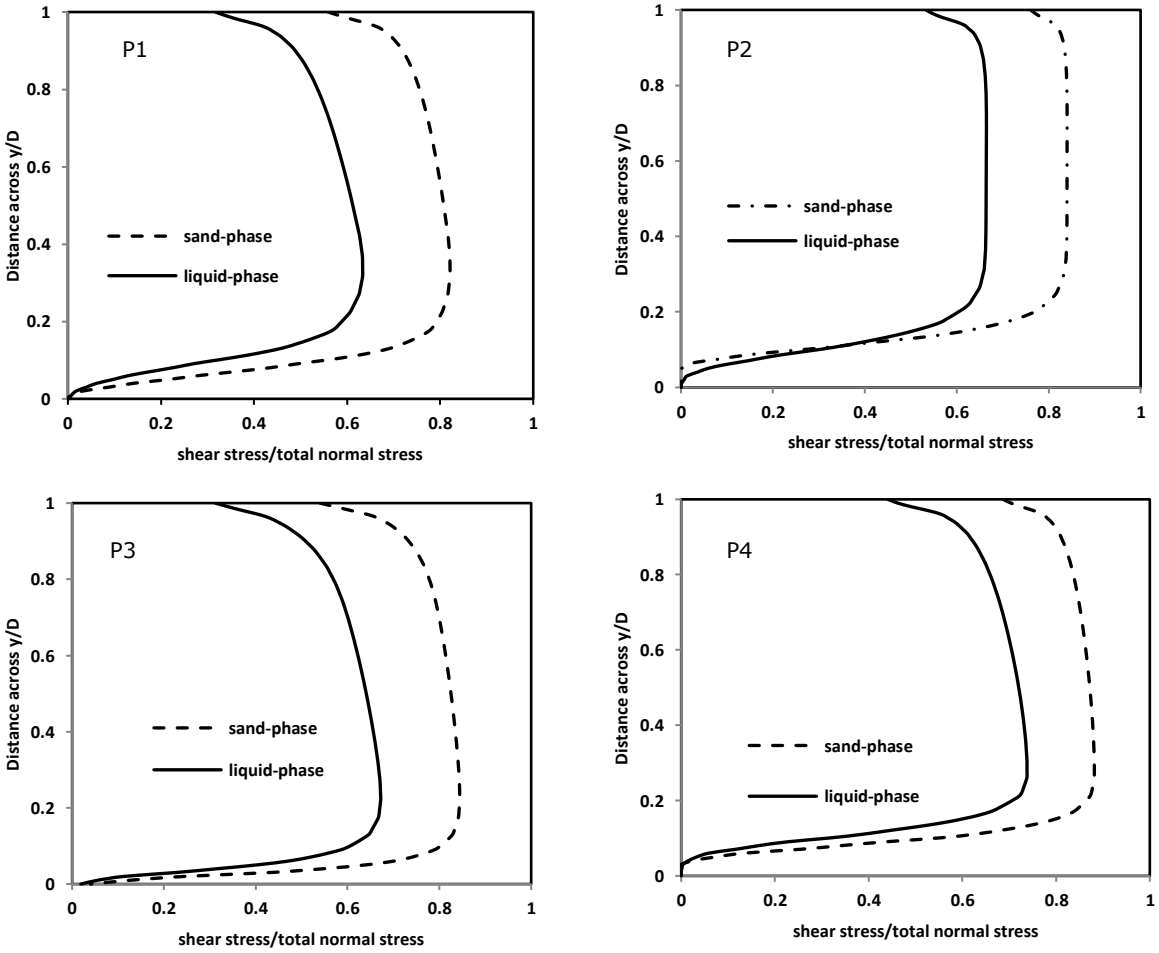

Figure 5.14: Curves of ratio of predicted sand and liquid phase stresses to the total stress in ±6° bend pipe sections at 2.5 m/s

In addition, it is observed that the liquid phase **R**-value is non-zero at certain region where, $^{y}/_{D} < 0.07$, in which the sand phase is non-shearing at section P2, as can be seen in Figure 5.14. This observation indicated that certain layer of the stationary sand bed thickness at section P2 is mobile, which can be described as a moving bed layer on a stationary bed layer at the pipe bottom wall at 3 m/s. The various sand transport flow regimes observed at 3m/s and 2.5 m/s velocities from the profiles of sand concentration in Figure 5.3 and the curves of $\mathbf{R}$ in Figure 5.14 indicated that immobile sand bed already existed in the bend pipe at the velocities above the 1.5 m/s MTV estimated for an equivalent horizontal pipe. The immobile sand bed is significant at sections P2 and P4 of the bend pipe.

Figures 5.15 and 5.16 present curves of $\mathbf{R}$ at 1.5 m/s and 1 m/s, velocities at the MTV estimated for horizontal pipe and below, respectively. It is observed that the **R**=0 in the pipe bottom region, $^{y}/_{D} \leq 0.15$ at all the pipe sections at the velocities of 1.5 m/s and 1m/s. The **R**-value is also zero at the pipe dip-exit, section-P3 where the liquid turbulence intensity has been observed to be favoured by the perturbation in the flow between section P2 and P3. This observation indicated that the sand-phase is immobile in the entire bend pipe bottom region at the 1.5 m/s and 1 m/s. The thickness of the region where the **R**=0 varies at the various pipe sections. The various thickness of the immobile sand zone indicated that moving and stationary sand beds of various thicknesses existed in the majority of the bend pipe sections, particularly at sections P1 and P4.

It should be noted that the frictional component of the inter-particles interactions of the sand phase is dominant at the pipe wall region, where **R**=0. It is observed that the fullness of the curves reduced as the thickness of the zone where particle frictional interactions increased, as evident in Figure 5.16. The interstitial liquid in the stationary sand bed region is stagnant as indicated by the **R**=0 for the liquid phase at the pipe bottom region. This observation indicated that the contributions of the liquid turbulence and the sand-phase translational-collisional stresses have reduced significantly at 1 m/s. The condition in the ±6^{o} bend pipe may be described as partial pipe blockage at the velocity range of 1.5 m/s and 1 m/s, considering the sand concentration at the pipe bottom in Figure 5.3 and the features of the curves of **R** at 1.5 and 1 m/s in Figures 5.15 and 5.16.

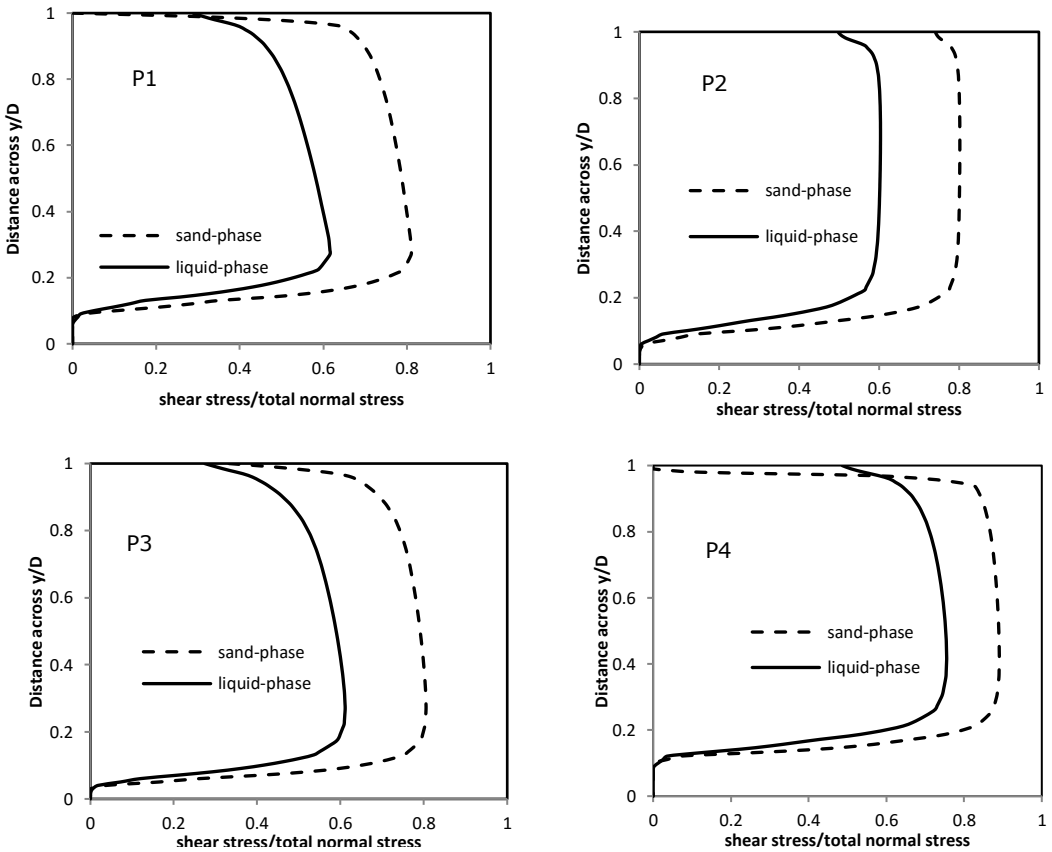

Figure 5.15: Curves of ratio of predicted sand and liquid phase stresses to the total stress in ±6° bend pipe sections at 1.5 m/s.

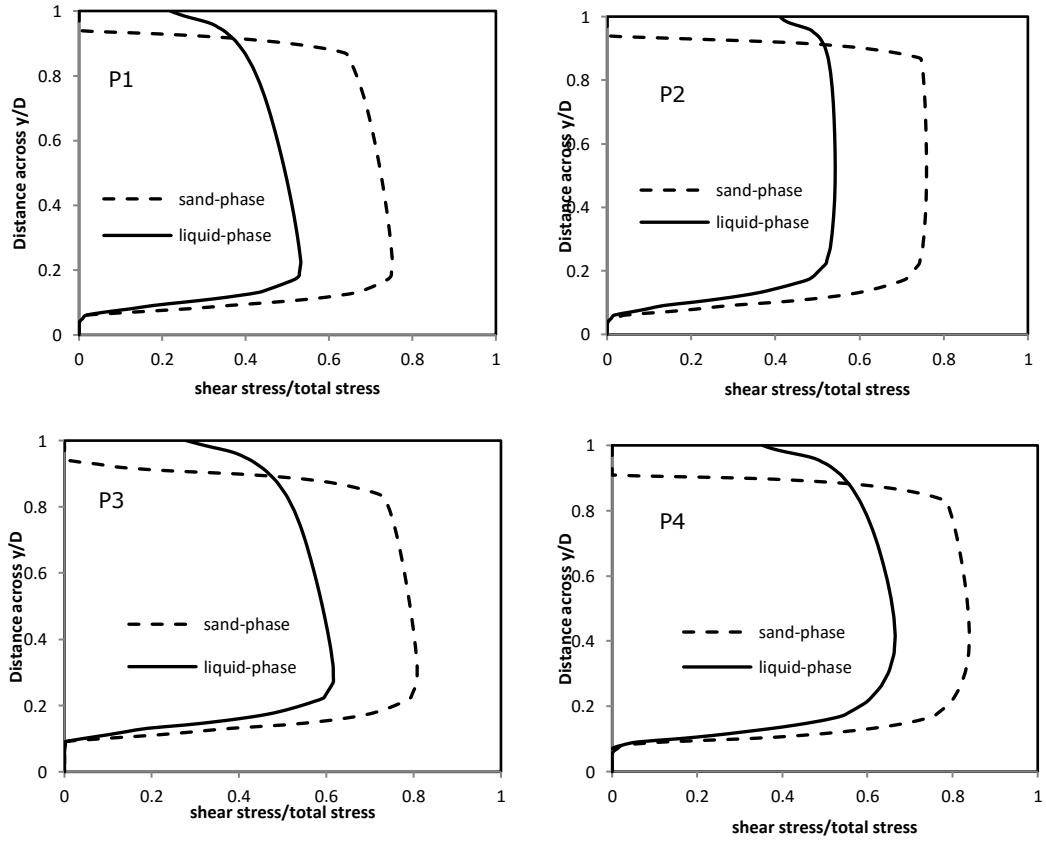

Figure 5.16: Curves of ratio of predicted sand and liquid phase stresses to the total stress in ±6° bend pipe sections at 1 m/s.

5.4 Parametric study

5.4.1 Pipe inclination angle effect

Figure 5.17 presents the effect of pipe inclination angle on immobile sand bed formation and the limit stationary sand bed velocity. The limit velocity corresponds to the minimum transport velocity (MTV) below which the onset of a stationary sand bed deposit formed in the pipe. Significant difference is observed in the predicted thickness of the stationary sand bed and MTV for the $\pm 6^0$, $\pm 4^0$ V-pipe and horizontal inclined pipes. It can be observed in Figure 5.17 that the predicted stationary sand bed in the $\pm 6^0$ bend pipe is ≈120% thicker than that of the $\pm 4^0$ bend pipe at 2.5 m/s, whereas the sand phase is completely mobile in the equivalent horizontal pipe at the 2.5m/s velocity. This observation indicated that the bend pipe angle and pipe inclination have significant effect on immobile sand deposit formation in pipes. The velocities at which the immobile sand bed formed in the bend pipes and the sand bed thickness observed in the $\pm 4^0$ and $\pm 6^0$ bend pipes indicated that for the $\pm 6^0$ bend pipe, MTV ≅ 3m/s, whereas for the $\pm 4^0$ bend pipe, 3m/s > MTV ≥ 2.5 m/s. However, for the equivalent horizontal pipe, 2 m/s > MTV ≥1.5m/s, as can be seen in Figure 5.17.

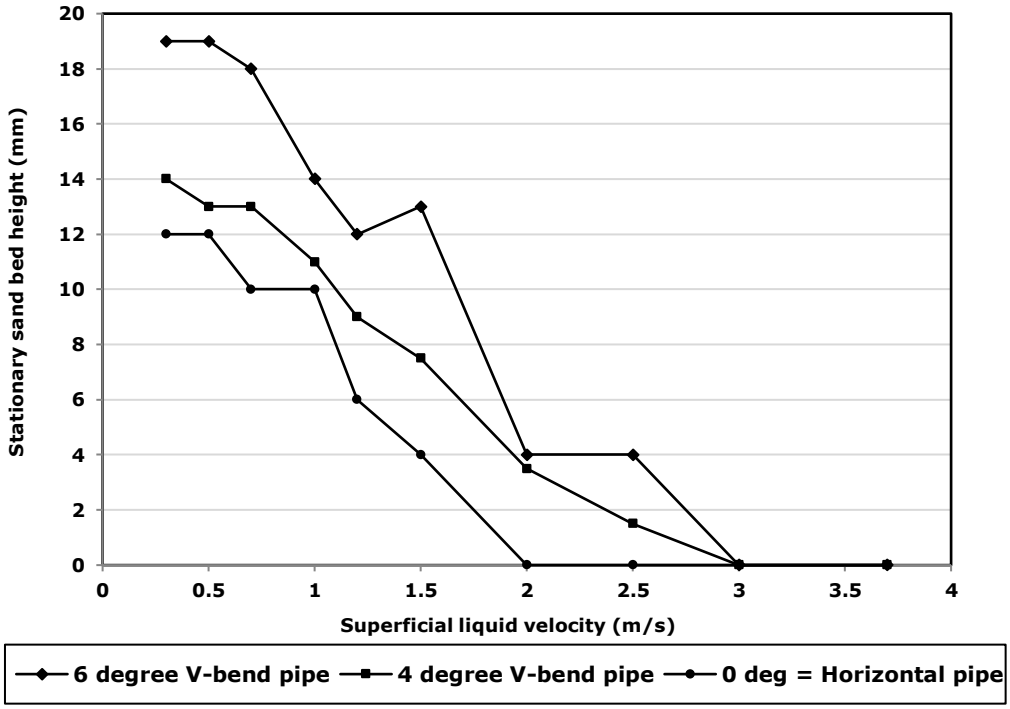

Figure 5.17: Effect of pipe angle on the limit stationary sand bed velocity (MTV)

5.4.2 Particle size effect

Figure 5.18 presents the dependence of MTV and stationary sand bed thickness on particle size, for 120 μm, 180 μm and 255 μm particle sizes. It is observed that the predicted MTV and stationary sand bed thickness are different for the different particle sizes. The MTV and stationary sand bed height increased as the particle size increased. This observation indicated that the smallest particles tend to follow the liquid phase more closely. Also, the MTV of 0.5 m/s predicted for the smallest, 120 μm particles is significantly less than the MTV of 3 m/s predicted for the largest particle of 255 μm,. The flow Reynolds number at 0.5 m/s is ≈17% of that at 3 m/s. The significant difference in the magnitude of Reynolds number at the MTV predicted for the 255 μm and 120 μm particle sizes indicated that larger driving force is required to sustain the motion of the 255 μm particles compared to the 120 μm particles. The larger driving force that is required to transport the 255 μm particle is evident in the considerable sand bed thickness predicted for the 255 μm particles compared to that of the 120 μm, as can be seen in Figure 5.18.

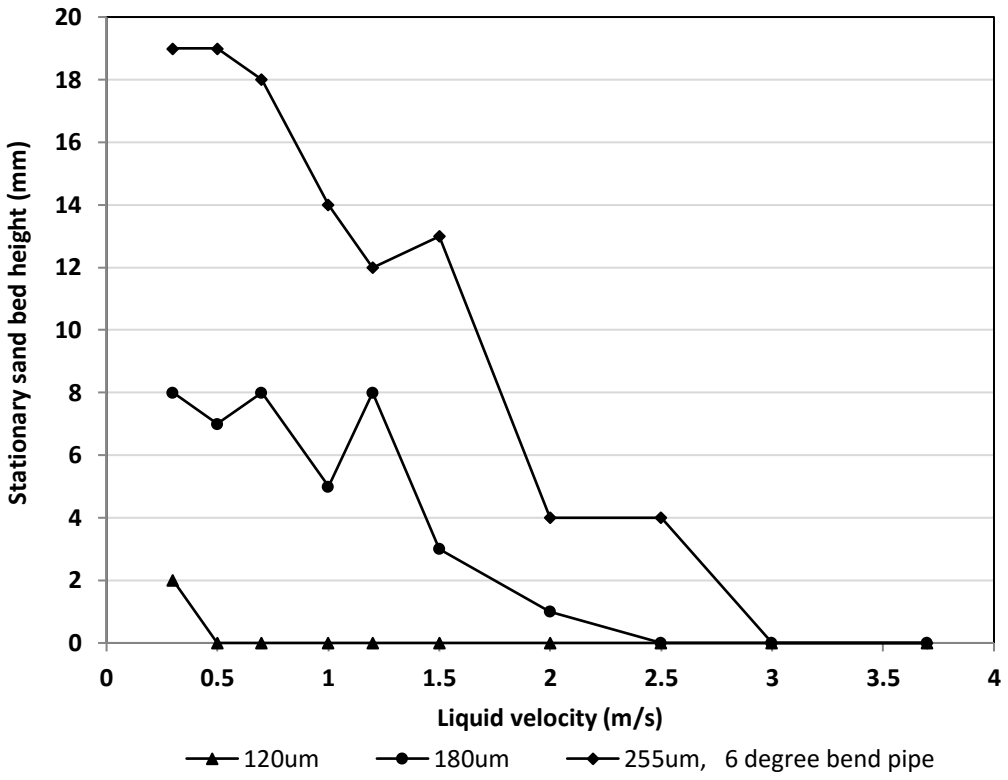

Figure 5.18: Effect of particle size on the limit stationary sand bed velocity (MTV)

An interesting feature observed in the predicted stationary sand bed height as the velocity is reduced is the counter-intuitive reduction in the bed height at certain velocity range, as can be seen between the range of velocity change from 1.5 - 1.2 m/s for the 255 μm particles and 1.2 - 0.5 m/s for 0.18mm particles in Figure 5.18. This feature suggested that a certain portion of the stationary sand bed yielded to the shear stress present above the stationary bed layer as the thickness of the bed layer developed into the shearing zone in the pipe lower half region, when the velocity is reduced. The presence of the sheared layer above the stationary bed is evident in the previous Figures 5.14 and 5.15, in which the zone of the **R**=0 for the liquid phase is slightly less than that for the sand phase at the bend pipe sections P2 at 2.5m/s and P4 at 1.5 m/s, respectively. Such feature observed in Figure 5.18 suggested the sand transport flow regime at certain velocity range may be characterised by sand dunes or moving sand bed layer on a stationary sand bed layer at the bottom of a pipe.

5.4.3 Pipe diameter effect

Figure 5.19 presents a comparison of the predicted stationary sand bed height and MTV for flow in $\pm 4^0$ bend pipes of 0.05 m and 0.1 m diameter pipe sizes with 255 μm particle size. The comparison indicated that the sand bed height in the larger pipe of 0.1 m diameter is significantly higher than that of the smaller pipe of 0.05 m diameter. The significant difference in the predicted stationary sand height in the pipes indicated that sand deposition rate is dependent on pipe size. Also, it can be observed in Figure 5.19 that the MTV in which the stationary sand bed formed in the larger pipe is $\cong$ 3 m/s, whereas that of the smaller pipe is $\cong$ 2 m/s. This observation suggested that stationary sand bed formed rapidly in the larger pipe compared to the smaller pipe, as the predicted MTV is higer for the larger pipe. The dependence of the sand bed height and MTV on pipe size may be best explained by the effect of the viscous sublayer thickness, δ, of the turbulent flow boundary layer in the pipes. The viscous sublayer corresponds to the region in the pipe bottom where the flow viscous effect is most dominant in a turbulent pipe flow (King, Fairhurst and Hill 2001).

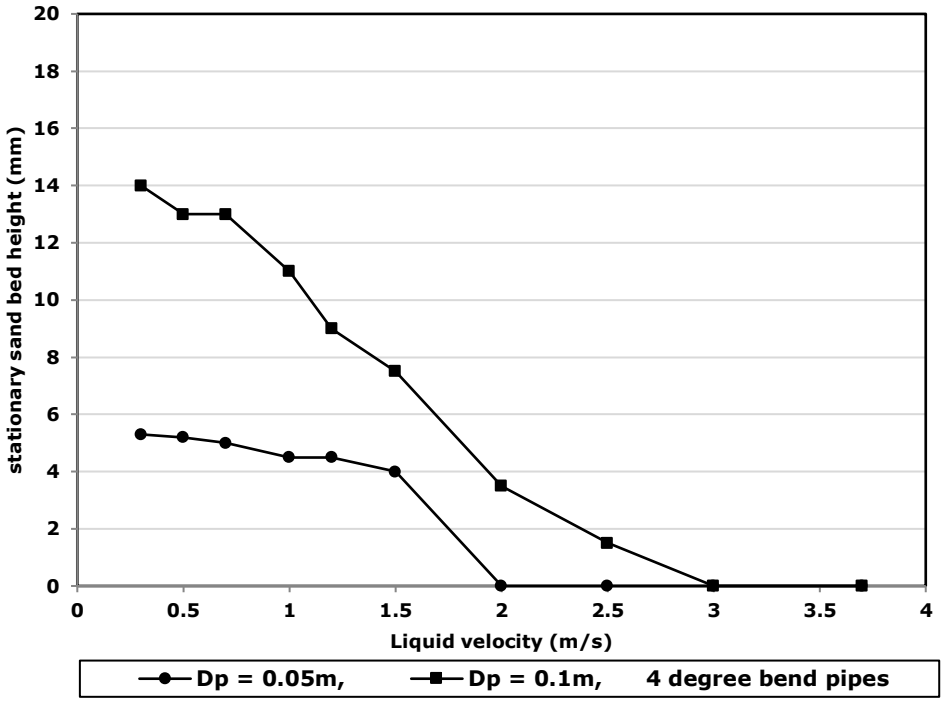

Figure 5.19: Effect of pipe size (D) on the limit stationary sand bed velocity (MTV)

The viscous sublayer height has been evaluated using, $\delta = 62\mathrm{D}(\mathrm{DV_l}\rho_l/\mu_l)^{-7/8}$ for Reynolds number below 10^7 (King, Fairhurst and Hill 2001). The evaluated viscous sublayer height for the 0.05 m and 0.1 m pipes are 100 micron and 170 micron ($\mu\mathrm{m}$), respectively, at velocity of 2.5 m/s. The 2.5 m/s velocity corresponds to the velocity at which the difference in the sand bed height in the pipes is observed, as can be seen in Figure 5.19. The evaluated sublayer thickness for the two pipes indicated that a thicker region is dominated by viscous effect in the larger pipe compared to the smaller pipe. Consequently, the velocity gradient at the bottom of the 0.05 m pipe is expected to be higher than that of the 0.1 m pipe, as evident in the profiles in Figure 5.20 (a), the region, $^{\mathrm{y}}/_{\mathrm{D}} \leq 0.1$, which the velocity profile of the smaller pipe is thinner.

The higher velocity gradient observed at the bottom of the smaller pipe indicated that the slip velocity, which represents the difference in the in-situ liquid and sand phase velocity $(V_l - V_s)$ is higher at the bottom of the smaller pipe compared to the bigger pipe, which is evident in Figure 5.20 (b). The larger slip velocity at the pipe bottom of the smaller pipe indicated that larger drag force acted on the sand particles at the bottom of the 0.05 m pipe than that of the 0.1 m pipe. Consequently more particles tend to follow the liquid phase in the bottom of the smaller pipe compared to the bigger pipe, which may have resulted in the higher sand bed height observed in the larger pipe at the same velocity.

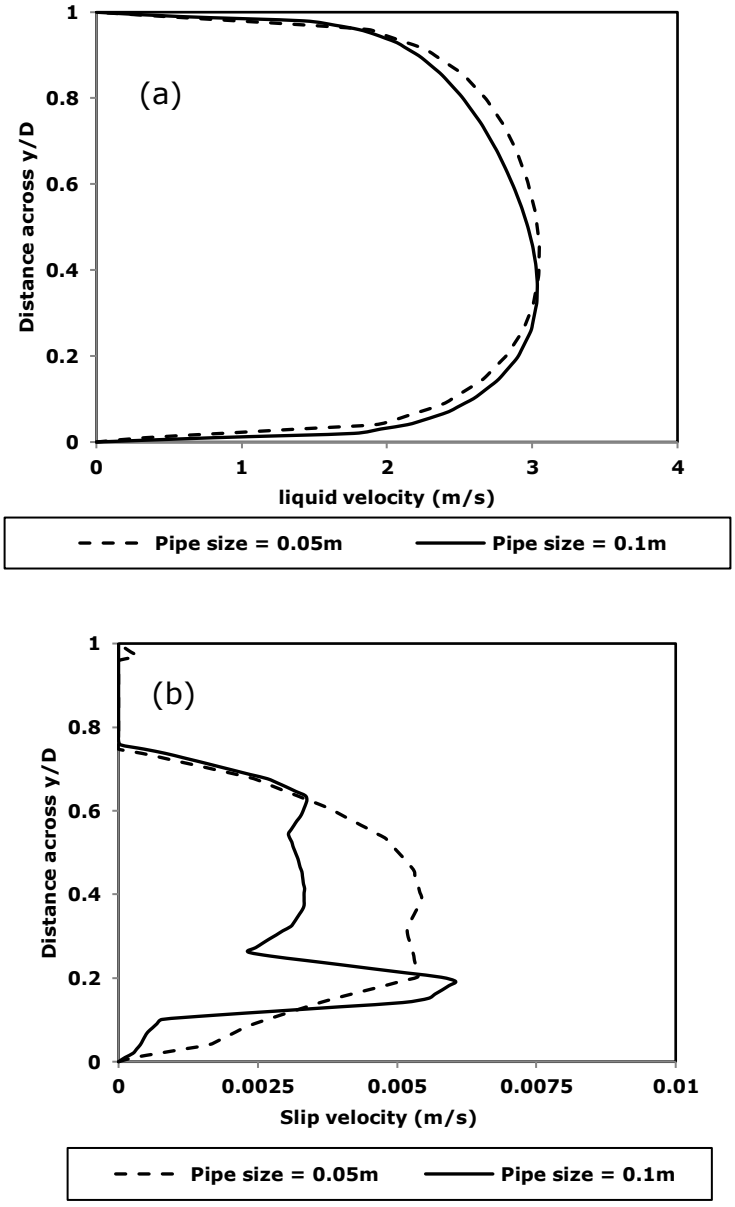

Figure 5.20: Effect of pipe size on sand deposition in pipe (a) single-phase liquid velocity profiles (b) slip velocity profiles

5.5 Conditions of stationary sand deposit in pipe bend

The stationary sand-bed flow regime is considered the most undesirable and severe flow regime that can impede fluid flow in pipelines. Therefore, it is considered important to examine all the possible modes of occurrence of immobile sand deposit in the pipe bend sections P1-P4. The modes include whether or not the sand-phase is stationary at a section, or at multiple sections of the pipe bend under a certain operating condition. The possible modes have been determined by the concept of factorial design of experimental, in which certain factors are used to determine the possible scenarios in a single experiment in order to examine all possible outcomes. The pipe sections P1, P2, P3 and P4 are the independent components in the present case, while the levels of possibilities of the presence of immobile sand phase in any of the pipe sections are defined by 'Yes' or 'No', which is determined by the R-value at region, $^{y}/_{D} = 0.05$ of the $\pm 6^{o}$ and $\pm 4^{o}$ V-inclined pipe bends. Therefore, the present case has four factors and two levels, which resulted to $2^4 = 16$ possible conditions of stationary sand deposit in the pipe bend. Tables 5.2 and 5.3 present the possible stationary sand bed conditions in $\pm 6^{o}$and $\pm 4^{o}$ pipe bends, respectively.

Although the design of experiment suggested that 16 possible conditions of stationary sand deposit formation may occur in the pipe bend sections. However, 6 of the conditions have been observed in the $\pm 6^{o}$ pipe bend and 7 conditions in the $\pm 4^{o}$ pipe bend investigated, as can be seen in Tables 5.2 and 5.3, respectively. The Tables show that the critical transport velocity to ensure complete sand transport without sand deposit in the 6 pipe bend is 3 m/s, but the velocity may be as low as 2.5 m/s for the $\pm 4^{o}$ pipe bend. The effect of the pipe curvature angle on turbulence intensity in the pipe bend is revealed by the condition code-8, which represents the presence of stationary deposit in the downward, dip and dip-exit of the pipe bend. The condition is observed in the $\pm 4^{o}$ pipe bend, but not observed in the $\pm 6^{o}$ pipe bend. This observation indicates that the turbulence energy at the dip-exit, P3 is enhanced with increase in pipe bend angle, as the sand is entrained by flow turbulence longer at the dip-exit of the $\pm 6^{o}$ pipe bend compared to the $\pm 4^{o}$ pipe bend. The condition code-16 which represents the presence of stationary sand deposit in the entire pipe bend is the most critical condition. The pipe may be described as completely plugged by sand deposit at the condition code-8. This condition will occur in the pipe bends when the flow velocity is $\leq$ 1.2 m/s

Table 5.2: Matrix of conditions for stationary sand deposit formation in $\pm 6^{o}$ V-inclined Pipe bend

Condition code	$R = 0$ at $^{y}/_{D} = 0.05$ of the bend pipe				Velocity range (m/s)	Comment
	P1	**P2**	**P3**	**P4**		
1	No	No	No	No	3.7-3	Mobile sand phase throughout pipe bend
2	Yes	No	No	No	< 3-2.5	stationary sand deposit at the downhill section
3	No	Yes	No	No	-	Unobserved condition
4	Yes	Yes	No	No	< 3-2	Stationary sand deposit at the downhill and dip sections
5	No	No	Yes	No	-	Unobserved condition
6	Yes	No	Yes	No	-	Unobserved condition
7	No	Yes	Yes	No	< 0.3	Plugged pipe-dip
8	Yes	Yes	Yes	No	-	Unobserved condition
9	No	No	No	Yes	-	Unobserved condition
10	Yes	No	No	Yes	-	Unobserved condition
11	No	Yes	No	Yes	-	Unobserved condition
12	Yes	Yes	No	Yes	1.5	Mobile sand phase at the dip-exit towards upward inclined pipe bend section
13	No	No	Yes	Yes	-	Unobserved condition
14	Yes	No	Yes	Yes	-	Unobserved condition
15	No	Yes	Yes	Yes	-	Unobserved condition
16	Yes	Yes	Yes	Yes	1.2-0.3	Stationary sand deposit throughout the pip bend Plugged pipe condition

Table 5.3: Matrix of conditions for stationary sand deposit formation in $\pm 4^{o}$ V-inclined Pipe bend

Condition code	$R = 0$ at $^{y}/_{D} = 0.05$ of the bend pipe				Velocity range (m/s)	Comment
	P1	**P2**	**P3**	**P4**		
1	No	No	No	No	3.7-2.5	Mobile sand phase throughout pipe bend
2	Yes	No	No	No	2	stationary sand deposit at the downhill section
3	No	Yes	No	No	-	Unobserved condition
4	Yes	Yes	No	No	< 2-1.2	Stationary sand deposit at the downhill and dip sections
5	No	No	Yes	No	-	Unobserved condition
6	Yes	No	Yes	No	-	Unobserved condition
7	No	Yes	Yes	No	< 0.3	Plugged pipe-dip
8	Yes	Yes	Yes	No	1.2	Stationary deposit at the downward, dip and dip exit
9	No	No	No	Yes	-	Unobserved condition
10	Yes	No	No	Yes	-	Unobserved condition
11	No	Yes	No	Yes	-	Unobserved condition
12	Yes	Yes	No	Yes	1.5	Mobile sand phase at the dip-exit in upward inclined pipe bend section
13	No	No	Yes	Yes	-	Unobserved condition
14	Yes	No	Yes	Yes	-	Unobserved condition
15	No	Yes	Yes	Yes	-	Unobserved condition
16	Yes	Yes	Yes	Yes	1-0.3	Stationary sand deposit throughout the pip bend Plugged pipe condition

5.6 Discussion of results

The results presented in the preceding sections show that the seemingly small V-inclined pipe bend angles of $\pm 4^0$ - $\pm 6^0$ significantly influence sand transport in pipes differently from that of horizontal pipes. The findings show the dependence of concentration of sand deposit, streamwise pressure gradient, turbulence intensity and critical transport velocity on pipe inclination. The figures 5.6 and 5.7 clearly show that bend pipe curvature induces vortex-like force on flow and imbalance pressure gradient in the dip region of V-inclined bend pipes. The other parameters that strongly affect sand deposition in pipes are the degree of pipe bend angle, pipe size and particle size, as shown in Figures 5.17, 5.18 and 5.19. The turbulence modulation result in Figure 5.11 provides a clear view of how turbulence activity in bend pipes is different from that of horizontal pipes.

There is a big difference in the formation of stationary sand bed in the downward and upward sections of the pipe bends. At velocities above the estimated MTV for an equivalent horizontal pipe, immobile sand bed formed at the downward section into the dip section of the bend pipe, prior to that of the upward section of the pipe. This observation agrees with the observation reported in previous study by Stevenson and Thorpe (1999), which mentioned that downward inclined flowline is more susceptible to sand deposition than upward inclined flowline. Therefore, it can be said that the sand-phase is stratified in the flow in the downward section of the bend pipe, whereas most of the sand is entrained in the flow at the upward section towards the downstream of the pipe where the turbulence energy dissipated. The study by Tippet and Priestman (1997) also reported similar observation in sand deposition in their experimental study of solids transport in a low angle pipe bend, which is similar to the pipe bend of the present study.

The upward section of the bend pipe is favoured by the secondary vortices and perturbation from the pressure imbalance formed at the vicinity of the dip, which enhanced sand entrainment in the upward section. The experimental study on sand transport in elbow pipe by Kesena et al. (2014) also reported the presence of additional forces in bend pipe that are not present in straight pipe, which acted on solid particles and multiphase fluids, due to secondary vortices in the pipe elbow. The presence of the forces in V-inclined pipes due to the pipe curvature are indications of additional phenomena in bend pipe that are not present in other forms of inclined pipe, which play varying degree of role in sand transport in bend pipes.

The forces observed in bend pipes are the critical factors that differentiate sand transport characteristics in V-inclined bend pipes from other forms of inclined pipes. Therefore, the results of the present study provide evidences that suggest that it is important to distinguish the implications of V-inclined bend pipes from those of other forms of inclined pipes when mitigation strategies for solids deposition in pipelines are being developed, particularly in the design of offshore subsea petroleum pipelines, in which V-inclined bend pipe sections are inevitable due to seabed undulations. The inexact generalization of the characteristics of sand transport in low angle V-inclined bend pipes with those of other forms of inclined pipes may be attributed to the classifications of inclined pipes in research investigations in solids transport and the intricate nature of the flow phenomena that differentiate the flow in V-inclined pipes from other forms of inclined pipes.

The previous studies by Danielson (2007) and Al-Lababidi, Yan and Yeung (2012) concluded that critical transport velocity for liquid-solids flow has no dependence on the seemingly small inclined pipe angles. It should be noted that these studies investigated sand transport in inclined pipes by treating the downward and upward inclined pipe sections as separate standalone inclined pipe sections. Conversely, these inclined pipes rarely exist as separate standalone pipe sections in subsea petroleum pipelines, but usually as V-inclined bend pipe sections. In addition, most of the studies on solids transport in inclined pipes are based on experimental method. This method may not easily provide sufficient evidences that reveal the additional intricate forces present in bend pipes; the underlying intricate physical phenomena may be obscured.

Computational fluid dynamics method if correctly performed provides the benefit of revealing the localized flow properties that are unique to V-inclined bend pipe flows, as evident in the results of the present study. The literatures with such evidences of the forces present in V-inclined bend pipe of the seemingly small angles are scarce. The knowledge of the local intricate forces in bend pipes is necessary to advance the science of solids transport in pipes and predictions of the flow characteristics in more complex inclined pipes. As with most numerical modelling studies, relevant assumptions have been made in the present study in order to focus on key parameters, given the wide range of parameters in a typical petroleum pipeline system. The sand particles are treated as mono-size particles and the investigation focused on a liquid-solids system.

The typical petroleum systems usually contain liquid hydrocarbon and produced gas phase in addition to the solids phase, which is usually sand of varying particle size. However, the primary consideration of pipeline design is to ensure the solid particles, which usually reside in the liquid phase do not settle at the pipe bottom to form stationary solids bed. Therefore, the knowledge of the forces such as the multi-phase turbulence kinetic energy presented in Figure 5.10, which is required to keep the solids in motion in the liquid-phase is very relevant. The intricate physics of sand transport in petroleum systems is very dynamic and the numerical modelling of the entire flow phenomena is very difficult. The difficulties manifested mainly as an impossibility to obtain converged solution of the iterative process in the 3D calculations, which posed some limitations in the present study. A number of effective approaches were developed in efforts to obtain realistic results, which include mesh refinement and extensive validation of the numerical models capable of accounting for the important flow properties.

The identification of the various sand transport regimes with less subjectivity posed enormous challenges. The dynamic nature of the transport mechanisms in sand transport and the varying role played by several parameters in sand transport flow regimes are factors responsible for the subjectivity in recognition of solids transport regimes. The sand concentration profiles steepness and the **R**-value evaluated from the stress distribution ratio in the pipe as demonstrated in the results, provide useful guide in the flow regime recognition, particularly in

recognition of the flow regimes when solids contact load is dominant, which is attributable to the moving bed and stationary bed flow regimes.

The stationary sand-bed flow regime is regarded as the most undesirable flow regime, which can impede hydrocarbon flow in pipelines. The findings in the parametric study show that the V-inclined bend pipe increases the critical transport velocity required to limit stationary sand bed formation in pipes when compared to that for a horizontal pipe. The results also show that the minimum sand transport velocity (MTV) depends on a wide range of parameters. The pipe size (D) is arguably a parameter that is common to all the existing correlations for predicting solids MTV. The result in Figure 5.20 provides the evidence of the key factors responsible for the dependence of MTV on pipe size. The knowledge of the identified factors is important to improve the precision of pipe sizing for solids transport and MTV correlations.

Chapter 6

Conclusions and Recommendations for Future

6.1 Conclusions

A 3D computational fluid dynamics (CFD) model has been developed in Eulerian-Eulerian methodology with kinetic theory of granular flow to investigate sand transport in turbulent pipe flow. The CFD model predictions have been validated with published experimental data. The good agreement between the CFD model predictions and the experimental data shows that the treatment of the solids-phase turbulence kinetic energy in addition with the transport equation for the turbulence kinetic energy of the liquid phase is essential for modelling the various liquid-solids transport flow regimes. The CFD model takes into account the co-existence of inter-particle collisional-frictional interactions to represent the intermediate-heterogeneous conditions of solids transport flow regime. The following important conclusions have been drawn from the present study:

1. The finite volume CFD simulation method has the capability to produce realistic data of local solids concentration distribution, liquid and solids velocities, pressure, turbulence kinetic energy in the transport of solids in liquid in pipelines, where measurement of such local quantities may be impossible. Such data are useful for pipe designers to visualize the local conditions in pipelines, to understand how solids transport rate changes as operating conditions vary and inform the design process. The analysis and interpretation of numerical data require relevant expertise to reveal the significant underlying physical phenomena relevant to defined hypotheses.

2. The Eulerian-Eulerian approach with the kinetic theory of granular flow constitutive relations treatment of liquid-solids flow enables a complete coupling of all the possible interactions between the phases and the drag force acting on the solids-phase attributable to the various sand transport flow regimes in pipes. Turbulent dispersion force plays important role in accuracy of prediction of solids deposition for the range of particle size

investigated. For modelling the pseudo-homogeneous sand transport regime, omission of the particle-phase turbulence kinetic energy may be a valid approximation, whereas in heterogeneous transport regime in which significant sand stratification exists, the particle phase turbulence is of great importance. Therefore, extensive validation of CFD predictions for the various sand transport flow regimes is imperative.

3. The sand transport characteristics and MTV are strongly dependent on the seemingly small V-inclined bend pipes investigated. The results show that slight bend pipe curvatures of subsea petroleum pipelines may cause adverse pressure surge and partial pipe blockage in certain sections of the pipelines at relatively high velocity due to positive streamwise pressure gradient and formation of unexpected stationary sand deposit at the vicinity of pipe dips. The shear stress analysis provides a quantitative criterion for identification of stationary sand deposit formation and estimation of obstructive sand bed height at the bottom of pipes.

4. The correlations for predicting minimum sand transport velocity (MTV) developed based on data obtained from horizontal pipe and other forms of inclined pipe may be inaccurate for predicting the limit sand deposit velocity in V-inclined bend pipe sections. The threshold velocity to keep sand entrained in liquid in V-inclined bend pipe is significantly higher than that for horizontal pipes. Therefore, it is important for researchers and operators of petroleum pipelines to know the limitations of a correlation used for the solids MTV predictions.

5. The results show that optimum pipe diameter may be selected to minimize solids settling in pipelines based on the knowledge of flow boundary layer. Generally, the build-up of stationary sand deposit is more likely if pipe size is too large, because the viscous sublayer which traps particulate solids is thicker in larger pipes compared to smaller pipes, as evident in the parametric study results presented. Therefore, the size of multiphase pipelines in which solids is transported should be specified by considering the smallest size that will contain the product and as well sustain a predetermined transport velocity which will keep the solids in continuous motion in the pipeline.

6. The importance of having an accurate MTV correlation for solids transport in low angle pipe bends is evident in the mode of stationary sand formation predicted for the $\pm 4^{o}$ and $\pm 6^{o}$ V-inclined pipe bends, as summarized in the condition matrix in Table 5.2 and 5.3. It can be said that the critical sand transport velocity that prevents stationary sand deposit in horizontal pipe may be that at which plugged pipe condition may exist in pipe bend sections of undulating pipelines. Therefore, a predetermined critical sand transport velocity in which the effect of the pipe bends section has been incorporated will enable unhindered flow through pipe bend sections and the entire sections of long undulating pipelines such as subsea petroleum pipelines.

7. The mode of turbulence modulation in bend pipe suggests that flow impingement on pipe wall is likely at the inner surface of the bend pipe section where sand entrainment is favoured by turbulence intensity at high velocity. The implication of such phenomenon may be related to rapid pipe wear at the upper pipe wall of bend pipe dip exit.

6.2 Recommendations for future work

The following recommendations for future research work have been identified from the presents study:

1. The possibility of flow impingement in pipe bends has been inferred by the result in the present study. The implication of the flow impingement may be related to pipe erosion induced by particle-impact. Therefore, the findings in the present study provide a relevant base for future research study to investigate the effects of low angle pipe bend on erosion of subsea multiphase pipelines.

2. The modelling of the pipe near-wall boundary conditions for particles-wall collision still posed a major problem. The description of particle-wall collision depends on several parameters such as the wall restitution coefficient and specularity coefficient whose values in turn depend on specific properties of the particles and the pipe, as has been experienced in the course of the present study. To effectively account for these parameters, a wide range of particle properties and pipe wall properties must be investigated. Therefore, more focused research on the particles-wall collision characteristics is imperative to improve the understanding and accuracy of predictions of particle-wall boundary conditions in pipe flows.

3. The solids transport investigated in the present study is relatively dominated by collisional and frictional inter-particles interactions, which exhibit particles-phase turbulence. Although, some of the implications of the solids phase turbulence energy on solids deposition in pipes have been revealed in the test cases of the present study. However, the detailed influence of the molecular multiphase turbulence interaction may be more complicated than have been observed. Probably, a more detailed high-resolution numerical investigation would provide better insight of how the different phase turbulent energy influences solids transport of relatively medium particle size and low solids concentration.

4. The sub-models in CFD codes such as those of the Eulerian-Eulerian multiphase models and the kinetic theory of granular flow constitutive relations are developed based on certain assumptions. A key challenge in the application of the model codes for solids transport multiphase pipe flow modelling is the wide range of spatial and time scales encountered in solids transport in turbulent pipe flows. For example, the KTGF models become less valid as the particles collision and enduring contact interaction increase. Although, the frictional models developed based on soil mechanics study provides a reasonable approximate description of the frictional stress. However, the models are very empirical, which may be limited in certain conditions and require extensive validation to be applied correctly. Therefore, more fundamental and experimental research studies, which cover a wider range of condition are needed to reduce the inherent uncertainties in some of the models and provide a platform for development of more CFD codes for wider applications.

5. The development of accurate MTV correlation for predicting sand critical transport velocity requires sufficient data. Therefore, more CFD studies which account for the detailed intricate physics of sand transport characteristic in low angle pipe bends are required in order to generate sufficient data base in which predictive correlation for sand transport and sand transport flow regimes in low angle V-inclined bend pipes can be developed.

References

AL-SAFRAN, E. et al 2005. Investigation of slug flow characteristics in the valley of a hilly-terrain pipeline. *International Journal of Multphase Flow*, 31(3), pp. 337-357.

ALBION, K. et al., 2007. Flow regime determination in horizontal pneumatic transport of fine powders using non-intrusive acoustic probes. *Journal of Powder technology,* 172, pp. 157-166.

ALEXANDRE, R. G., and RASTEIRO, M. G., 2001. Pipe flow of solid-liquid suspensions with a broad size range. *Proceedings of International Congress for Particle Technology.* 27-29 March 2001. pp. 3-8.

AL-LABABIDI, S., YAN, W., and YEUNG, H., 2012. Sand transportations and deposition characteristics in multiphase flows in pipelines. *Journal of Energy Resources Technology*. 134, pp. 1-13.

ANDERSSON, B., ANDERSSON, R., HÅKANSSON, L., MORTENSEN, M., SUDIYO, R. and VAN WACHEM, B., 2012. *Computational fluid dynamics for engineers*. New York: Cambridge University Press.

ANDRZEJ, A.K. and SUSAN, E.L., 2001. Emergence of flow assurance as a technical discipline specific to deepwater: Technical challenges and integration into subsea system engineering. *Offshore Technology Conference, OTC 13123*. 30 April-3 May, 2001: Houston, Texas, USA.

ANSYS, F., 2012. Fluent 14.0 Documentation. *Lebanon, NH: ANSYS Inc*.

ANTAYA, C.L., ADANE, K.F.K. and SANDERS, R.S., 2012, July. Modelling Concentrated Slurry Pipeline Flows. In *ASME 2012 Fluids Engineering Division Summer Meeting collocated with the ASME 2012 Heat Transfer Summer Conference and the ASME 2012 10th International Conference on Nanochannels, Microchannels, and Minichannels* pp. 1659-1671. American Society of Mechanical Engineers.

AZIZ AL, A. I. and MOHAMED, H. I., 2013. A study of the factors affecting transporting solid-liquid suspension through pipelines. *Scientific Research Open Journal of fluid dynamics*, 3, pp. 152-162.

BAGNOLD, R.A., 1956. The flow of cohesionless grains in fluids. *Philosophical Transactions of the Royal Society of London A: Mathematical, Physical and Engineering Sciences*, *249*(964), pp.235-297.

BARTOSIK, A., 2010. Influence of Coarse-Dispersive Solid Phase on the 'Particles-Wall'Shear Stress in Turbulent Slurry Flow with High Solid Concentration. *Archive of Mechanical Engineering*, *57*(1), pp.45-68

BELLO, K. O., OYENEYIN, M. B. and OLUYEMI, G. O., 2011. Minimum transport velocity models for suspended particles in multiphase flow revisited. *Proceeding of the Society of Petroleum Engineers Annual Technical Conference and Exhibition SPE 147045*. 30 October -2 November 2011. Denver, Colorado. pp. 1-10.

BELLO, O. O., REINICKE, K. M., and TEODORIU, C. T., 2006. Experimental study on particle behaviour in simulated gas-oil-sand multiphase production and transfer operations. *Proceedings of the ASME Joint US-European Fluids Engineering Summer Meeting*. 17-20 July. Miami, Florida. pp. 1-8.

BELLO, O. et al., 2011. A mechanistic model for predicting and optimising oil-sand flow in horizontal wells. *Oil and Gas Technology,* 66(6), pp. 979-989.

BENYAHIA, S., SYAMLAL, M. and O'BRIEN, T.J., 2005. Evaluation of boundary conditions used to model dilute, turbulent gas/solids flows in a pipe. *Powder Technology*, *156*(2), pp.62-72.

BRENNEN, C.E., 2005. *Fundamentals of multiphase flow*. Cambridge University Press.

BURNS, A.D., FRANK, T., HAMILL, I. and SHI, J.M., 2004. The Favre averaged drag model for turbulent dispersion in Eulerian multi-phase flows. In *5th international conference on multiphase flow, ICMF*. May 2004. Volume. 4, pp. 1-17.

CAPECELATRO, J. and DESJARDINS, O., 2013. An Euler–Lagrange strategy for simulating particle-laden flows. *Journal of Computational Physics*, *238*, pp.1-31.

CAPECELATRO, J., PEPIOT, P. and DESJARDINS, O., 2015. Numerical investigation and modeling of reacting gas-solid flows in the presence of clusters.*Chemical Engineering Science*, *122*, pp. 403-415.

CHAPMAN, S. and COWLING, T.G., 1970. *The mathematical theory of non-uniform gases: an account of the kinetic theory of viscosity, thermal conduction and diffusion in gases.* Cambridge university press.

CHEMIOUL, S. N., CHAIB, K., and MOSTEFA, K., 2009. Simultaneous measurement of solid particles velocity and concentration profiles in two phase

flow by pulsed ultrasonic Doppler velocimetry. *Journal of the Braz. Soc. of Mech. Sci. and Eng.* 31(4), pp. 333-343.

CHOONG, K. W. et al., 2014. A comparative study of sand transport modelling for horizontal multiphase pipeline. *Research Journal of Applied Science and Technology*, 7(6), pp. 1017-1024.

CROWE, C.T., TROUTT, T.R. and CHUNG, J.N., 1996. Numerical models for two-phase turbulent flows. *Annual Review of Fluid Mechanics*, *28*(1), pp.11-43.

CUSICK, D. 2013. Global demand for fossil fuel continues to rise. *ClimateWire.* E&E Publishing, LLC Report, October 25. Available from: http://www.eenews.net/stories/1059989393 [Accessed 31st March 2014]

DABIRIAN, R., MOHAN, R.S., SHOHAM, O. and KOUBA, G., 2015, September. Sand Transport in Stratified Flow in a Horizontal Pipeline. In *SPE Annual Technical Conference and Exhibition*. Society of Petroleum Engineers.

DANIELSON, T. J., 2007. Sand transport modelling in multiphase pipelines. *Proceedings of the Offshore Technology Conference, OTC 18691.* 30 April-3 May 2007. Houston, Texas. pp. 1-11.

DAVIES, J. T., 1987. Calculation of critical velocities to maintain solids in suspension in horizontal pipes. *Journal of Chemical Engineering Science*, 45(7), pp. 1667-1670.

DE HENAU, V. and RAITHBY, G.D., 1995. A study of terrain-induced slugging in two-phase flow pipelines. *International journal of multiphase flow*, *21*(3), pp.365-379.

DORON, P., and BARNEA, D., 1996. Flow pattern maps for solid-liquid flow in pipes. *International Journal of Multiphase Flow*, 22(2), pp. 273-283.

DORON, P. and BARNEA, D., 1995. Pressure drop and limit deposit velocity for solid-liquid flow in pipes. *Chemical Engineering Science*, 50(10), pp. 1595-1604.

DORON, P., and BARNEA, D., 1993. A three-layer model for solid-liquid flow iin horizontal pipes. *International Journal of Multiphase Flow*, 19(6), pp. 1029-1043.

DORON, P., GRANICA, D. and BARNEA, D., 1987. Slurry flow in horizontal pipes-experimental and modelling. *International Journal of Multiphase Flow*, 13(4), pp. 535-547.

DOAN, Q., et al., 1996. Simulation of sand transport in a horizontal well. *Proceedings of the SPE International Conference on Horizontal Well Technology*. SPE 37106. 18-20 November. pp. 581-593.

DURAND, R., 1953. Basic relationships of the transportation of solids in pipes experimental research. *Proceedings Minnesota International Hydraulics Convention*, pp. 89-103.

DREW, D. 1983. Mathematical modelling of two-phase flow. *Annual Reviews of Fluid Mechanics*. 15, pp. 261-291.

ELGHOBASHI, S., 1991. Particle-laden turbulent flows: direct simulation and closure models. *Applied Scientific Research*, *48*(3-4), pp.301-314.

El-SEBAKHY, E.A., 2010. Flow regimes identification and liquid-holdup prediction in horizontal multiphase flow based on neuro-fuzzy inference systems. *Mathematics and Computers in Simulation*, *80*(9), pp.1854-1866.

ENWALD, H., PEIRANO, E. and ALMSTEDT, A.E., 1996. Eulerian two-phase flow theory applied to fluidization. *International Journal of Multiphase Flow*, *22*, pp.21-66.

ERGUN, S., 1952. Fluid flow through packed columns. *Chem. Eng. Prog.*, *48*, pp.89-94.

ESKIN, D., 2012. A simple model of particle diffusivity in horizontal hydrotransport pipelines. *Journal of Chemical Engineering Science*, 82, pp. 84-94.

EKAMBARA, K., SANDERS, R.S., NANDAKUMAR, K. and MASLIYAH, J.H., 2009. Hydrodynamic simulation of horizontal slurry pipeline flow using ANSYS-CFX. *Industrial & Engineering Chemistry Research*, *48*(17), pp.8159-8171.

EWIDA, A.A., HURLEY, S.J., EDISON, S.H. and TEH, C.E., 2004. Shallow to deepwater facilities and flow assurance challenges in offshore newfound land. *The International Society of Offshore and Polar Engineers*, Tuolone, France. May 23-28.

FARAJ, Y., WANG, M. and JIA, J., 2015. Automated horizontal slurry flow regime recognition using statistical analysis of the ERT signal. *Procedia Engineering*, *102*, pp.821-830.

GIDASPOW, D., 1994. *Multiphase flow and fluidization: continuum and kinetic theory descriptions*. Academic press.

GIGUERE, R. et al., 2008. Characterization of slurry flow regime transitions by ERT. *Chemical Engineering Research and Design*, 86, pp. 989-996.

GIGUERE, R. et al., 2009. Analysis of slurry flow regimes downstream of a pipe bend. *Chemical Engineering Research and Design*, 87, pp. 943-950.

GILLIES, R. G. et al., 2000. Deposition velocities for Newtonian slurries in turbulent flow. *The Canadian Journal of Chemical Engineering*, 78, pp. 704-708.

GIILLIES, R. G., MCKIBBEN, M. J., and SHOOK, C. A., 1996. Flow of sand-water mixtures at velocities below the deposition condition. *Journal of Particulate Science and Technology*, 14(4), pp. 293-314.

GILLIES, R. G., SHOOK, C. A., and XU, J., 2004. Modelling heterogeneous slurry flows at high velocities. *Canadian Journal of Chemical Engineering*, 82(5), pp. 1060-1065.

GILLIES, R. G., and SHOOK, C. A., 2000. Modelling high concentration settling slurry flows. *Canadian Journal of Chemical Engineering*, 74(4), pp. 709-716.

GILLIES, R.G. and SHOOK, C.A., 1994. Concentration distributions of sand slurries in horizontal pipe flow. *Particulate science and technology*, *12*(1), pp.45-69.

GOHARZADEH, A., RODGERS, P. and WANG, L., 2013. Experimental Characterization of Slug Flow on Solid Particle Transport in a 1 Deg Upward Inclined Pipeline. *Journal of Fluids Engineering*, *135*(8), p. 081304.

GORE, R.A. and CROWE, C.T., 1989. Effect of particle size on modulating turbulent intensity. *International Journal of Multiphase Flow*, *15*(2), pp. 279-285.

GUZMAN, J. E. V. and ZENIT, R., 2011. Application of the euler-lagrange method to model developed hydrodynamic slugs in conduits. *Journal of fluids engineering,* 133, pp. 1-9.

HASHEMI, S. A. et al., 2014. Solid velocity and concentration fluctuations in highly concentrated liquid-solids (slurry) pipe flows. *International Journal of Multiphase Flow*, 66, pp. 46-61.

HERNANDEZ, F. H., BLANCO, A. J., and SOLORZANO, L. R., 2008. Cfd modelling of slurry flows in horizontal pipes. *Proceedings of the 2008 ASME Fluids Engineering Conference*. 10-14 August 2008. Jacksonville, Florida. pp. 1-7.

HILL, A. L. et al., 2011. Critical liquid velocities for low concentration transport. *Proceedings of the ASME-JSME-KSME Joint Fluids Engineering Conference*. 24-29 July 2011. Hamamatsu, Shizouka. pp. 1-6.

HILTUNEN, K. et al. 2009. Multiphase flow dynamics. *Theory and Numerics. Tech. Rep*, *722*.

HUANG, S., ZHANG, B., LU, J. and WANG, D., 2013. Study on flow pattern maps in hilly-terrain air–water–oil three-phase flows. *Experimental Thermal and Fluid Science*, *47*, pp.158-171.

HUNT, J.N., 1954, July. The turbulent transport of suspended sediment in open channels. In *Proceedings of the Royal Society of London A: Mathematical, Physical and Engineering Sciences*, 224 (1158) pp. 322-335.

IBARRA, R., MOHAN, R.S. and SHOHAM, O., 2014. Critical sand deposition velocity in horizontal stratified flow. In *SPE International Symposium and Exhibition on Formation Damage Control*. February. Louisiana, USA.

INTERNATIONAL ENERGY AGENCY, 2015. *Secure sustainable together: world energy outlook*. Paris: OECD/IEA

ISHII, M. and HIBIKI, T., 2011. *Thermo-fluid dynamics of two-phase flow*. 2nd ed. New York, NY: Springer.

ISSA, R. I., and KWEMF, M. H. W., 2003. Simulation of slug flow in horizontal and nearly horizontal pipes with the two-fluid model. *International Journal of Multiphase Flow*, 29, pp. 69-95.

ISSA, R.I. and OLIVEIRA, P.J., 1997. Assessment of a particle-turbulence interaction model in conjunction with an Eulerian two-phase flow formulation. *Turbulence, Heat and Mass Transfer*, *2*, pp. 113-120.

ISSA, R.I. and OLIVEIRA, P.J., 1993. Modelling of turbulent dispersion in two phase flow jets. *Engineering turbulence modelling and experiments*, *21993*, pp.947-957.

JAKOBSEN, H.A., 2014. *Chemical Reactor Modeling. Multiphase Reactive Flows*, 2nd ed. Berlin, Germany: Springer-Verlag.

JAYARAJU, S.T., SATHIAH, P., ROELOFS, F. and DEHBI, A., 2015. RANS modelling for particle transport and deposition in turbulent duct flows: Near wall model uncertainties. *Nuclear Engineering and Design*, *289*, pp. 60-72

JAYAWARDENA, S., DYKHNO, L. and HUDSON, J., 2002. Challenges in pigging of subsea gas flowlines. Society of Petroleum Engineers Annual Technical Conference *SPE*, *77576*. 29 Sept – 2 Oct. San Antonio.

JENKINS, J. and SAVAGE, S.B., 1983. A theory for the rapid flow of identical, smooth, nearly elastic, spherical particles. *Journal of Fluid Mechanics*, *130*, pp. 187-202.

JOHNSON, P.C., NOTT, P. and JACKSON, R., 1990. Frictional–collisional equations of motion for participate flows and their application to chutes. *Journal of fluid mechanics*, *210*, pp. 501-535.

JOHNSON, P.C. AND JACKSON, R., 1987. Frictional–collisional constitutive relations for granular materials, with application to plane shearing. *Journal of Fluid Mechanics*, 176, pp.67-93.

JORDAN, M.M., SJURAETHER, K., COLLINS, I.R., FEASEY, N.D. and EMMONS, D., 2001, January. Life cycle management of scale control within subsea fields and its impact on flow assurance, Gulf of Mexico and the North Sea basin. In *SPE Annual Technical Conference and Exhibition*. Society of Petroleum Engineers.

KAUSHAL, D. R., and TOMITA, Y., 2013. Prediction of concentration distribution in pipeline flow of highly concentrated slurry. *Particulate Science and Technology: An International Journal*, 31(1), pp. 28-34.

KAUSHAL, D. R., et al. 2013. Flow of mono-dispersed particles through horizontal bend. *International Journal of Multiphase Flow*, 52, pp. 71-91.

KAUSHAL, D. R., TOMITA, Y., and DIGHADE, R. R., 2002. Concentration at the pipe bottom at deposition velocity for transportation of commercial slurries through pipeline. *Journal of Powder Technology*, 125, pp. 89-101.

KAUSHAL, D. R. et al., 2012. Cfd modelling for pipeline flow of fine particles at high concentration. *International Journal of Multiphase Flow,* 43, pp. 85-100.

KESENA, N. R. et al., 2014. Experimental study of sand particle concentration profiles in straight and pipe elbow for horizontal and pipe elbow for horizontal multiphase flows. *Journal of Energy Resources Technology*, 136, pp. 1-11.

KING, M. J. S., FAIRHURST, C. P., and HILL, T. J., 2001. Solids transport in multiphase flows-application to high viscosity systems. *American Society of Mechanical Engineers ASME*, 123, pp. 200-204.

KUBICKI, D., and SIMON, L., 2012. Slurry transport in a pipeline-comparison of cfd and dem models. *Proceedings of the 9th International Conference on cfd in the mineral sand process industries*. 10-12 December 2012. Melbourne. pp. 1-6.

LAHIRI, S. K., and GHANTA, K. C., 2010. Slurry flow modelling by cfd. *Chemical Industry and Chemical Engineering Quarterly*, 16(4), pp. 295-308.

LEE, S.L. and WIESLER, M.A., 1987. Theory on transverse migration of particles in a turbulent two-phase suspension flow due to turbulent diffusion—I. *International journal of multiphase flow*, *13*(1), pp. 99-111.

LONDON, M., CAMERON, S., and PIERCE, G. Flow loop for x-ray ct imaging of sand transport. *Proceedings of the SPE Heavy Oil Conference*. SPE 157897. Alberta. 12-14 June 2012. pp. 1-15.

LUN, C.K.K., SAVAGE, S.B., JEFFREY, D.J. and CHEPURNIY, N., 1984. Kinetic theories for granular flow: inelastic particles in Couette flow and slightly inelastic particles in a general flowfield. *Journal of fluid mechanics*, *140*, pp. 223-256.

MA, D. and AHMADI, G., 1990. A thermodynamical formulation for dispersed multiphase turbulent flows—II: Simple shear flows for dense mixture. *International Journal of Multiphase Flow*, *16*(2), pp. 341-351.

MAKKAWI, Y.T., WRIGHT, P.C. and OCONE, R., 2006. The effect of friction and inter-particle cohesive forces on the hydrodynamics of gas–solid flow: a comparative analysis of theoretical predictions and experiments. *Powder Technology*, *163*(1), pp.69-79.

MARCHIOLI, C., PICCIOTTO, M. and SOLDATI, A., 2006. Particle dispersion and wall-dependent turbulent flow scales: implications for local equilibrium models. *Journal of Turbulence*, (7), p. N60.

MATIDA, E.A., NISHINO, K. and TORII, K., 2000. Statistical simulation of particle deposition on the wall from turbulent dispersed pipe flow. *International Journal of Heat and Fluid Flow*, *21*(4), pp. 389-402.

MATOUSEK, V., KRUPICKA, J., and CHARA, Z., 2014. Stationary and sliding beds in pipe flows of settling slurry. *15th International Freight Pipeline Society Symposium 2014 Czech Association of Scientific and Technical Societies*. 24-26 June 2014. Czech Republic.

MATOUSEK, V., KRUPICKA, J. and PENIK, V., 2014. Distribution of medium-to-coarse glass beads in slurry pipe flow: evaluation of measured concentration profiles. *Particulate Science and Technology*, 32, pp. 186-196.

MATOUSEK, V., and KRUPICKA, J., 2013. Analysis of concentration profiles in dense settling-slurry flows. *Proceedings of the ASME 2013 Fluids Engineering Division Summer Meeting.* 7-11 July 2013. pp. 1-8.

MATOUŠEK, V., 2005. Research developments in pipeline transport of settling slurries. *Powder Technology*, *156*(1), pp. 43-51.

MENTER, F.R., 1994. Two-equation eddy-viscosity turbulence models for engineering applications. *AIAA journal*, *32*(8), pp. 1598-1605.

MESSA, G. V., and MALAVASI, S., 2014. Numerical prediction of particle distribution of solid-liquid slurries in straight pipes and bends. *Journal of Engineering Applications of Computational Fluid Mechanics,* 8(3), pp. 356-372.

MEZA-DIAZ, B., and SAWATZKY, R., 2012. Sand on demand: a laboratory investigation on improving productivity in horizontal wells under heavy-oil primary production-part 2. *Society of Petroleum Engineers Journal*, pp. 1012-1028.

NAJMI, K., MCLAURY, B. S., and SHIRAZI, S. A., 2014. Experimental study of low concentration sand transport in low liquid loading water-air flow in horizontal pipes. *BHR Group 2014 Multiphase 9.* pp. 17-27.

NOSSAIR, A.M., RODGERS, P. and GOHARZADEH, A., 2012, November. Influence of Pipeline Inclination on Hydraulic Conveying of Sand Particles. In *ASME 2012 International Mechanical Engineering Congress and Exposition* pp. 2287-2293.

OLIVEIRA, P.J. and ISSA, R.I., 2003. Numerical aspects of an algorithm for the Eulerian simulation of two-phase ows. *Int. J. Numer. Meth. Fluids, 43*, pp. 1177-1198.

OROSKAR, A. R., and TURIAN, R. M., 1980. The critical velocity in pipeline flow of slurries. *American Institute of Chemical Engineers Journal*, 26(4), pp. 55-558.

OSHO, A.J., YAN, W., and YEUNG, H., 2012. Experimental study of air-water flow in undulating pipeline and implication on sand transport. *Offshore Technology Conference, OTC 23331*. 30 April-3 May. Houston, Texas, USA.

OUDEMAN, P., 1993. Sand transport and deposition in horizontal multiphase trunklines of subsea satellite developments. *Society of Petroleum Engineers Production and Facilities.* November 2013. pp. 237-241.

OUDEMAN, P., 1992. Sand transport and deposition in horizontal multiphase trunklines of subsea satellite developments. *Proceedings of the Offshore Technology Conference, OTC 7059*. 4-7 May 1992. Houston, Texas. pp. 659-667.

PAN, Y. and BANERJEE, S., 1996. Numerical simulation of particle interactions with wall turbulence. *Physics of Fluids (1994-present)*, *8*(10), pp.2733-2755.

PEIRANO, E. and LECKNER, B., 1998. Fundamentals of turbulent gas-solid flows applied to circulating fluidized bed combustion. *Progress in Energy and Combustion Science*, *24*(4), pp. 259-296.

PORTELA, L.M., COTA, P. and OLIEMANS, R.V., 2002. Numerical study of the near-wall behaviour of particles in turbulent pipe flows. *Powder technology*,*125*(2), pp. 149-157.

PLETCHER, R.H., TANNEHILL, J.C. and ANDERSON, D., 2012. *Computational fluid mechanics and heat transfer*. 3rd ed. Florida: CRC Press.

PUGH, F.J. and WILSON, K.C., 1999. Velocity and concentration distributions in sheet flow above plane beds. *Journal of Hydraulic Engineering*, *125*(2), pp.117-125.

RAMADAN, A., SKALLE, P., and SAASEN, A., 2005. Application of a three-layer modelling approach for solids transport in horizontal and inclined channels. *Chemical Engineering Science*, 60, pp. 2557-2570.

RAWLINS, C.H., 2013, April. Sand Management Methodologies for Sustained Facilities Operations. In *North Africa Technical Conference and Exhibition*. Society of Petroleum Engineers

RICE, H. P. et al., 2015. Particle concentration measurement and flow regime identification in multiphase pipe flow using a generalised dual-frequency inversion method. *Proceedings of the 7th World Congress on Particle Technology, Procedia Engineering,* 102, pp. 986-995.

ROBINSON, M. P., WALTER, H., and GRAF, M., 1972. Critical deposit velocities for low-concentration sand-water mixtures. *American Society of Civil Engineers National Water Resources Engineering Meeting*. 24-28 January 1972. pp. 1-29.

ROCO, M. and BALAKRISHNAM, N., 1985. Multidimensional flow analysis of solid-liquid mixtures. *Journal of Rheology*, pp. 431-456.

ROUSE, H., 1937. Modern conceptions of the mechanics of fluid turbulence. Transaction of ASCE, 102, pp. 463-563

SALAMA, M. M., 2000. Sand production management. *Journal of Energy Resources Technology*, 122, pp. 29-33.

SALAMA, M. M., 2000. Influence of sand production on design and operation of piping systems. *Corrosion2000. Proceedings of the NACE International Conference*. Houston, Texas. Paper No. 00080.

SAMBATH et al., 2014. A new model for solids transport in multiphase flows. *BHR Group Multiphase 9*, PP. 215-221.

SANDERS, R. S. et al., 2004. Deposition velocities for particles of intermediate size in turbulent flow. In: N. Heywood, ed. *Hydrotransport. Proceedings of the 16th International Conference of BHR Group.* Cranfield: BHR Group LTD. pp. 429-442.

SANKARANARAYANAN, K., SHAN, X., KEVREKIDIS, I.G. and SUNDARESAN, S., 2002. Analysis of drag and virtual mass forces in bubbly suspensions using an implicit formulation of the lattice Boltzmann method. *Journal of Fluid Mechanics*, *452*, pp. 61-96.

SAVAGE, S.B., 1984. The mechanics of rapid granular flows. *Advances in applied mechanics*, 24, pp. 289-366.

SAVAGE, S.B. and JEFFREY, D.J., 1981. The stress tensor in a granular flow at high shear rates. *Journal of Fluid Mechanics*, *110*, pp. 255-272.

SCHAEFFER, D.G., 1987. Instability in the evolution equations describing incompressible granular flow. *Journal of differential equations*, *66*(1), pp. 19-50.

SHOOK, C.A., GILLIES, R., HAAS, D.B., HUSBAND, W.H.W. and SMALL, M., 1982. Flow of coarse and fine sand slurries in pipelines. *Journal of Pipelines*, *3*(1), pp. 13-21.

SHEN, X. and NAKAMURA, H., 2014. Spherical-bubble-based four-sensor probe signal processing algorithm for two-phase flow measurement. *International Journal of Multiphase Flow*, *60*, pp. 11-29.

SIMONIN, O. and VIOLLET, P.L., 1990. Modelling of turbulent two-phase jets loaded with discrete particles. *Phase-Interface Phenomena for Multiphase Flow*, pp. 259-269.

SOEPYAN, F. B. et al., 2014. The use of single continuous-phase solids transport models for near horizontal stratified liquid/gas flow. *BHR Group Multiphase 9.* pp. 223-235.

SOEPYAN, F. B. et al., 2014. Solids transport models comparison and fine-tuning for horizontal low concentration flow in single-phase carrier fluid. *America Institute of Chemical Engineers Journal*, 60 (1), pp. 76-121.

SOHN, H.Y. and MORELAND, C., 1968. The effect of particle size distribution on packing density. *The Canadian Journal of Chemical Engineering*, *46*(3), pp. 162-167.

SOMMERFELD, M., 2003. Analysis of collision effects for turbulent gas–particle flow in a horizontal channel: Part I. Particle transport. *International journal of multiphase flow*, *29*(4), pp. 675-699.

SPEZIALE, C.G., ABID, R. and ANDERSON, E.C., 1992. Critical evaluation of two-equation models for near-wall turbulence. *AIAA journal*, *30*(2), pp. 324-331.

SPILLANE, C., and LEGGOE, J., 2011. Investigation into sand deposition of transportation in multiphase pipelines. *Proceedings of the CEED Seminar 2011*. pp. 13-18.

STEVENSON, P., and THORPE, R. B., 2002. Method calculates sand velocity hold-up in flowlines. *Oil and Gas Journal*, 29 July 2002, pp. 47-50

STEVENSON, P. et al., 2001. The transport of particles at low loading in near-horizontal pipes by intermittent flow. *Journal of Chemical Engineering Science*, 56, pp. 2149-2159.

STEVENSON, P. and THORPE, R. B., 1999. Towards understanding sand transport in subsea flowlines. *In: A. P. BURNS, ed. frontier technology comes of age. Proceedings of the 9th International Conference on Multiphase 1999*. Vol. 35. Bury St Edmunds. Professional Engineering Publications. pp. 583-594.

SYAMLAL, M., ROGERS, W. and O'BRIEN, T.J., 1993. MFIX documentation: Theory guide. *National Energy Technology Laboratory, Department of Energy, Technical Note DOE/METC-95/1013 and NTIS/DE95000031.*

SYAMLAL, M. and O'BRIEN, T.J., 1989. Computer simulation of bubbles in a fluidized bed. In *AIChE. Symp. Ser.* 85 (1) pp. 22-31.

TAITEL, Y., SARICA, C. and BRILL, J.P., 2000. Slug flow modelling for downward inclined pipe flow: theoretical considerations. *International Journal of Multiphase Flow*, *26*(5), pp. 833-844.

TIPPET, J. R. and PRIESTMAN, G. H., 1997. Mobility of solids in multiphase undulating pipeline. *In: A. P. BURNS, ed. how deep? how far? how soon? Proceedings of the 8th International Conference on Multiphase 1997.* Vol. 24. London. Mechanical Engineering. pp. 125-132.

THOMAS, A. D., 1979. Predicting the deposit velocity for horizontal turbulent pipe flow of slurries. *International Journal of Multiphase Flow*, 5, pp. 113-129.

TREMBLAY, B., 2005. Modelling of sand transport through wormholes. *Journal of Canadian Petroleum Technology*, *44* (04).

TRYGGVASON, G., BUNNER, B., ESMAEELI, A., JURIC, D., AL-RAWAHI, N., TAUBER, W., HAN, J., NAS, S. and JAN, Y.J., 2001. A front-tracking method for the computations of multiphase flow. *Journal of Computational Physics*, *169*(2), pp.708-759.

TURIAN, R. M., HSU, F. L., and MA, T. W., 1987. *Estimation of the critical velocity in pipeline flow of slurries*. Journal of Powder Technology, 51, pp. 35-47.

TURIAN, R. M., and YUAN, T. F., 1977. Flow of slurries in pipelines. *American Institute of Chemical Engineers Journal*, 23(3), pp. 232-243.

SHOOK, C.A., et al. 1982. Flow of Coarse and Fine Sand Slurries in Pipelines. *Journal of Pipelines,* 3, pp. 13-21

VAN WACHEM, B.G.M. and ALMSTEDT, A.E., 2003. Methods for multiphase computational fluid dynamics. *Chemical Engineering Journal*, *96*(1), pp.81-98.

VAN WACHEM, B.G.M. et al. 2001. Comparative analysis of CFD models of dense gas–solid systems. *AIChE Journal*, *47*(5), pp. 1035-1051.

VERSTEEG, H.K. and MALALASEKERA, W., 2007. *An introduction to computational fluid dynamics: the finite volume method*. 2nd ed. Harlow, England: Pearson Education.

WASP, E.J., KENNEY, J. P., and Ghandi, R. I., 1977. *Solid liquid flow slurry pipeline transportation*, Trans Tech Publications.

WEBER, M.W. and HRENYA, C.M., 2006. Square-well model for cohesion in fluidized beds. *Chemical Engineering Science*, *61*(14), pp. 4511-4527.

WEN, C.Y. and YU, Y.H., 1966. A generalized method for predicting the minimum fluidization velocity. *AIChE Journal*, *12*(3), pp. 610-612.

WHITFIELD, S., 2016. Finding New Ground in Subsea Integrity Management. *Oil and Gas Facilities*, *5*(01), pp. 10-14.

WICKS, M., 1971. Transport of solids at low concentration in horizontal pipes. In: I. ZANDI*,* ed*. Advances in solid-liquid flow in pipes and its application. Proceedings of International Symposium in Solid-Liquid Flow*. 1971. Oxford: Permagon. pp. 101-124.

WILSON, A., 2013. Facilities Sand-Management Techniques Fall Into Two Types: Inclusionary and Exclusionary. *Journal of Petroleum Technology*,*65*(10), pp. 166-16

WILSON, K.C. and PUGH, F.J., 1988. Dispersive-force modelling of turbulent suspension in heterogeneous slurry flow. *The Canadian Journal of Chemical Engineering*, *66*(5), pp. 721-727.

WILSON, K.C., SANDERS, R.S., GILLIES, R.G. and SHOOK, C.A., 2010. Verification of the near-wall model for slurry flow. *Powder Technology*, *197*(3), pp.247-253.

WILSON, K. C., and SELLGREN, A., 2008. Revised method for calculating stratification ratios for heterogeneous flows. *Proceedings of the 14th International Conference on Transport and Sedimentation of Solid Particles*. 23 June. pp. 334-340.

WILSON, K. C., and SELLGREN, A., 2003. Interaction of particles and near-wall lift in slurry pipelines. *Journal of Hydraulic Engineering*, 129, pp. 73-76.

WORLD ENERGY COUNCIL, 2013. *World energy resources.* London: World energy council.

XU, Y., and SUBRAMANIAN, S., 2010. Effect of particle clusters on carrier flow turbulence a direct numerical simulation study. *Journal of Flow Turbulence Combust*, 85, pp. 735-761.

YANG, Z. L. et al., 2007. Simulation of sand transport in stratified gas-liquid two-phase pipe flow. *BHR Group 2007 Multiphase Production Technology 13*. pp. 327-341.

YAN, W., HU, X. Osho, Y and YEUNG, H., 2011. Experimental study on sand transport characteristics in water and air-water flow in dip pipeline. *BHR Group Multiphase* 15, pp. 51-68.

YOUNG, J., and LEEMING, A., 1997. A theory of particle deposition in turbulent pipe flow. *Journal of Fluid Mechanics*, 340, pp. 129-159.

ZHANG, P. et al., 2010. Modelling turbulent flow with particle deposition in curved pipes. *Proceedings of the 7th International Conference on Multiphase Flow*. 30 May -4 June 2010. Tampa, Florida. pp. 1-9.

ZHENG, G., BRLL, J. P., and SHOHAM, O., 1993. Hilly terrain effects on slug flow characteristics. *Proceedings of the 68th Annual Technical Conference and Exhibition of the Society of Petroleum Engineers. SPE 26566*. Houston, Texas, 3-8 October 1993. pp. 529-541.

ZHU, Z., SAND, K.W., and TEEVENS, P.J., 2010. Solids deposition in liquids petroleum (oil) and wet-gas pipelines for internal corrosion predictive modelling (ICPM). *Nace International*

Appendix: Publications

Conference and Symposium Papers

Tebowei, R., Hossain, M., Oluyemi, G. and Islam, S., 2015. Modelling effects of particle size and pipe gradient on sand transport in multiphase pipes. *Computational Methods in Multiphase Flow VIII*, 20-22 April, Valencia. 89, pp.323.

R. Tebowei, M. Hossain & S. Islam, 2014. CFD Modelling of sand-liquid flow for prediction of sand distribution pattern in horizontal pipes. 1st IDEAS Symposium on Innovation, Design and Sustainability, May 2014, IDEAS Research Institute, RGU, Aberdeen.

Poster Presentation

R.Tebowei & M. Hossain, 2014. 3-D Modelling of sand distribution pattern in multiphase pipeline. Poster presented at Sand Management Network (SMN) Technology Forum, April, 2014, Aberdeen, UK.